Assessing the Capabilities of a Multispectral Unmanned Aerial System (UAS) at the Santa Rosa Environmental Monitoring Super Site, Costa Rica

by

Carlos Andres Campos Vargas

A thesis submitted in partial fulfilment of the requirements for the degree of

Master of Science

Department of Earth and Atmospheric Sciences
University of Alberta

Abstract

The main objective of this thesis was to assess the capabilities of an Unmanned Aerial System (UAS) equipped with a multispectral camera at the Santa Rosa Environmental Monitoring Super Site, Guanacaste, Costa Rica (SR-EMSS). Nowadays, available solutions for processing UAS multispectral imagery consist of end-user solutions that are mostly composed of commercial software that follows predefined processing chains. In many cases, these processing changes are created without an understanding of the effects its various steps might or will have on final data quality. As such, this thesis is divided into four chapters. *Chapter One* of this thesis explored the gaps and opportunities regarding the use of UAS in environmental monitoring and research at the SR-EMSS. *Chapter Two* compared the error at the band-level as well as spectral vegetation indexes (VI) generated from at a grass-covered firebreak using two methods to calibrate the surface reflectance at four different acquisition altitudes. *Chapter Three* of this thesis quantified the extension of dead woody components using a multispectral UAS and machine learning (ML) techniques in five temporary plots of a secondary tropical dry forest. *Chapter Four* synthesised the main challenges of this thesis, as well as discussed future paths and scientific gaps on topics related to work presented here. Results from *Chapter Two* demonstrated that using at least three reference materials for the calibration of the observed UAV surface reflectance; it can be possible to increase the accuracy of those values associated to a given spectral band. However, differences between calibration methods were statistically significant only for bands on Blue, Red, Red Edge, and NIR spectrum of light; no significant differences were observed for the Green band. *Chapter Two* also demonstrated that spectral errors associated to a given band can be up to 10% when compared with information derived from a field spectrometer. The comparison of ten Vegetation Indexes (VIs) generated from the multispectral camera and those

from a field spectrometer, indicated that seven out of ten camera derived VIs were lower than those derived from the field spectrometer. In the context of *Chapter Three,* this thesis demonstrated the advantages of using Machine Learning (ML) techniques to conduct UAV derived land cover classification tasks associated to the determination of dead woody components (e.g. dead trees). Ten ML techniques were tested and compared. Results indicate that neither of the ten algorithms used and tested (with a single set of parameters) overperformed all others in all situations. In this study multispectral UAS proved to be a useful tool to develop monitoring programs aimed to estimate the extent of tree mortality in a tropical dry forest environment. The use of future hyperspectral and thermal cameras integrated into UAVs, as well as their integration with both terrestrial and drone base LiDAR technologies, provide new emerging opportunities towards the monitoring of the impact of climate change in tropical regions.

Keywords: Machine Learning, radiometric transformation, tropical dry forests, Unmanned Aerial Systems, Unmanned Aerial Vehicle.

Preface

This thesis is an original work by Carlos Andres Campos Vargas. No part of this thesis has been previously published. However, Chapter Two incorporates the changes suggested from Raymond Soffer, from the NRCC, who review the first draft of that chapter.

Acknowledgements

I would like to thank the following: Dr Sanchez and Dr Rivard for their guidance during my studies and in the elaboration of this thesis. Raymond Soffer for his comments and suggestions on chapter two which significantly enhanced that chapter. Michael Hesketh for his help with the English proofread and comments of this document.

To my family, which has always been there. Alina, Myriam, Simon, and obviously, Whisky.

To the *Universidad Estatal a Distancia*, Costa Rica for its financial support that made it possible to conduct my studies at the University of Alberta. To Andres Segura from the Laboratorio de Investigación e Innovación Tecnológica (LIIT) for all its support. To all people from AMI and COBI, especially to Diana Hernandez, Heidy Rosales, Lizette Brenes, Marianela Salas and Yelitza Fong.

To all my friends at UofA Branko, Naty, Sofia, Wei, Toño for all his help.

To the people from the *Área de Conservación Guanacaste*, for all its support and inspiration. Especially to Didi Guadamuz, Julio Diaz, María Marta Chavarría and Roger Blanco. To all people who helped me in the field Daniela, Diana, Henry, José, Katherine, Rebeca, Ruta, and others that help me in some way or another.

Finally, I would like to acknowledge the Inter-American Institute for Global Change Research (IAI) - CRN3-025 TROPI-DRY, Universidad Estatal a Distancia de Costa Rica (UNED), and the University of Alberta for their institutional and financial support.

List of abbreviations

DVI	Difference Vegetation Index
EVI	Enhanced Vegetation Index
EMSS	Environmental Monitoring Super Site
GDVI	Green Difference Vegetation Index
GRVI	Green Ratio Vegetation Index
GNDVI	Green Normalized Difference Vegetation Index
IPVI	Infrared Percentage Vegetation Index
MSR	Modified Simple Ratio
NDVI	Normalized Difference Vegetation Index
NLI	Non-Linear Index
TDF	Tropical Dry Forests
SR-EMSS	Santa Rosa National Park Environmental Monitoring Super Site
SR	Simple Ratio
VI	Vegetation index(es)
UAV	Unmanned Aerial Vehicle
UAS	Unmanned Aerial System

Definitions

Multispectral sensor	Referred as a sensor that captures radiance values in a small number of discrete and broad spectral bands across some regions of the electromagnetic spectrum.
Spectral band	Measured as the sections of a wavelength of light captured by optical sensors.
Spectral signature	Measured as the response of the reflectance across the electromagnetic spectrum.
Spectral index	Referred as a mathematical expression that combines two or more spectral bands to express a trait of an observed target.
Spatial resolution	The measure of the pixel size as a projection of a detector element into the ground.
UAV	Referred to an aircraft remotely piloted by a human pilot.
UAS	Referred as an encompassing description that encapsulates the aircraft (UAV), the ground-based controller, and system communication that connect them.

References

Jensen, J. R. 2005. Introductory digital image processing: a remote sensing perspective. (3rd Edition). Prentice Hall Inc, Upper Saddle River, New Jersey.

Lillesand, T. M., R. W. Kiefer, and Chipman, J. W. 2004. Remote sensing and image interpretation Seventh. John Wiley & Sons, Ltd., New York, New York.

Table of Contents

List of Tables

Chapter Two

Chapter Three

List of Figures

Chapter Two

Chapter Three

1. Chapter One – Introduction

1.1. Introduction

Tropical Dry Forests (TDFs) have been described as an ecosystem with the highest structural and physiological diversity of life forms in the world (Sánchez-Azofeifa et al. 2013). TDFs are forests with a pronounced seasonality in rainfall distribution and several months of drought (Portillo-Quintero and Sanchez-Azofeifa, 2010). As a consequence of this long dry season, the common phenological response for most of the woody species is deciduousness, with almost 50% of trees present being drought deciduous (Kalacska et al. 2004). However, the number of species and individuals with this response varies strongly with successional stage and topography (Hilje et al. 2015; Kalacska et al. 2004). The mean annual temperature is >25 °C, the total annual precipitation ranges between 700 and 2000 (Portillo-Quintero and Sanchez-Azofeifa, 2010), and the potential evapotranspiration exceeds the precipitation (Van Bloem, Murphy, and Lugo 2004). Furthermore, TDFs are considered the most endangered and threatened ecosystems in comparison with others tropical forests (Sánchez-Azofeifa et al. 2013). As of today, there has been a loss of almost 60% of their original total extent, and the remaining forests are experiencing high levels of forest fragmentation (Portillo-Quintero and Sanchez-Azofeifa, 2010). Nowadays the Neotropical dry forests exist as fragments of a once large forest that reached from Mexico to Northern Argentina (Portillo-Quintero and Sanchez-Azofeifa 2010).

In 2003,Sanchez-Azofeifa et al. (2003) foresaw remote sensing research priorities in the TDF for a better understanding of this ecosystem. These priorities included: i). the development of techniques for the identification and characterisation of tropical dry secondary forests and ii) the development of baseline spectral data and tools for the characterisation and detection of single tree species. These priorities led to a series of studies to: i) understand the relationships between the spectral reflectance observed by Landsat TM and forest structural characteristics of dry forest succession in Costa Rica (Arroyo-Mora et al. 2005), ii) use MODIS surface reflectance imagery at 500m resolution to assess the extent of Neotropical dry forests (Portillo-Quintero and Sanchez-Azofeifa 2010), iii) use EO-1 Hyperion hyperspectral satellite imagery for mapping structure and floristic diversity as a way of assessing a regional ecological fingerprint (Kalacska et al. 2007). In addition, short-wave infrared information (SWIR, 1000 to 2500 nm) and a

multiple criteria spectral mixture analysis was used to study the structural variability of different successional forests (Cao et al. 2015).

More recently Sanchez-Azofeifa et al. (2017a) reviewed trends in remote sensing technologies for the conservation and the study of tropical forests. In this review, six emerging trends where highlighted in relation to: i) passive remote sensors, ii) passive hyperspectral and multi-angular sensors, iii) light detection and ranging sensor (LIDAR), iv) near-surface remote sensing, v) ground-based observatories, and vi) sensor fusion. Ensuing publications that include Sánchez-Azofeifa et al. (2017b) have examined how the abundance of liana affects the prediction of Terrestrial Laser Scanner and Hemispherical Photos in detecting the level of a succession of a given forest stand. Li et al. (2017) pursued the identification of tropical dry forests and their succession, and the determination of their extent via the use of machine learning techniques and fusion of LiDAR and hyperspectral imaging data. As well as, Li et al. (2018) that quantified the relative coverage of dead trees, liana-infested, and non-liana-infested trees, using multispectral UAS data and ML techniques.

This thesis aims to contribute to the development of near-surface remote sensing at the Santa Rosa Environmental Monitoring Super Site (SR-EMSS). The main objective of *Chapter Two* was to evaluate the impact on the error values of two radiometric transformations used to translate digital numbers to reflectance values of a MicaSense RedEdge ^{3M} multispectral camera onboard an UAS at SR-EMSS's grass-covered firebreaks. The primary objective of *Chapter Three* was to detect and quantify dead stand trees, fallen trees and decaying trees with dead structures using a multispectral UAS and ML techniques at SR-EMSS' secondary dry forests.

Though there has been significant remote sensing research of TDF, under humid conditions, the application of optical remote sensor data can suffer constraints as a consequence of the high humidity (Sanchez-Azofeifa et al. 2017). For example, Kalacska et al. (2016) on the "Quality Control Assessment of the Mission Airborne Carbon 13 (MAC-13) Hyperspectral Imagery from Costa Rica" reported a spectral misalignment in some flights attributed to the acquisition of data under extremely humid conditions. Specifically, Kalacska et al. (2016) highlighted that in consultation with the sensor manufacturer that the issue was not previously reported.

Near-surface remote sensing has been rapidly evolving through the use of Unmanned Aerial Systems (UAS). It has been claimed that UAS offer timely and cost-effective solutions to gather

data at large-scales, low-altitude and high spatial resolution, with little atmospheric interference (Anderson and Gaston 2013; Colomina & Molina, 2014; Ballesteros *et al.*, 2014). However, available solutions for processing UAS imagery consisted of end-users solutions that follow predefined processing chains in commercial software; that only allows the use of a single white reference panel in the radiometric calibration. In this context, *chapter Two* compared the relative error of reflectance values at the band-level as well as spectral vegetation indexes (VI) from a MicaSense Red Edge ™ 3 multispectral camera onboard of a Draganfly XP-4 helicopter at the SR-EMSS' grass-covered firebreaks. This was done using two radiometric transformations and four acquisition altitudes. The first transformation, named as single-point, only considers the values of a single-white reference panel as suggested by Ahmed et al. (2017). The second transformation suggested by Smith and Milton (1999) and Pozo et al. (2014) is the empirical line method that was developed with three reference panels.

UAS have been used in many fields such as, estimation of canopy attributes (Chianucci et al. 2016), quantification of tree high (Bendig et al., 2015; Panagiotidis *et al.*, 2016; Zarco-Tejada *et al.*, 2014), vegetation structure (Cunliffe, Brazier, and Anderson 2016; Panagiotidis et al. 2017), and biomass (Li et al. 2016). UAS has also been contributing to the monitoring of wildfires (Yuan, Zhang, & Liu, 2015; Ambrosia et al., 2011), and ecological restoration monitoring (Knoth *et al.*, 2013; Zahawi *et al*., 2015).

There is growing evidence suggesting that many forests could be increasingly vulnerable to extensive tree mortality triggered by drier and hotter climatic conditions (Anderegg, Kane, and Anderegg 2012). These conditions are causing tree mortality to become a dominant driver of forest aboveground carbon turnover (Carvalhais et al. 2014).

Severe and recurrent widespread mortality events can have long-term impacts on a wide range of populations, communities, and ecosystems (Zeppel, Anderegg, and Adams 2013). Tree mortality can also impact biodiversity, and ecosystem functions such as nutrient and carbon cycling, ecosystem services, and biophysical and biogeochemical climate feedbacks.

In general, ML has become a significant component of remote sensing data analysis, mainly because, a computer algorithm can acquire knowledge from existing data using specific inference strategies such as induction or deduction (Ghamisi et al. 2017; Maxwell, Warner, and Fang 2018; Plaza et al. 2009). A number of studies have found that these methods tend to

produce higher accuracy compared to traditional parametric models (Kuhn and Johnson 2013; Maxwell et al. 2018). For instance, on the identification of the extent and succession of tropical dry forests at SR-EMSS using ML and hyperspectral data (Li et al. 2017), and a multiple criteria spectral mixture analysis and SWIR data (Cao et al. 2015). On the quantification of the relative coverage of dead trees, liana-infested, and non-liana-infested trees in a temporary plot at SR-EMSS using multispectral UAS data and ML techniques.

Chapter Three contributed to the quantification of dead woody components in a gradient of secondary tropical dry forests at the SR-EMSS, using a broadband multispectral UAS and machine learning (ML) models. Ten state-of-the-art machine learning algorithms in remote sensing were used: Averaged Neural Network (ANN), Conditional Inference Tree (CIT), C4.5-like Trees (C45), Deep Neural Network (DNET), Gradient Boosting Machines (GBM), Random Forest (RF), Neural Network (NNT), Support Vector Machines with Linear Kernel (SVML), Support Vector Machines with Polynomial Kernel (SVMP), and Support Vector Machines with Radial Kernel (SVMR).

1.2. References

Ahmed, Oumer S., Adam Shemrock, Dominique Chabot, Chris Dillon, Griffin Williams, Rachel Wasson, and Steven E. Franklin. 2017. "Hierarchical Land Cover and Vegetation Classification Using Multispectral Data Acquired from an Unmanned Aerial Vehicle." *International Journal of Remote Sensing* 38 (8–10). Taylor & Francis: 2037–52. https://doi.org/10.1080/01431161.2017.1294781.

Ambrosia, V. G., S. Wegener, T. Zajkowski, D. V. Sullivan, S. Buechel, F. Enomoto, B. Lobitz, S. Johan, J. Brass, and E. Hinkley. 2011. "The Ikhana Unmanned Airborne System (UAS) Western States Fire Imaging Missions: From Concept to Reality (2006–2010)." *Geocarto International* 26 (2): 85–101. https://doi.org/10.1080/10106049.2010.539302.

Anderegg, William R L, Jeffrey M Kane, and Leander D L Anderegg. 2012. "Triggered by Drought and Temperature Stress." *Nature Climate Change*, 9. September. Nature Publishing Group. https://doi.org/10.1038/nclimate1635.

Anderson, Karen, and Kevin J. Gaston. 2013. "Lightweight Unmanned Aerial Vehicles Will Revolutionize Spatial Ecology." *Frontiers in Ecology and the Environment* 11 (3): 138–46. https://doi.org/10.1890/120150.

Arroyo-Mora, Pablo, G Arturo Sánchez-Azofeifa, Margaret E R Kalacska, Benoit Rivard, Julio C Calvo-Alvarado, Daniel H Janzen, Juan Pablo Arroyo-mora, et al. 2005. "Secondary Forest Detection in a Neotropical Dry Forest Landscape Using Landsat 7 ETM + and IKONOS Imagery. Association for Tropical Biology and Conservation." *Biotropica* 37 (4): 497–507. https://doi.org/10.1111/j. 1744-7429.2005.00068.x.

Ballesteros, R., J. F. Ortega, D. Hernández, and M. A. Moreno. 2014. "Applications of Georeferenced High-Resolution Images Obtained with Unmanned Aerial Vehicles. Part I: Description of Image Acquisition and Processing." *Precision Agriculture* 15 (6): 579–92. https://doi.org/10.1007/s11119-014-9355-8.

Bendig, Juliane, Kang Yu, Helge Aasen, Andreas Bolten, Simon Bennertz, Janis Broscheit, Martin L. Gnyp, and Georg Bareth. 2015. "Combining UAV-Based Plant Height from Crop Surface Models, Visible, and near Infrared Vegetation Indices for Biomass Monitoring in Barley." *International Journal of Applied Earth Observation and Geoinformation* 39. Elsevier B.V.: 79–87. https://doi.org/10.1016/j.jag.2015.02.012.

Bloem, S Van, P Murphy, and A Lugo. 2004. "Tropical Dry Forests." Encyclopedia of Forest Sciences 24 (1): 1767–75. https://doi.org/http://dx.doi.org/10.1016/B0-12-145160-7/00176-9.

Cao, Sen, Qiuyan Yu, Arturo Sanchez-Azofeifa, Jilu Feng, Benoit Rivard, and Zhujun Gu. 2015. "Mapping Tropical Dry Forest Succession Using Multiple Criteria Spectral Mixture Analysis." ISPRS Journal of Photogrammetry and Remote Sensing 109 (November 2017). *International Society for Photogrammetry and Remote Sensing*, Inc. (ISPRS): 17–29. https://doi.org/10.1016/j.isprsjprs.2015.08.009.

Carvalhais, Nuno, Matthias Forkel, Myroslava Khomik, Jessica Bellarby, Martin Jung, Mirco Migliavacca, Mingquan Mu, et al. 2014. "Global Covariation of Carbon Turnover Times with Climate in Terrestrial Ecosystems." *Nature* 514 (7521): 213–17. https://doi.org/10.1038/nature13731.

Chianucci, Francesco, Leonardo Disperati, Donatella Guzzi, Daniele Bianchini, Vanni Nardino, Cinzia Lastri, Andrea Rindinella, and Piermaria Corona. 2016. "Estimation of Canopy Attributes in Beech Forests Using True Colour Digital Images from a Small Fixed-Wing UAV." *International Journal of Applied Earth Observation and Geoinformation* 47. Elsevier B.V.: 60–68. https://doi.org/10.1016/j.jag.2015.12.005.

Colomina, I., and P. Molina. 2014. "Unmanned Aerial Systems for Photogrammetry and Remote Sensing: A Review." ISPRS Journal of Photogrammetry and Remote Sensing 92. *International Society for Photogrammetry and Remote Sensing*, (ISPRS): 79–97. https://doi.org/10.1016/j.isprsjprs.2014.02.013.

Cunliffe, Andrew M., Richard E. Brazier, and Karen Anderson. 2016. "Ultra-Fine Grain Landscape-Scale Quantification of Dryland Vegetation Structure with Drone-Acquired Structure-from-Motion Photogrammetry." *Remote Sensing of Environment* 183. The Authors: 129–43. https://doi.org/10.1016/j.rse.2016.05.019.

Dunford, R., K. Michel, M. Gagnage, H. Piégay, and M. L. Trémelo. 2009. "Potential and Constraints of Unmanned Aerial Vehicle Technology for the Characterization of Mediterranean Riparian Forest." *International Journal of Remote Sensing* 30 (19): 4915–35. https://doi.org/10.1080/01431160903023025.

Ghamisi, Pedram, Javier Plaza, Yushi Chen, Jun Li, and Antonio J. Plaza. 2017. "Advanced Spectral Classifiers for Hyperspectral Images: A Review." *IEEE Geoscience and Remote Sensing* Magazine 5 (1): 8–32. https://doi.org/10.1109/MGRS.2016.2616418.

Kalacska, M., G. A. Sanchez-Azofeifa, J. C. Calvo-Alvarado, M. Quesada, B. Rivard, and D. H. Janzen. 2004. "Species Composition, Similarity and Diversity in Three Successional Stages of a Seasonally Dry Tropical Forest." *Forest Ecology and Management* 200 (1–3): 227–47. https://doi.org/10.1016/j.foreco.2004.07.001.

Kalacska, M., G. A. Sanchez-Azofeifa, B. Rivard, T. Caelli, H. Peter White, and J. C. Calvo-Alvarado. 2007. "Ecological Fingerprinting of Ecosystem Succession: Estimating Secondary Tropical Dry Forest Structure and Diversity Using Imaging Spectroscopy." *Remote Sensing of Environment* 108 (1): 82–96. https://doi.org/10.1016/j.rse.2006.11.007.

Kalacska, Margaret, J. Pablo Arroyo-Mora, Raymond Soffer, and George Leblanc. 2016. "Quality Control Assessment of the Mission Airborne Carbon 13 (MAC-13) Hyperspectral Imagery from Costa Rica." *Canadian Journal of Remote Sensing* 42 (2): 85–105. https://doi.org/10.1080/07038992.2016.1160771.

Kalácska, Margaret, G. Arturo Sánchez-Azofeifa, Terry Caelli, Benoit Rivard, and Brent Boerlage. 2005. "Estimating Leaf Area Index from Satellite Imagery Using Bayesian

Networks." *IEEE Transactions on Geoscience and Remote Sensing* 43 (8): 1866–73. https://doi.org/10.1109/TGRS.2005.848412.

Knoth, Christian, Birte Klein, Torsten Prinz, and Till Kleinebecker. 2013. "Unmanned Aerial Vehicles as Innovative Remote Sensing Platforms for High-Resolution Infrared Imagery to Support Restoration Monitoring in Cut-over Bogs." *Applied Vegetation Science* 16 (3): 509–17. https://doi.org/10.1111/avsc.12024.

Kuhn, Max, and Kjell Johnson. 2013. Applied Predictive Modeling. *Applied Predictive Modeling*. https://doi.org/10.1007/978-1-4614-6849-3.

Li, Wang, Zheng Niu, Hanyue Chen, Dong Li, Mingquan Wu, and Wei Zhao. 2016. "Remote Estimation of Canopy Height and Aboveground Biomass of Maize Using High-Resolution Stereo Images from a Low-Cost Unmanned Aerial Vehicle System." *Ecological Indicators* 67. Elsevier Ltd: 637–48. https://doi.org/10.1016/j.ecolind.2016.03.036.

Li Wei, Campos-Vargas Carlos, Marzahn Phillip, Sanchez-Azofeifa Arturo 2018. On the estimation of tree mortality and liana infestation using a deep self- encoding network. *International Journal of Applied Earth Observation and Geoinformation* 73:1–13. https://doi.org/10.1016/j.jag.2018.05.025.

Li, Wei, Sen Cao, Campos-Vargas, Carlos, and Sanchez-Azofeifa, Arturo. 2017. "Identifying Tropical Dry Forests Extent and Succession via the Use of Machine Learning Techniques*." International Journal of Applied Earth Observation and Geoinformation* 63 (July). Elsevier: 196–205. https://doi.org/10.1016/j.jag.2017.08.003.

Maxwell, Aaron E., Timothy A. Warner, and Fang. 2018. "Implementation of Machine-Learning Classification in Remote Sensing: An Applied Review." *International Journal of Remote Sensing* 39 (9). Taylor & Francis: 2784–2817. https://doi.org/10.1080/01431161.2018.1433343.

Panagiotidis, Dimitrios, Azadeh Abdollahnejad, Peter Surový, and Vasco Chiteculo. 2017. "Determining Tree Height and Crown Diameter from High-Resolution UAV Imagery." *International Journal of Remote Sensing* 38(8–10):2392–2410. https://doi.org/10.1080/01431161.2016.1264028.

Plaza, Antonio, Jon Atli Benediktsson, Joseph W. Boardman, Jason Brazile, Lorenzo Bruzzone, Gustavo Camps-Valls, Jocelyn Chanussot, et al. 2009. "Recent Advances in Techniques for Hyperspectral Image Processing." *Remote Sensing of Environment* 113 (SUPPL. 1). Elsevier Inc.: S110–22. https://doi.org/10.1016/j.rse.2007.07.028.

Portillo-Quintero, C. A., and G. A. Sanchez-Azofeifa. 2010. "Extent and Conservation of Tropical Dry Forests in the Americas." *Biological Conservation* 143 (1). Elsevier Ltd: 144–55. https://doi.org/10.1016/j.biocon.2009.09.020.

Pozo, Susana Del, Pablo Rodríguez-Gonzálvez, David Hernández-López, and Beatriz Felipe-García. 2014. "Vicarious Radiometric Calibration of a Multispectral Camera on Board an Unmanned Aerial System." *Remote Sensing* 6 (3): 1918–37. https://doi.org/10.3390/rs6031918.

Sanchez-Azofeifa, Arturo, Jose Antonio Guzmán, Carlos A. Campos, Saulo Castro, Virginia Garcia-Millan, Joanne Nightingale, and Cassidy Rankine. 2017. "Twenty-First Century Remote Sensing Technologies Are Revolutionizing the Study of Tropical Forests." *Biotropica* 49 (5): 604–19. https://doi.org/10.1111/btp.12454.

Sánchez-Azofeifa, Arturo, Julio Calvo-Alvarado, Mário Marcos do Espírito-Santo, Geraldo Fernandes, and Jennifer Powers. 2013. "*Tropical Dry Forests in the Americas*." Tropical Dry Forests in the Americas, 1–15. https://doi.org/10.1201/b15417-2.

Sanchez-Azofeifa, G. A., K. L. Castro, B. Rivard, M. R. Kalascka, and R. C. Harriss. 2003. "Remote Sensing Research Priorities in Tropical Dry Forest Environments." *Biotropica* 35 (2): 134–42. https://doi.org/10.1111/j.1744-7429.2003.tb00273.x.

Sánchez-Azofeifa, Arturo, J. Antonio Guzmán-Quesada, Mauricio Vega-Araya, Carlos Campos-Vargas, Sandra Durán, Nikhil D'Souza, Thomas Gianoli, Carlos Portillo-Quintero, and Iain Sharp. 2017. "Can Terrestrial Laser Scanners (TLSs) and Hemispherical Photographs Predict Tropical Dry Forest Succession with Liana Abundance?" *Biogeosciences* 14 (4): 977–88. https://doi.org/10.5194/bg-14-977-2017.

Smith, Geoffrey M., and Edward J. Milton. 1999. "The Use of the Empirical Line Method to Calibrate Remotely Sensed Data to Reflectance." *International Journal of Remote Sensing* 20 (13): 2653–62. https://doi.org/10.1080/014311699211994.

Yuan, Chi, Youmin Zhang, and Zhixiang Liu. 2015. "A Survey on Technologies for Automatic Forest Fire Monitoring, Detection, and Fighting Using Unmanned Aerial Vehicles and Remote Sensing Techniques." *Canadian Journal of Forest Research* 45 (7): 783–92. https://doi.org/10.1139/cjfr-2014-0347.

Zahawi, Rakan A., Jonathan P. Dandois, Karen D. Holl, Dana Nadwodny, J. Leighton Reid, and Erle C. Ellis. 2015. "Using Lightweight Unmanned Aerial Vehicles to Monitor Tropical Forest Recovery." *Biological Conservation* 186: 287–95. https://doi.org/10.1016/j.biocon.2015.03.031.

Zarco-Tejada, P. J., R. Diaz-Varela, V. Angileri, and P. Loudjani. 2014. "Tree Height Quantification Using Very High-Resolution Imagery Acquired from an Unmanned Aerial Vehicle (UAV) and Automatic 3D Photo-Reconstruction Methods." *European Journal of Agronomy* 55. Elsevier B.V.: 89–99. https://doi.org/10.1016/j.eja.2014.01.004.

2. Chapter Two – Effect of acquisition altitude and radiometric transformation of multispectral data acquired with an Unmanned Aerial Vehicle on Vegetation Indexes at SR-EMSS.

2.1. Keywords

Tropical grasslands, radiometric transformations, near remote sensing, vegetation index, unmanned aerial system.

2.2. Introduction

With the increasing accessibility and payload versatility of Unmanned Aerial Vehicles (UAV), many researchers are now exploring scientific applications to study ecosystems that would otherwise be difficult or impossible to achieve using satellite or airborne data. Small and low-cost UAV with multispectral, hyperspectral and infrared imaging sensors are particularly well-suited for addressing current issues in remote sensing of tropical ecology and conservation (Sanchez-Azofeifa et al. 2017a). It has been suggested that Unmanned Aerial Systems (UAS) are a viable option for mapping canopy structure even under cloudy conditions (Aasen et al. 2018; Sanchez-Azofeifa et al. 2017a; Dandois, Olano, and Ellis 2015).

Multispectral data can provide information about leaf properties from leaf reflectance by making use of absorption features associated with foliar organic compounds. Vegetation in the visible-near infrared (VNIR, 400 – 1000 nm) and shortwave infrared (SWIR,1000 to 2500 nm) presents five spectral absorption regions, as a result of electron transitions in chlorophylls and the bending/stretching of the Oxygen-Hydrogen bond in water and other chemicals (Curran 1989). However, the radiance or reflectance measurement at one single band cannot be used as a metric for chemicals concentrations (Gamon and Surfus 1999) because absorption features are broadened by the scattering within the leaf, resulting in interference between adjacent bands (Harris et al. 2014). Besides, some organic compounds absorb at similar wavelength regions, distorting many absorption features (Sánchez-Azofeifa et al. 2009). In consequence, a single band is never uniquely related to a specific chemical (Banninger 1988; Curran 1989).

Spectral vegetation indexes (VI) are mathematical combinations of different spectral bands mostly in the VNIR region of the electromagnetic spectrum. The main purpose of VI is to enhance the information contained in spectral reflectance data, by extracting the variability due

to vegetation characteristics while minimizing soil, atmospheric, and sun-target-sensor geometry effects (Viña et al. 2011). Comparisons of VI with extracted pigment concentrations suggest that in vegetation, there are broad and species-specific relationships between VI and leaf pigments and leaf structural components (Castro-Esau, Sánchez-Azofeifa, and Caelli 2004; Harris et al. 2014). In general, high values of NDVI are associated with healthy photosynthetic foliage result of high water and pigments concentrations (Rullan-Silva et al. 2013). Contrary to senescence foliage that is associated with a drop in NDVI values (Dash et al. 2017).

Though significant research in remote sensing in tropical environments, under humid conditions, has resulted from the use of remote optical equipment, such equipment can suffer constraints in the application of the data (Sanchez-Azofeifa et al. 2017a). This is because of the interference from aerosols, water vapour and clouds that can restrict the extent to which the imagery acquired from a UAS can be immediately used as a management tool (Dunford et al. 2009; Sanchez-Azofeifa et al. 2017). Kalacska et al. (2016) detected a significant spectral misalignment in a number of flights, which was attributed to the acquisition of data under extremely humid conditions because atmospheric constituents such as water vapour can vary significantly over short distances (Gao, Goetz, and Zamudio 1991). On the other hand, to acquire multispectral or hyperspectral data compensation for differences in illumination during the acquisition time must be made. In a field collection even with a remarkably uniform cloud cover, the uniformity of the downwelling illumination is questionable which can could cast doubt on the accuracy of the in-scene calibration results. Therefore, observed reflectance obtained under diffuse conditions could differ from those observed under illumination conditions dominated by a direct illumination which in turn would impact any spectral component.

As the commercial use of multispectral sensors from UAS grows, tools for processing UAS multispectral imagery have become more accessible. However, those tools consist of commercial end-users software such as *PIX4D* or *Agisoft-photoscan* that follow predefined processing chains without a complete understanding of the effects that various steps might have on data quality. In these programs, the radiometric transformation of digital numbers (DN) to reflectance values only considers the values from a single white panel (single point method). On the other hand, in remote sensing there have been other methods which use at least three reference panels, also known as the empirical line method (Smith and Milton 1999; Pozo et al. 2014).

The single and multiple points methods let to measure of radiance ($W \cdot m^{-2} \cdot sr^{-1} \cdot nm^{-1}$) for any pixel from a single image in a particular camera and channel. However, both methods rely on assumptions that need to be recognized to interpret results accurately. These assume that there are no differences in illumination across the image; consequently, changes in radiance due to clouds, shadowing or topography could be ignored (Smith and Milton 1999). Also, they assume that the Earth's surface consists of Lambertian reflectors, and the effects of the atmosphere are uniform across scenes (Smith and Milton 1999). The use of UAS can solve some of those assumptions, for instance, the flight time of a UAV is limited to 10 to 15 min, in consequence, the chance of changes in illumination and radiance are diminished. Therefore, the relatively low acquisition altitude can reduce the effects of the atmosphere and clouds shadowing. This study compared the relative error of reflectance values at the band-level as well as spectral vegetation indexes (VI) from a multispectral camera onboard of an UAV at the SR-EMSS' grass-covered firebreaks. Using two radiometric transformations and four acquisition altitudes.

2.3. Materials and methods

2.3.1. Study site

The study area is located at SR-EMSS, Guanacaste, Costa Rica (Figure 2.1). The mean temperature is 25 °C, and the annual rainfall ranges from 900 to 2600 mm. The dry season lasts for a minimum of 5–6 months, it usually extends from late December to mid-May (Sánchez-Azofeifa et al. 2017b). Historically, *Jaragua* grass (*Hyparrhenia rufa*) from East Africa was introduced around 1940 (Janzen 2000) to create grass pastures for cattle as part of an intense deforestation process, traditionally associated with anthropogenic fires. Santa Rosa was extensively managed as a cattle ranch until the mid-1960s when a significant portion of the ranch was expropriated and subsequently transformed into a national park. Nowadays, the landscape comprises a mosaic of pastures and forests in various stages of regeneration that once suffered from anthropogenic fires and intense deforestation (Cao et al. 2015; Sánchez-Azofeifa et al. 2017b). Specifically, the data collection was conducted in grassland areas dominated by *Jaragua* grass that are used as firebreaks.

2.3.2. Data collection and processing

2.3.2.1. Panel calibration and instrument optimization

Instrument optimization and reflectance reference measurements were performed prior to sample measurements. Two U*niSpec* spectroradiometers (PP Systems, USA), two *ASD Illuminator* lamps, and a *MicaSense RedEdge* ™ 3 camera were used to collect directional-directional reflectance. The *MicaSense RedEdge* ™ 3 provides five separate 16-bit GeoTIFF images, each covering a specific spectral range. The blue band (B1) is centered at 475 nm, the green band (B2) is centered at 560 nm, the red band (B3) is centered at 668 nm, the red edge band (B4) is centered at 717 nm, and the NIR band (B5) is centered at 840 nm (Table 2.2).On the other hand, the *UniSpec* spectroradiometers (Table 1) are capable of measuring continuous reflectance from 310 to 1100 nm (Harris et al. 2014).

The spectral signatures and images of the manufacturer calibrated white panel that is used only in laboratory activities (Spectralon, LabSphere, North Sutton, NH, USA), the Spectralon white panel the MicaSense's halon panel (As a grey panel), and a black presentation cardboard were collected in laboratory with controlled illumination, temperature, and humidity. Specifically,the spectral signatures were adquired following the protocol of Castro-Esau, Sánchez-Azofeifa, and Rivard (2006). A dark scan was taken for every ten sample measurements. The integration time was adjusted with the fibre-optic exposed to white reference conditions, in order to the spectrum would peak but not saturate. A white reference measurement was taken prior to each panel measurement. The white reference measurements were obtained with the lamps directed toward the laboratory reference panel. In all cases, reflectance spectra were obtained by determining the ratios of data (Equations 1 and 2) acquired for a sample (an average of 10 scans) to data acquired for a laboratory white reflectance panel.

The *UniSpec* spectroradiometers are available in two configurations, for a single channel (*UniSpec-SC*) and dual channel (*UniSpec-DC*). In this study, a *UniSpec-DC* was used in the field to collect spectral signatures of the reference materials. However, before using the *UniSpec-DC* in the field, it was cross-validated at laboratory conditions with the *Unispec-SC* to verify the precision of its recorded values. The *UniSpec-DC* was equipped with an upward looking sensor head fitted with a cosine diffuser that simultaneously measured solar irradiance and target reflectance to minimise the impact of changes in the atmosphere on reflectance measurements.

During the laboratory acquisition, the upward sensor was located next to the sampled panels and the same altitude. In consequence, the reflectance from the *UniSpec-DC* was obtained by applying equation (1).

$$R_{DC} = \frac{R\ target / I\ downwelling}{R\ panel / I\ downwelling} \quad (1)$$

In equation (1) R_{DC} is the corrected reflectance, *R target / I downwelling* is the raw reflectance factor and *R panel / I downwelling* is the cross-calibration function. Using the laboratory white reflectance panel, dedicated only to laboratory activities, as the *R panel* and the three reference panels as *R target*. On the other hand, the readings the *UniSpec-SC* (equation 2), R_{SC} is the corrected reflectance, *R target* is the radiance from the three reference panels, and *R panel* is the radiance from the white reference panel that is dedicated only to laboratory activities. The *UniSpec-SC* required measures of the laboratory white reference panel after every collected sample.

$$R_{SC} = \frac{R\ target}{R\ panel} \quad (2)$$

The MicaSense data was acquired in the same laboratory conditions with controlled illuminated conditions. 80 multispectral images were acquired from the four reference panels. Precisely, 20 samples from the laboratory white *Spectralon* panel, 20 samples from the white *Spectralon* panel, 20 samples from the Mica Sense's halon panel, and 20 samples from the black presentation cardboard were collected.

A Pearson correlation analysis was performed to cross-validate the reflectance values (R_{DC} *and* R_{SC}) from the *Unispec* spectroradiometers. Comparing 10 datasets of 15 spectral signatures per calibrated panel, for a total of 150 spectral signatures of the three calibrated panels. Because of the differences in spectral resolution and wavelength coverage between the MicaSense camera and the *UniSpec-DC* spectroradiometer, the *UniSpec* values were resampled to match the spectral resolution of the *MicaSense* bands (Table 2.2), using the spectral resampling process available in *ENVI* (Exelis Visual Information Solutions, Boulder, Colorado, EEUU, v.*5.3*).

2.3.2.2. Dark signal noise correction

Previous studies of calibration of remote sensing data pointed out that instruments are susceptible to the readout noise and thermal noise related to sensor temperature and integration time, which is known as the dark signal noise (Aasen et al. 2018). Practical approaches for dark signal noise removal include i). acquired closed shutter images; ii). thermal characterization of the dark signal non-uniformity in the laboratory at multiple integration times and iii). measures of "black pixels" within the image using no illumination (Aasen et al. 2018; Babey and Soffer 1992). In this study, the dark signal noise from the field spectrometer was acquired while the shutter was closed, while for the camera it was measured using 30 images of a black panel acquired under no illumination in the laboratory.

2.3.2.3. Field acquisition

From June 2017 through July 2017, 12 UAS flights missions were performed at six sites located within the SR-EMSS (Figure 2.1a). Each location was situated in a firebreak patch with a ground surface cover composed of a mixture of *Jaragua* grass and exposed bare soils, which belong to the orders *Inceptisols* and *Entisols* according to the USDA soil taxonomy (Figure 2.1b, 2.1c, 2.1d). A total of 180 samples delineated with polyvinylchloride (PVC) square frames were collected with a multispectral UAS and field spectrometer (Figure 2.1b, 2.1c), adapting the protocols of Smith and Milton (1999) and Miura and Huete (2009). *The UniSpec-DC* spectrometer (Table 2.1) mounted in a tripod at 0.75m from the ground was used to collect spectral signatures of vegetation and soil samples delineated by PVC frames of 0.5 m by 0.5 m. On each site were spread 30 PVC frames in a linear orientation with a distance between frames of 0.5 m (Figure 2.1b, 2.1c, 2.1d).

The UAS multispectral data were obtained using a *MicaSense RedEdge* ™ 3 camera onboard a *Draganflyer X4-P* (Table 2.3 and Figure. 2.2b). The field data collection was limited to clear and sunny conditions, to mimic the reflectance acquired during the laboratory calibration, bidirectional reflectance. The 30 UAS multispectral samples per site were collected on two flight missions (with a time difference of less than 10 min.), acquiring 15 PVC frames per flight mission. On each flight mission, three to five images were systematically acquired at four different altitudes from the ground: at 100 m, 75 m, 50 m and 25 m to investigate any effect of

the acquisition altitude in the MicaSense reflectance values. To perform a radiometric transformation, immediately before and after each UAS's flight mission five multispectral images at 1.5m from the ground (Figure 2.2d) and 30 spectral signatures of the three calibrated reference materials were acquired with the *UniSpec-DC* spectrometer and the MicaSense camera, adapting the calibration framework of Miura and Huete (2009) and Smith and Milton (1999). Specifically, that calibration data was acquired following the protocol of Miura and Huete (2009); however, in this study was used three reference materials following the findings of Smith and Milton (1999). Because of Miura and Huete (2009) only considered white reference materials.

A spectrally independent angular correction factor of 0.95 was applied to the dark reference panel, following the suggestions of Kalacska et al. (2016). In the case of the white and grey (MicaSense panel) panels this factor was not applied because the material of both panels is barium sulphate, hence, those panels are lambertian surfaces.

2.3.2.4. Data processing

As previously pointed out available commercial solutions for processing UAS multispectral imagery such as *PiX4D* or *Agisoft* follow predefined processing chains mostly designed to end user. The supporting material of those solutions does not provide enough technical information to fully understand the effects that various processing steps might have on data quality. Preliminary products from those solutions provided unusual and useless values when the radiometric calibration was applied to the mosaicking process. Because at the time of the field collection, MicaSense released a firmware update that negatively affected the performance of the MicaSense's Downwelling Light Sensor (DLS). Consequently, an alternative framework to transform MicaSense raw values or Digital Numbers (DN) to sensor radiance ($W \cdot m^{-2} \cdot sr^{-1} \cdot nm^{-1}$) and reflectance at surface values was implemented. This framework consisted of a radiometric transformation, vignetting correction, mosaicking, and bands co-registration.

Two radiometric transformations on raw-individual *MicaSense* images to transform *MicaSense* DN to reflectance at the surface were performed. The first transformation, named single point method, used a reflectance factor from a single white panel such as Miura and Huete (2009), Candiago et al. (2015), Ahmed et al. (2017), and Li et al. (2018).On the other hand, the second

transformation, called the empirical line method, required the use of three reference panels such as Smith and Milton (1999) and Pozo et al. (2014).

Vignetting is an effect of radial falloff of intensity from the centre of the image that occurs in all digital cameras (Goldman and Jiun-Hung 2010). Vignetting carries problems for a wide variety of applications due to its effects when sequences of images are combined (Goldman and Jiun-Hung 2010). Consequently, a vignetting correction was performed on *R program* (R Foundation for Statistical Computing, Vienna, Austria, *v 3.2.1*), applying equation (3) to all single images. Based on the principles of Goldman and Jiun-Hung (2010).

$$P_{x,i} = R\ (t_i f_{d,f} M(r_{x,i})) \quad (3)$$

In Equation 3 R is the camera response curve provided by the camera manufacturer,

M is the image as a matriz of x rows and i columns, $r_{x,i}$ is the radiance value at any point in the image, t_i is the exposure time of frame i, and $f_{d,v}$ is funtion of the observation distance and the field of view of the camera. Assuming that the vignetting was radially symmetric about the centre of the image and in a given sequence of images.

The *MicaSense* camera provides five separate GeoTIFF, each covering a specific spectral range and a FOV. Those differences in position and FOV, result of the MicaSense imager, imply that the five bands are not inherently co-registered, and each band covers a different area. Consequently, the generation of mosaics from MicaSense images means that each band provides a single band mosaic with a specific spectral range and covered area. In this study the mosaicking process was performed in *Image Composite Editor* (ICE, Microsoft Research Computational Photography Group, v.2.0), employing three to five MicaSense images per altitude level. For each flight mission, five single band mosaics were generated for four different altitudes including 100 m, 75 m, 50 m and 25 m.

An orthorectification and an image-co-resgistration were applied to the mosaics generated with ICE because the mosaics generated had no geographical coordinates. Each blue mosaic was orthorectified in ENVI, using five ground control points acquired with a *Trimble GeoXT6000* differential GPS with a Hurricane antenna (average precision of 0.5 m horizontal and 0.75 m

vertical). Then, an image-to-image co-registration to the four remaining band mosaics (RMSE 0.6191 ± 0.1482) was performed, using as a based image the orthorectified blue mosaics. A minimum of 60 ground control points per mosaic or tile were selected, employing the corners of all PVC frames within each tile as reference points. The spatial resolutions of all mosaics were homogenized within the altitude levels, and as a result, all tiles acquired at 100 m altitude were resampled to a pixel resolution of nine cm, those at 75 m to seven cm, those at 50 m to 4.5 cm, and those at 25 m to 2.5 cm.

The reflectance values from all mosaics were extracted with a sequential model on *ModelBuilder* of *ArcGIS* (Environmental Systems Research Institute, Redlands, CA. v. 10.3). First, centroid points in all PVC targets were created using the ground control points generated during the co-registration process. A buffer zone of 15cm in radius was created for all centroids to coincide with the area sampled with of the *UniSpec-DC* radiometer. Finally, the reflectance values from all mosaics were extracted, using the tool extract from raster available in ArcGIS.

2.3.3. Vegetation Indexes

Ten common VI were calculated using the estimated average reflectance from all delineated targets (Table 2.4), making use of 4 of the 5 *MicaSense* channels from the two radiometric transformations. Likewise, the same VI were estimated using the resampled values of the field spectrometer, in order to estimate an approximation error between the camera and spectrometer values.

2.3.4. Comparison of radiometric transformations and statistical analysis

The effects of the two radiometric transformations and acquisition altitudes on reflectance values of the multispectral camera were assessed by estimating the relative error from every single band and the vegetation index estimated. Using in equation (4) the values from the field spectrometer as the *expected values* and the values from the MicaSense camera as *observed values*.

$$error_r = \frac{expected\ value - observed\ value}{100} \quad (4)$$

The statistical analysis was performed in *R program*. A Shapiro-Wilk normality test was performed to estimate the normality of the error distribution from the transformed bands and their derived vegetation indexes. Likewise, a *repeated measures ANOVA* analysis was performed to compare the camera reflectance values estimated by the two radiometric transformations and the four adquisition altitudes, following equation (5):

$$error_{band,VI} \sim \text{height} * \text{trans} + \text{Error}\left(\text{fid}/_{\text{height} * \text{trans}}\right) \quad (5)$$

In equation (5) $error_{band,\ VI}$ referred to the relative error value in percentage (Equation 5) of each band and each vegetation index; *height* referred to the altitude from the ground at which the image was acquired; *trans* refers to the transformation method used to estimate reflectance, and *fid* refers to the number of samples or PVC frames.

2.4. Results

2.4.1. Instruments validation and panel calibration

A strong correlation between *UniSpec-DC* and *UniSpec-DC* instruments was found using five resampled bands to match the MicaSense spectral resolution (Figure 2.3). The Blue band showed a $R^2 = 0.9820$, Green band $R^2 = 0.9930$, Red band $R^2 = 0.9920$, RedEdge band $R^2 = 0.9820$, and NIR band $R^2 = 0.9980$. Likewise, a strong linear correlation between MicaSense raw values and *UniSpec-DC* reflectance for all bands was found: Blue band $R^2 = 0.9935$, Green band $R^2 = 0.9931$, Red band $R^2 = 0.9919$, RedEdge band $R^2 = 0.9863$, and NIR band $R^2 = 0.9746$ (Figure 2.4).

The three panels showed a relative uniform reflectance in laboratory and field conditions (Figure 2.4f). Although some absorption features were observed for the black and white panels near 950 nm (Figure 2.4f), those absorption features did not affect our data because the *MicaSense* camera does not cover that spectral region.

2.4.2. Comparison of radiometric transformations and acquisition altitude on multispectral bands

In general, the two transformation methods at the band level showed maximum error values close to 10%. The distribution of error values displayed differences in their grouping patterns

(Figure 2.5). Disregarding the acquisition altitude, the Blue, Green, and Red bands show a normal distribution, contrary to bands RedEdge and NIR (Figure 2.5e). A *Shapiro-Wilk* normality test confirmed that the distribution of the data for the Blue (W = 0.96743, *p-value* = 0.1091), Green (W = 0.66743, *p-value* = 0.1021, and Red (W = 0.96743, *p-value* = 0.1091) bands were not significantly different from a normal distribution as opposed to the Red Edge (W = 1.00743, *p-value* = 0.0051) and NIR (W = 1.16773, *p-value* = 0.0121) bands.

In regard to the effect of acquisition altitude on the error distribution, the error of the MicaSense bands changed distribution as altitude changed. However, these changes were more evident in some bands than others (Figure 2.5). For instance, for the green band the error distributions at 25 m (Figure 2.5a) and the general distribution (Figure 2.5e) were similar; however, the distribution at 50 m (Figure 2.5b), 75 m (Figure 2.5c), and 100 m (Figure 2.5d) were different. Similar patterns were observed on the other four bands, which revealed some changes in their error distribution as a result of the acquisition altitude (Figure 2.5).

The *repeated measures ANOVA* indicated that the bands' reflectance between transformation methods had some significant differences (Table 2.5). The Blue (f= 8.98, *p-value* = 0.01), Red (f = 41.41, *p-value* = 0.0000), Red Edge (f = 14.76, *p-value* = 0.000) and NIR (f = 3.33, *p-value* = 0.05) bands showed significant differences in their distribution in contrast to the Green band (t = 53.02, *p-value* = 0.5125). Thus, the error distribution shows that for the multiple panel approach all bands are nearer to zero than the single panel method (Figure 2.5). This indicates that the multiple panel values were closer to that of the field spectrometer than those generated by the single panel transformation. Furthermore, the repeated measures ANOVA indicates that there was no link between the transformation method and the acquisition altitude (Table 2.5).

2.4.3. Comparison of radiometric transformations and acquisition altitude on vegetation indexes

The vegetation indexes displayed larger error values than single bands, reaching error values of up to 20%. The results showed that the indexes for six of the ten images were lower than the indexes obtained with the field spectrometer suggesting that our field measurements have a degree of inaccuracy and generally under-estimated the reflectance and that errors can behave in a multiplicative way instead of an additive way. Specifically, DVI, GDVI, GNDVI, IPVI, MSR, and NDVI aggregate below the zero-value because the estimated values (transformed reflectance

values) were lower than the expected values (field spectrometer). Instead, GRVI, NLI, and SR values aggregated above zero. NLI also had a high number of negative error values (Figure 2.6 e).

At the VI level, the transformation method did not affect all indexes equally. DVI, GDVI, GNDVI, GRVI, and NLI showed significant differences as a result of the transformation method. On the other hand, the vegetation indexes that did not report changes on their error distribution as a result of the transformation method were EVI, IPVI, NDVI and SR (Table 2.5).

The *Repeated measures ANOVA* indicated that not all VI changed their distribution as the acquisition altitude changes. The indexes DVI, GDVI, GNDVI, GRVI, MSR, and SR reported significant differences, at the 95% level of confidence, in the error distribution as a consequence of the acquisition altitude. On the other hand, EVI, IPVI, NDVI, NLI had no significant differences in their distribution caused by acquisition altitude (Table 2.5). The same test indicated that at the index level most of the indexes did not show a significant interaction between the transformation method and the acquisition altitude. Specifically, DVI, EVI, GNDVI, IPVI, MSR, NDVI, NLI, and SR reported no significant interactions between the transformation method and the acquisition altitude. This is contrary to GNDVI and GRVI that showed significant interactions at the 95% level of confidence (Table 2.5).

2.5. Discussion

2.5.1. Panel calibration and Instrument validation

The values from both UniSpec spectroradiometers and the MicaSense camera showed high correlation, indicating that those instruments can capture spectral in the five spectral regions; blue (475 nm), green (560 nm), red (668 nm), red edge (717 nm), and NIR (840 nm). The upward looking sensor of the *UniSpec-DC* minimises the impact of changes in the atmosphere on reflectance measurements, thus facilitating the field acquisition. However, the same upward looking sensor increase the complexity in the setup of the instruments at laboratory conditions. Kalacska et al. (2016) on the Quality Control Assessment of Hyperspectral Imagery from Costa Rica they recognized that the direct illumination is the dominant component at Santa Rosa field

conditions. Consequently, the upward looking sensor from the UniSpec-DC was able to capture most of the solar irradiation.

The white reference panel used as a white reference in the field was not a perfect Lambertian surface in the whole spectral region from 310 to 1100 nm, because of the presence of some sharp features around 450 and 950 nm in the spectral signature of the panel. The grey and black panels showed an increasing reflectance from 450 to 950 and a strong absorption feature around 950 nm. However, the all analysis performed in this study were not affected by those issues, because the absorption features and increasing reflectance occurred outside the spectral boundaries of MicaSense bands (Figure 2.4). In consequence, those issues were solved during the spectral resampling process, performed to match the MicaSense spectral resolution (Table 2.2).

2.5.2. Comparison of radiometric transformations and acquisition altitude on multispectral bands and vegetation indexes

Our results indicated that the radiometric transformation method used to translate DN to reflectance had a direct impact on both the derived band reflectance and spectral indexes values. The use of multiple reference panels in the transformation method significantly reduced the error values at the band level, in four of five bands (Blue, red, red edge, and NIR). The use of multiple calibration panels during the image acquisition provides better results than only using a single white reference panel. However, the statistical analysis indicated that the radiometric transformation not affected the green band. The same statistical analysis indicated that all five bands had significant changes in the distribution of errors as a function of the acquisition altitude. Those changes for Green, Red Edge, and NIR bands were attributed to the contributions of vegetation and soil in relation to variations of the spatial resolution, which generates a spectral mixture within the pixel. Because most clumps of grass would not provide 100% coverage of the sampled area, also even if it did it would have to be at least five leaves thick to be optically thick. Consequently, under field conditions, the soil spectra become an important contributor to consider, even when pure vegetation samples were collected.

In VI such as the DVI, IPVI, MSR, NDVI, NLI, and SR, the index values are mostly driven by photosynthetic activity in the red band and by water absorption in the NIR region. Other factors can also influence the response of vegetation in the NIR region. For example, NIR reflectance

increased slightly with increasing mesophyll thickness as a result of photon scattering within the spongy leaf mesophyll (Sánchez-Azofeifa et al. 2009). Instead, mature or senescing older leaves tended to have a higher NIR reflectance than younger leaves. VI such as GDVI, GNDVI, and GRVI were developed using the NIR band, but they use the Green band instead of the Red band. Consequently, it can be expected that for those indexes the NIR band has a more significant role than the red band because the Green band did not show differences due to the transformation method. The EVI and SR indexes showed a tighter distribution than the other indexes, although these indexes are very different in their formulas. In the case of EVI, it depends on three bands, using the blue band as a compensation factor. On the other hand, SR only considers a single ratio between two bands.

2.5.3. Uncertainties and sources of error

Several factors can increase the error during the field sampling collection; some are explicitly associated with the instrumentation used. Some are very variable and cannot be controlled such the ambient conditions and solar illumination. In this study, predefined protocols were followed to avoid or at least diminish the systematic errors in the measurements in the laboratory and field data. Likewise, the cross-validation of the instruments was performed to discard the existence of instrumentation issues.

Even with a calibrated reference panel and the upward looking sensor from the UniSpec-DC, it cannot be expected that the spectral values recorded in a laboratory entirely coincide with spectral values collected in field conditions due to several factors such as the aerosol column in the atmosphere, viewing angle, meteorological conditions. The surface calibration it has been used for decades in the remote sensing field providing high quality results (Babey and Soffer 1992; Leblanc et al. 2016).

Flying at low altitude from the ground can help to diminish the effect of atmospheric aerosols. However, it also can create or exacerbate some radiometric constraints related to water absorption features. When flying at low altitude, the transmittance of the atmosphere can rapidly change a result of absorption features by water vapour, because the atmospheric water vapour concentrations decrease with height (Gao et al. 1991). Especially, when flying above tropical forests, because the canopy transpiration that releases huge amounts of water vapour to the

atmosphere. Consequently, even if the data from an UAS are not affected by the whole atmospheric column like a spaceborne sensor or some airborne systems, these could suffer some restrictions result of water absorption features from vapour water (Sánchez-Azofeifa et al. 2017a).

The use of small UAS could mean reduced platform stability caused by winds and thermals, limited GPS accuracy, and more compressed exterior orientation data. Small digital consumer cameras used in UAS have considerably more distortions than traditional mapping cameras used on traditional piloted aircraft. As a consequence, the processing of the UAS imagery is more problematic than that of imagery obtained from more stable platforms provided by bigger aircraft (Laliberte 2009). Mostly the geometric rectification, not the radiometric correction as the path lengths from the center pixel vs border pixels is not substantially different at low altitudes, not enough to generate errors of concern in the derivation of at surface reflectance.

Even with the acquisition of data at noon, Kalacska et al. (2016) demonstrated the necessity to account for a spectrally independent angular correction factor to correct for illumination angles. Consequently, in this study, the acquisition time at noon and the use of the halon panels as Lambertian surfaces to calibrate the data helped to avoid this step in two calibration panels; however, the dark reference required a calibration factor of 0:95. The decision to avoid the acquisition of information at lower illumination angles is because, if the images are acquired at lower illumination angles than 45° illumination angle-0 degree view angle, a cross-calibration process to generate a specific spectrally independent angular correction factor is required (Kalacska et al. 2016). Likewise, the use of UAS on sunny days at the early morning or late afternoon with low solar angles could decrease the contrast between classes as a result of no direct lighting increasing the number of shadows (Dandois et al. 2015).

2.6. Conclusions

This study demonstrated that using at least three reference materials for the calibration to at surface reflectance can increase the accuracy of reflectance estimated values. The error at the band level stretched values up to 10% that we expect are dominated by random errors because the instrument calibration and the protocols used to mitigate the synthetic errors. Likewise, the vegetation indexes reported error values close to 20%. Suggesting that the error could behave in

an additive way. The error distribution of vegetation indexes exhibited an underestimation in comparison with indexes generated with a field spectrometer.

Finally, we point out that our vegetation indexes come from grass-like vegetation. Consequently, for further uses or comparisons with these data, it should be considered that throughout the VIS spectral region, grass species have consistently higher reflectance values than woody species (Asner 1998). Therefore, because of the broadband channels of the camera used, many small absorption features or second overtones could be hidden because of the low spectral resolution of the multispectral camera used. Also, it is strongly recommended to acquire 'pure' and mixed spectra of the grass and the background that allow knowing an average spectrum and its standard deviation, which could facilitate the data interpretation and processing.

2.7. References

Ahmed, Oumer S., Adam Shemrock, Dominique Chabot, Chris Dillon, Griffin Williams, Rachel Wasson, and Steven E. Franklin. 2017. "Hierarchical Land Cover and Vegetation Classification Using Multispectral Data Acquired from an Unmanned Aerial Vehicle." *International Journal of Remote Sensing* 38 (8–10). Taylor & Francis: 2037–52. https://doi.org/10.1080/01431161.2017.1294781.

Aasen H, Honkavaara E, Lucieer A, Zarco-Tejada P. 2018. Quantitative Remote Sensing at Ultra-High Resolution with UAV Spectroscopy: A Review of Sensor Technology, Measurement Procedures, and Data Correction Workflows. *Remote Sensing* 10(7):1091. https://doi.org/10.3390/rs10071091.

Asner, Gregory P. 1998. "Biophysical and Biochemical Sources of Variability in Canopy Reflectance." *Remote Sensing of Environment* 64 (3): 234–53. https://doi.org/10.1016/S0034-4257(98)00014-5.

Babey, S. K., and Raymond J. Soffer. 1992. "Radiometric Calibration of the Compact Airborne Spectrographic Imager (Casi)." *Canadian Journal of Remote Sensing* 18 (4): 233–42. https://doi.org/10.1080/07038992.1992.10855328.

Banninger, C. 1988. "Changes In Canopy Leaf Area Index And Biochemical Constituents Of A Spruce Forest As Measured By The AIS-2 Airborne Imaging Spectrometer." *In 12th Canadian Symposium on Remote Sensing Geoscience and Remote Sensing Symposium*, 4:2085–89. IEEE. https://doi.org/10.1109/IGARSS.1989.577783.

Candiago, Sebastian, Fabio Remondino, Michaela De Giglio, Marco Dubbini, and Mario Gattelli. 2015. "Evaluating Multispectral Images and Vegetation Indices for Precision Farming Applications from UAV Images." *Remote Sensing* 7 (4): 4026–47. https://doi.org/10.3390/rs70404026.

Cao, Sen, Qiuyan Yu, Arturo Sanchez-Azofeifa, Jilu Feng, Benoit Rivard, and Zhujun Gu. 2015. "Mapping Tropical Dry Forest Succession Using Multiple Criteria Spectral Mixture Analysis." *ISPRS Journal of Photogrammetry and Remote Sensing* 109. *International Society for Photogrammetry and Remote Sensing*, Inc. (ISPRS): 17–29. https://doi.org/10.1016/j.isprsjprs.2015.08.009.

Castro-Esau, K. L., G. A. Sánchez-Azofeifa, and T. Caelli. 2004. "Discrimination of Lianas and Trees with Leaf-Level Hyperspectral Data." *Remote Sensing of Environment* 90 (3): 353–72. https://doi.org/10.1016/j.rse.2004.01.013.

Curran, Paul J. 1989. "Remote Sensing of Foliar Chemistry." *Remote Sensing of Environment* 30 (3): 271–78. https://doi.org/10.1016/0034-4257(89)90069-2.

Dandois, Jonathan P., Marc Olano, and Erle C. Ellis. 2015. "Optimal Altitude, Overlap, and Weather Conditions for Computer Vision Uav Estimates of Forest Structure." *Remote Sensing* 7 (10): 13895–920. https://doi.org/10.3390/rs71013895.

Dash, Jonathan P., Michael S. Watt, Grant D. Pearse, Marie Heaphy, and Heidi S. Dungey. 2017. "Assessing Very High-Resolution UAV Imagery for Monitoring Forest Health during a

Simulated Disease Outbreak." *ISPRS Journal of Photogrammetry and Remote Sensing* 131. Scion (New Zealand Forest Research Institute): 1–14. https://doi.org/10.1016/j.isprsjprs.2017.07.007.

Dunford, R., K. Michel, M. Gagnage, H. Piégay, and M. L. Trémelo. 2009. "Potential and Constraints of Unmanned Aerial Vehicle Technology for the Characterization of Mediterranean Riparian Forest." *International Journal of Remote Sensing* 30 (19): 4915–35. https://doi.org/10.1080/01431160903023025.

Gamon, J. A., and J. S. Surfus. 1999. "Assessing Leaf Pigment Content and Activity with a Reflectometer." *New Phytologist* 143 (1): 105–17. https://doi.org/10.1046/j.1469-8137.1999.00424.x.

Gao, Bo Cai, Alexander Goetz, and J. Zamudio. 1991. "Retrievals of Surface Reflectance from AVIRIS data." In IGARSS'91 *Remote Sensing: Global Monitoring for Earth Management Geoscience and Remote Sensing Symposium*, 2077:2069–77.

Goldman, Daniel B., and Chen Jiun-Hung. 2010. "Vignette and Exposure Calibration and Compensation." *IEEE Transactions on Pattern Analysis and Machine Intelligence* 32 (12): 2276–88. https://doi.org/10.1109/TPAMI.2010.55.

Harris, A., J. A. Gamon, G. Z. Pastorello, and C. Y S Wong. 2014. "Retrieval of the Photochemical Reflectance Index for Assessing Xanthophyll Cycle Activity: A Comparison of near-Surface Optical Sensors." *Biogeosciences* 11 (22): 6277–92. https://doi.org/10.5194/bg-11-6277-2014.

Janzen, Daniel H. 2000. "Costa Rica's Area de Conservación Guanacaste: A Long March to Survival through Non-Damaging Biodevelopment." *Biodiversity* 1 (February): 7–20. https://doi.org/10.1080/14888386.2000.9712501.

Kalacska, Margaret, J. Pablo Arroyo-Mora, Raymond Soffer, and George Leblanc. 2016. "Quality Control Assessment of the Mission Airborne Carbon 13 (MAC-13) Hyperspectral Imagery from Costa Rica." *Canadian Journal of Remote Sensing* 42 (2): 85–105. https://doi.org/10.1080/07038992.2016.1160771.

Laliberte, Andrea. 2009. "Unmanned Aerial Vehicle-Based Remote Sensing for Rangeland Assessment, Monitoring, and Management." *Journal of Applied Remote Sensing* 3 (1): 033542. https://doi.org/http://dx.doi.org/10.1117/1.3216822.

Li, Wei, Campos-Vargas Carlos, Philip Marzahn, and Sanchez-Azofeifa Arturo. 2018. "Int J Appl Earth Obs Geoinformation On the Estimation of Tree Mortality and Liana Infestation Using a Deep Self- Encoding Network." *Int J Appl Earth Obs Geoinformation* 73 (May). Elsevier: 1–13. https://doi.org/10.1016/j.jag.2018.05.025.

Miura, Tomoaki, and Alfredo R. Huete. 2009. "Performance of Three Reflectance Calibration Methods for Airborne Hyperspectral Spectrometer Data." *Sensors* 9 (2): 794–813. https://doi.org/10.3390/s90200794.

Pozo, Susana Del, Pablo Rodríguez-Gonzálvez, David Hernández-López, and Beatriz Felipe-García. 2014. "Vicarious Radiometric Calibration of a Multispectral Camera on Board an

Unmanned Aerial System." *Remote Sensing* 6 (3): 1918–37. https://doi.org/10.3390/rs6031918.

Rullan-Silva, C. D., A. E. Olthoff, J. A. Delgado de la Mata, and J. A. Pajares-Alonso. 2013. "Remote Monitoring of Forest Insect Defoliation. A Review." *Forest Systems* 22 (3): 377–91. https://doi.org/10.5424/fs/2013223-04417.

Sanchez-Azofeifa, Arturo, Jose Antonio Guzmán, Carlos A. Campos, Saulo Castro, Virginia Garcia-Millan, Joanne Nightingale, and Cassidy Rankine. 2017a. "Twenty-First Century Remote Sensing Technologies Are Revolutionizing the Study of Tropical Forests." *Biotropica* 49 (5): 604–19. https://doi.org/10.1111/btp.12454.

Sánchez-Azofeifa, Arturo, Karen Castro, S. Joseph Wright, John Gamon, Margaret Kalacska, Benoit Rivard, Stefan A. Schnitzer, and Ji Lu Feng. 2009. "Differences in Leaf Traits, Leaf Internal Structure, and Spectral Reflectance between Two Communities of Lianas and Trees: Implications for Remote Sensing in Tropical Environments." *Remote Sensing of Environment* 113 (10): 2076–88. https://doi.org/10.1016/j.rse.2009.05.013.

Sánchez-Azofeifa, Gerardo Arturo, J. Antonio Guzmán-Quesada, Mauricio Vega-Araya, Carlos Campos-Vargas, Sandra Milena Durán, Nikhil D'Souza, Thomas Gianoli, Carlos Portillo-Quintero, and Iain Sharp. 2017b. "Can Terrestrial Laser Scanners (TLSs) and Hemispherical Photographs Predict Tropical Dry Forest Succession with Liana Abundance?" *Biogeosciences* 14 (4): 977–88. https://doi.org/10.5194/bg-14-977-2017.

Smith, Geoffrey M., and Edward J. Milton. 1999. "The Use of the Empirical Line Method to Calibrate Remotely Sensed Data to Reflectance." *International Journal of Remote Sensing* 20 (13): 2653–62. https://doi.org/10.1080/014311699211994.

Viña, A., Gitelson, A., Nguy-Robertson, A. L., & Peng, Y. 2011. Comparison of different vegetation indices for the remote assessment of green leaf area index of crops. Remote Sensing of Environment, 115(12), 3468–3478. https://doi.org/10.1016/j.rse.2011.08.010

2.8. Figures and Tables

Table 2.1. Technical specifications of UniSpec SC/DC spectroradiometers (PP Systems) used at SR-EMSS and in laboratory conditions.

PP Systems UniSpec SC/DC	
Specifications	**Value**
Wavelength range (nm)	310–1100
FWHM (nm)	10
Sampling interval (nm)	3.3
Downward FOV (°)	20
Operative temperature range (*C)	0 - 50

Table 2.2. Technical specifications of MicaSense RedEdge [3M] camera used at the SR-EMSS and in laboratory conditions.

MicaSense RedEdge 3 M		
Specifications		**Value**
Focal Length (mm)		5.5
FOV (°)		47.2
Imager Size (mm)		4.8 x 3.6
Imager resolution (pixels)		1280 x 960
Capture rate/ second		1
Band Name	**Center Wavelength (nm)**	**FWHM (nm)**
Blue (b1)	475	20
Green (b2)	560	20
Red (b3)	668	10
Red Edge (b4)	717	10
Near IR (b5)	840	40

Table 2.3. Technical specifications of the airframe Draganfly XP4 used at SR-EMSS and in laboratory conditions.

Draganfly X4ES airframe	
Specifications	**Value / units**
Maximum Takeoff Weight	2.50 kg (88.2oz)
Maximum payload weight	800 g (28.2oz)
Empty Weight	1.7 kg (59.9oz)
Climb rate	393.7 ft/min (2m/s)
Descend rate	393.7 ft/min (2m/s)
Maximum operating speed	26.9 knots (50km/hr)
Manoeuvring speed	26.9 knots (50km/hr)
Maximum endurance	25 minutes
Maximum Attitude angle	34 degrees
Max turn rate (yaw)	90 degrees/sec
Max Rotor RPM	5000 RPM
Yaw Torque limit	0.25N.m (Newton Meters)
Sound at 1 meter	72db
Sound at 3 meters	62db
Width	87cm (34.4”)
Length	87cm (34.4”)
Height	29cm (11.6”)
Top diameter	106cm (42.0”)
Service Ceiling	2438m (8000ft) ASL
Maximum controller signal range	1 km (0.62miles)
Accelerometer	Three Axes
Magnetometer	Three Axes
Gyrostabilizer	Three Axes
Luminous flux navigation lights	40 lm
Operating Temperature	-25C to +38C (-13F to 100.4F)
Max Wind speed	up to 35km/hr (21mph)
Relative humidity	0% to 90% non-condensing

Table 2.4. List of Spectral Vegetation Indexes (SVI) estimated across six firebreak patches covered by *Jaragua* grass at the SR-EMSS, Costa Rica.

Index	Acron.	Formula	Reference
Difference Vegetation Index	DVI	$DVI = NIR - Red$	(Tucker 1979)
Enhanced Vegetation Index	EVI	$\text{EVI} = 2.5 * \frac{(\text{NIR} - \text{Red})}{(\text{NIR} + 6\text{RED} - 7.5\text{Blue} + 1)}$	(Huete et al. 2002)
Green Difference Vegetation Index	GDVI	$GDVI = NIR - Green$	(Sripada et al. 2006)
Green Ratio Vegetation Index	GRVI	$GRVI = \frac{NIR}{Green}$	(Sripada et al. 2006)
Infrared Percentage Vegetation Index	IPVI	$IPVI = \frac{NIR}{NIR + Red}$	(Crippen 1990)
Green Normalized Difference Vegetation Index	GNDVI	$GNDVI = \frac{NIR - Green}{NIR + Green}$	(Gitelson and Merzlyak 1998)
Modified Simple Ratio	MSR	$MSR = \frac{(NIR/Red) - 1}{\left(\sqrt{NIR/Red}\right) - 1}$	(Vescovo et al. 2012)
Normalized Difference Vegetation Index	NDVI	$NDVI = \frac{NIR - Red}{NIR + Red}$	(Gitelson and Merzlyak 1998)
Non-Linear Index	NLI	$NLI = \frac{NIR^2 - Red}{NIR^2 + Red}$	(Goel and Qin 1994)
Simple Ratio	SR	$SR = \frac{NIR}{Red}$	(Birth and McVey 1968)

Table 2.5. F -values of some *Repeated measures ANOVA* on error values of bands and vegetation spectral indexes using a MicaSense RedEdge in *Jaragua* grass at SR-EMSS, Costa Rica.

	Bands				
	Blue (b1)	**Green (b2)**	**Red (b3)**	**Red Edge (b4)**	**NIR (b5)**
Treat (T)	8.98**	0.59	41.41***	14.76***	3.33*
Height (H)	103.46***	53.02***	11.57***	4.22**	41.10***
T*H	0.8	0.25	0.69	0.59	1.53

	Indexes									
	DVI	**EVI**	**GDVI**	**GNDVI**	**GRVI**	**IPVI**	**MSR**	**NDVI**	**NLI**	**SR**
Treat (T)	11.29***	1.73	60.80***	85.99***	50.41***	1.09	0	0.85	9.09**	0.24
Height (H)	2.68*	0.45	24.04***	32.99***	33.44***	0.92	2.86*	0.99	1.92	6.01***
T*H	2.13	1.63	3.01*	0.09	3.06*	0.07	0.06	0.06	0.04	0.08

Where the Significance is represented by these codes: 0 '***', 0.001 '**', 0.01 '*', 0.05 '.', 0.1 ' ' 1.

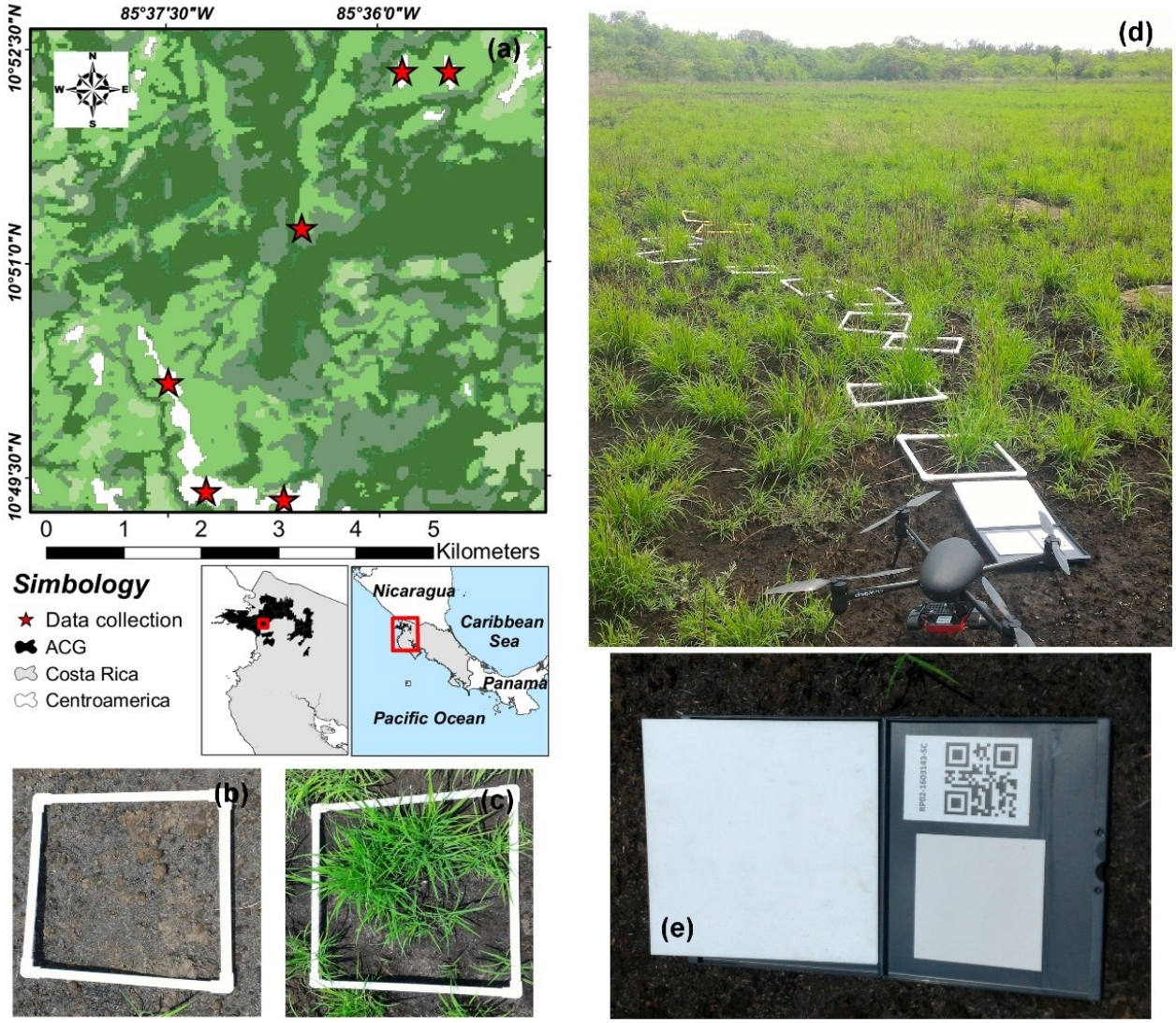

Figure 2.1. (a) Study area at the SR-EMSS, Costa Rica; (b) Soil dominate sample collection; (c) Vegetation dominated sample collection; (d) overview of field data collection; (e) reference panels white (50 cm) and grey (25 cm).

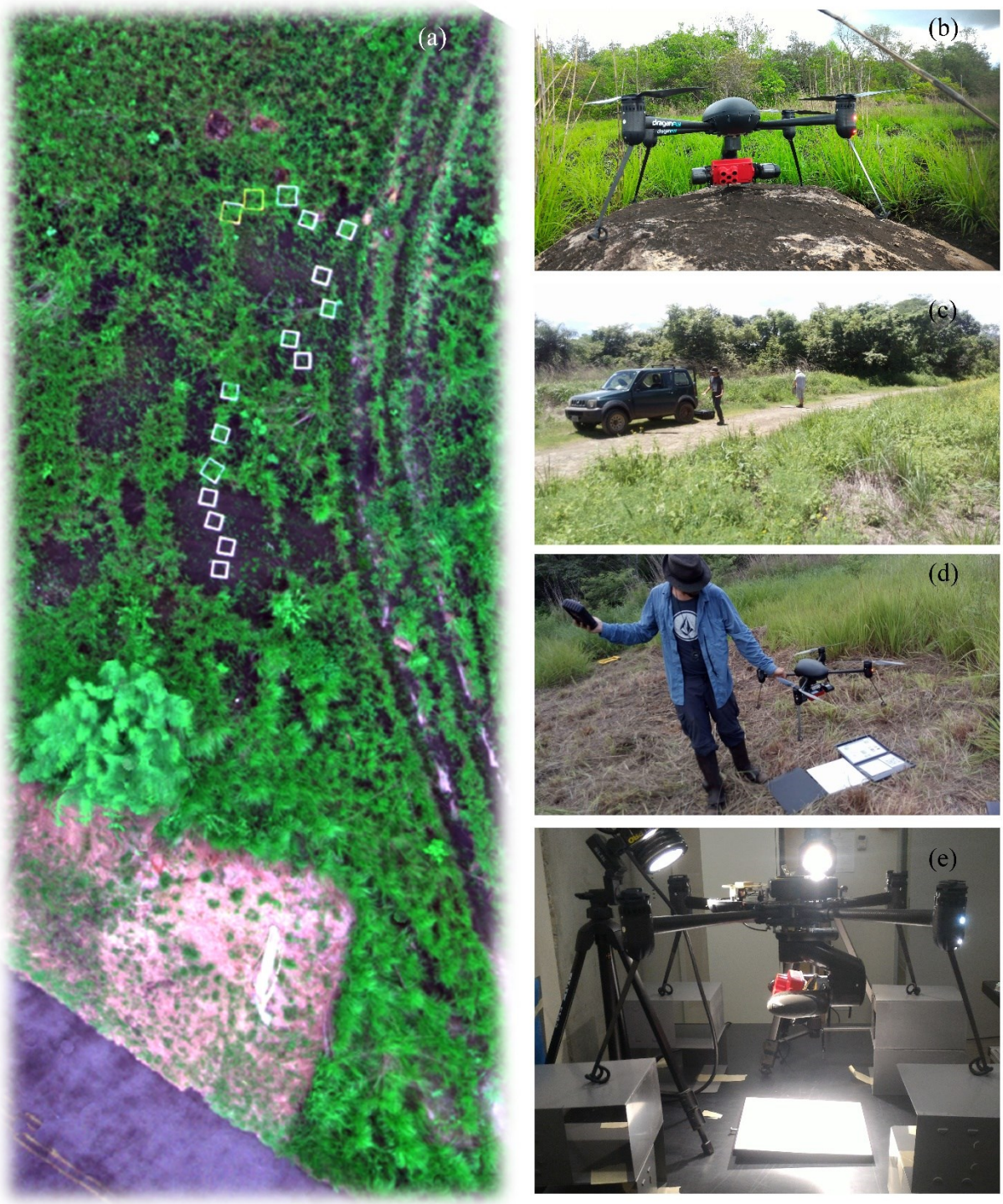

Figure 2.2.(a) Example of a multispectral image acquired at 25 m of altitude from the ground with an UAS. (b) *Draganfly X4ES* airframe at SR-EMSS. (c) Example of field acquisition conditions at SR-EMSS. (d). Example of panel calibration acquisition during the field campaign. (e) Example of data acquisition in laboratory conditions at the Centre for Earth Observations Sciences of the University of Alberta, Edmonton, Canada.

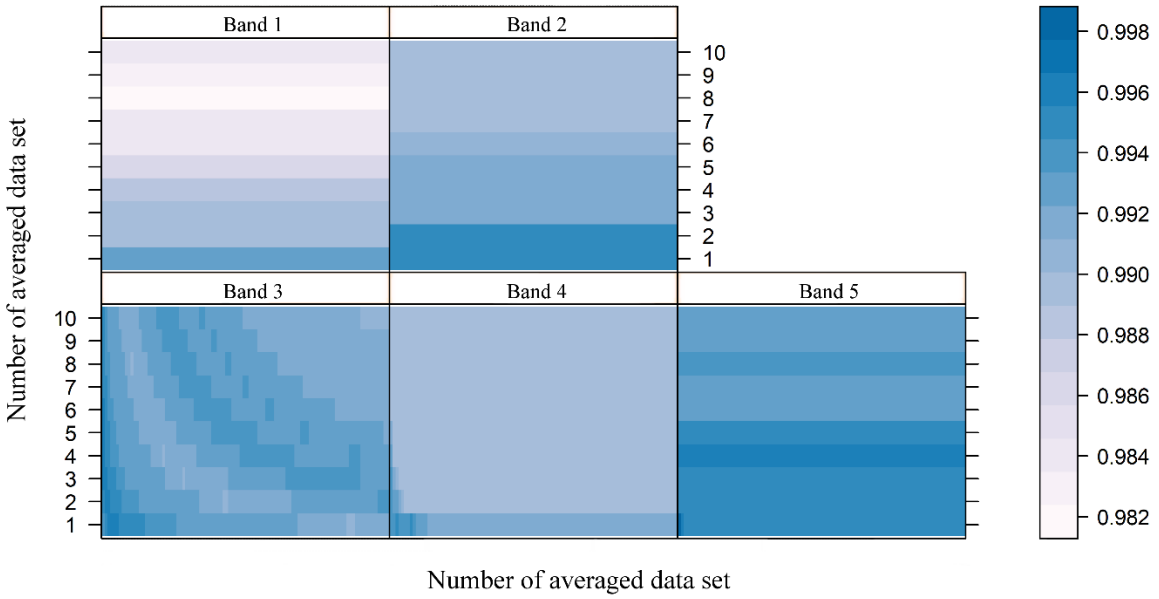

Figure 2.3. Correlation matrix between *UniSpec-DC* and *UniSpec-SC* spectroradiometers, using ten averaged data sets acquired at laboratory conditions in the Centre for Earth Observations Sciences of the University of Alberta, Edmonton, Canada.

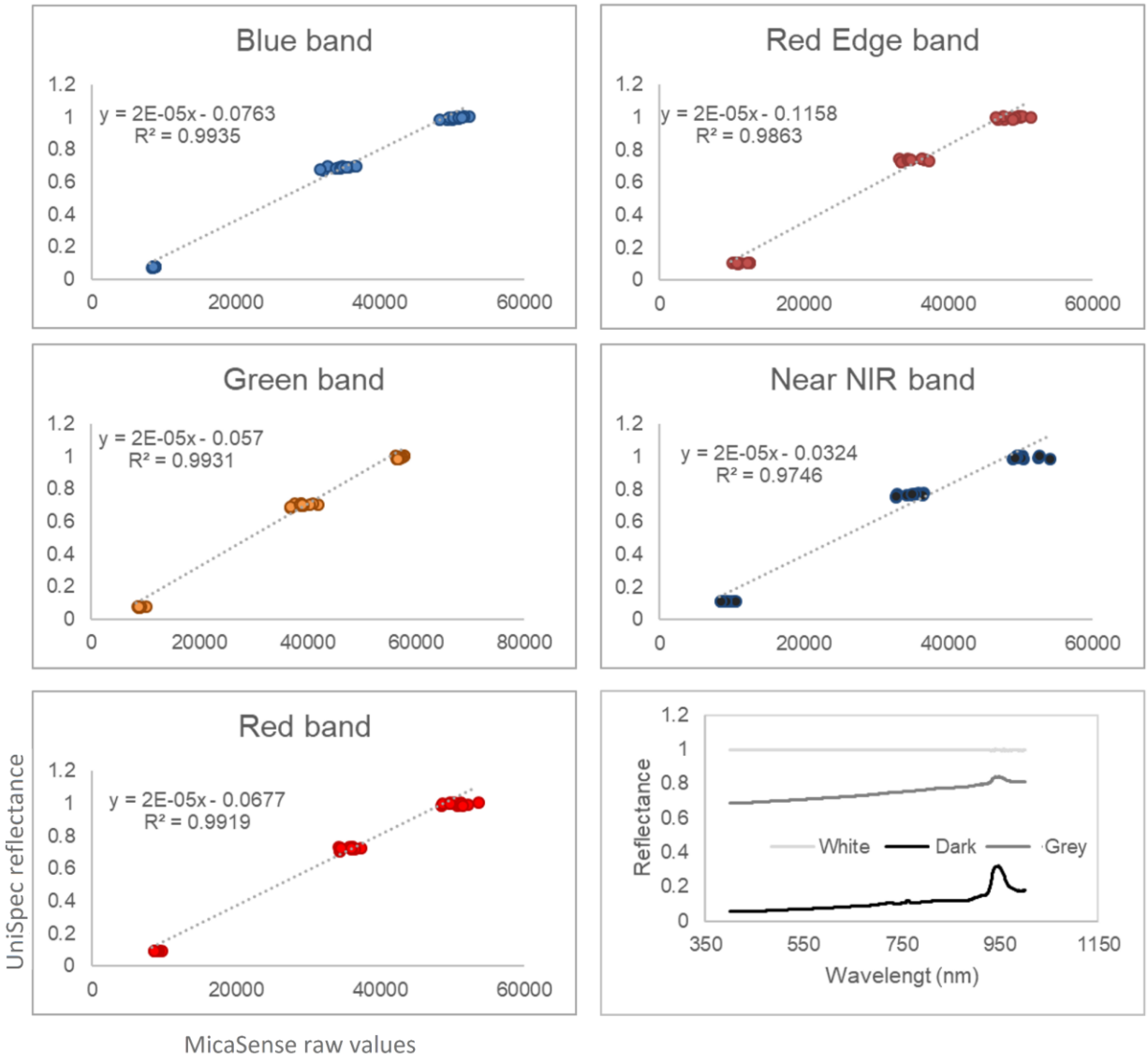

Figure 2.4. Linear relation between field spectrometer reflectance (y axis) and multispectral camera radiance (x axis) based on three reference panels acquired at laboratory conditions in the Centre for Earth Observations Sciences of the University of Alberta, Edmonton, Canada. Specifically, the axis *y* refers to measures from an *UniSpec-DC* spectrometer, and the axis *x* refers to measures from MicaSense *RedEdge* ™ 3.

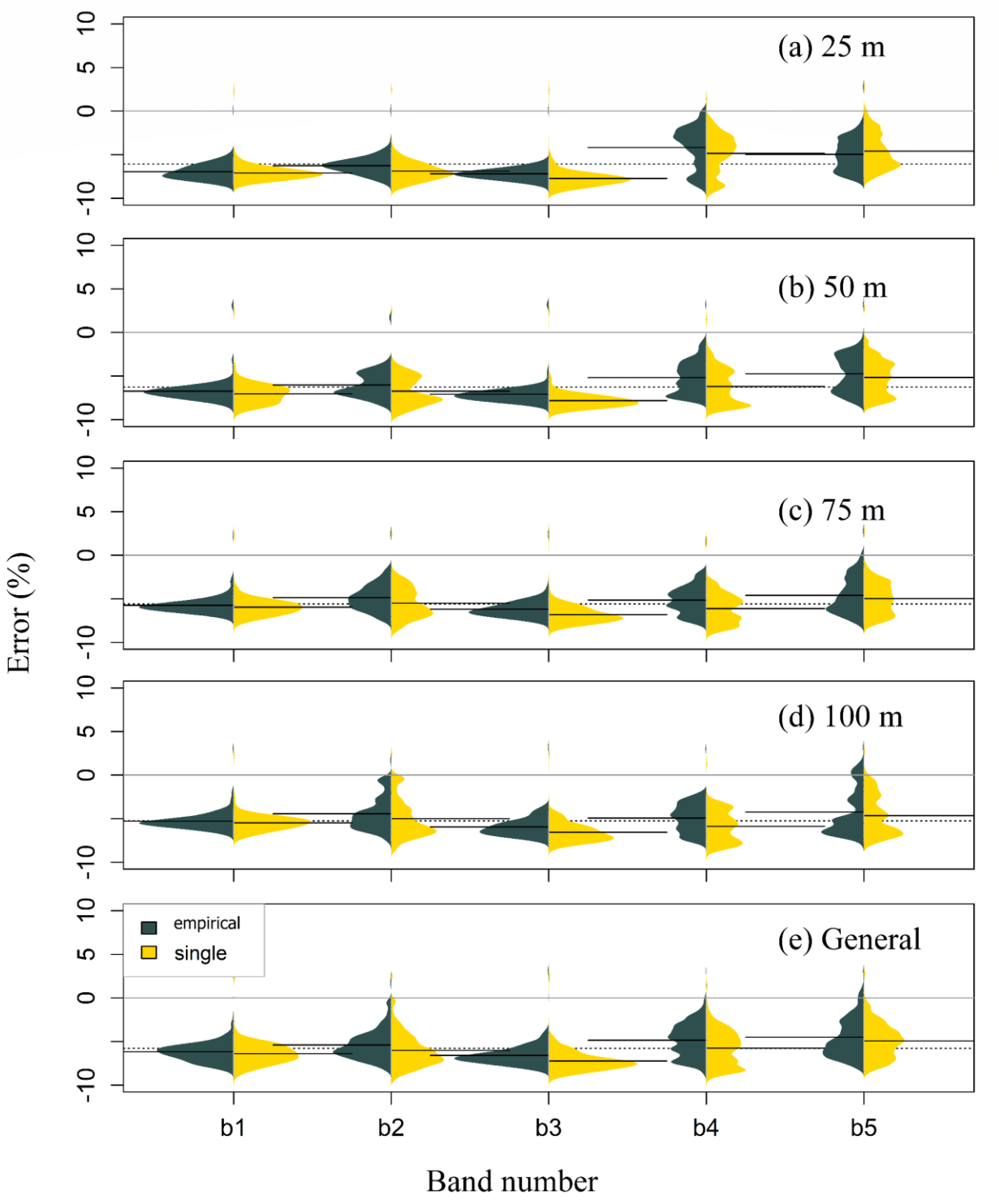

Figure 2.5. Error at band level for two radiometric transformations of MicaSense RedEdge bands across patches covered by *Jaragua* grass at SR-EMSS, Costa Rica. Obtained using a *MicaSense RedEdge* ™ 3 camera onboard a *Draganflyer X4-P at* (a) 25 m, (b) 50 m, (c) 75 m, and (d) 100 m from the ground level. Therefore, (e) represent the aggregated values from all bands disregarding the acquisition altitude.

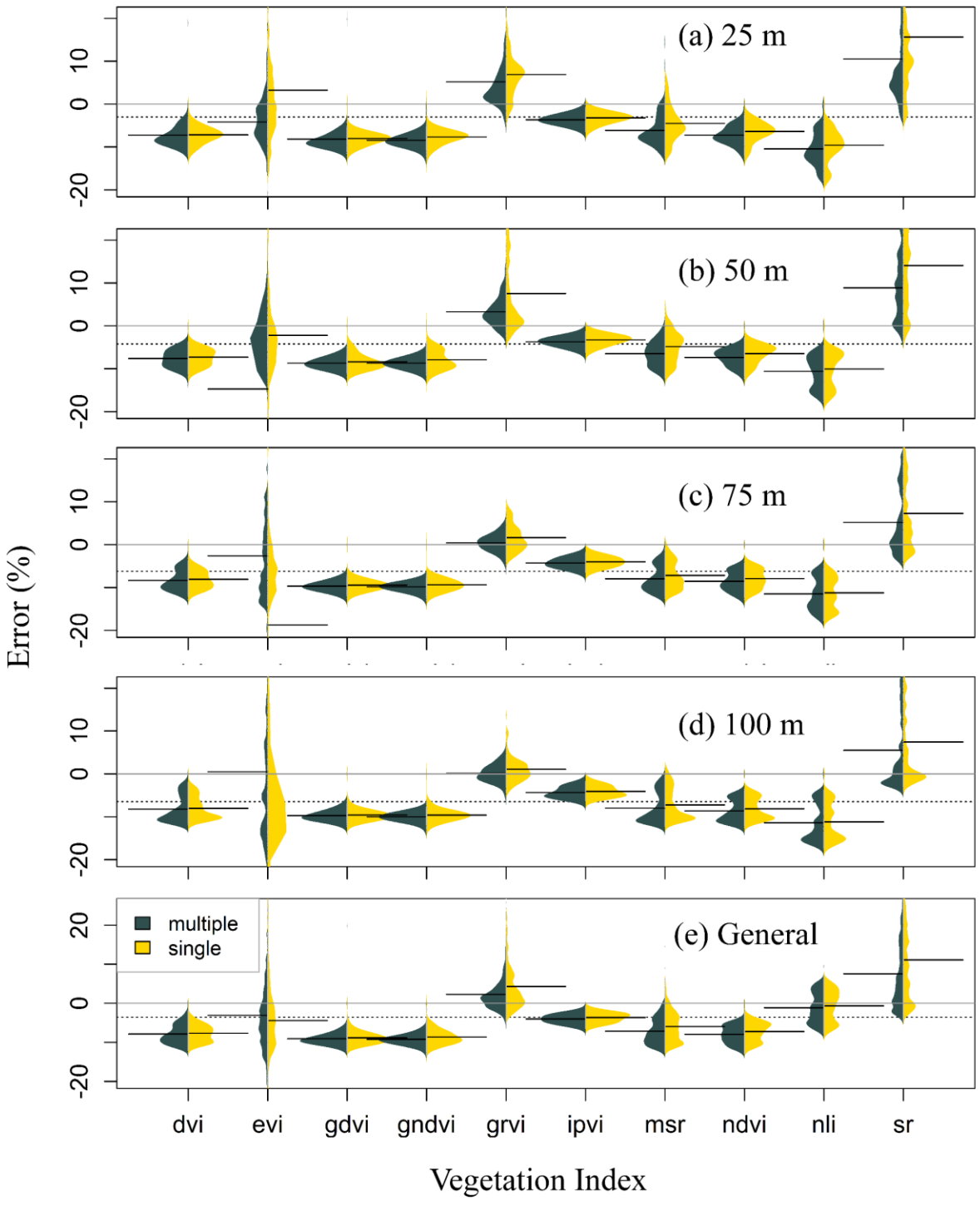

Figure 2.6. Error distribution of 10 vegetation indexes from two radiometric transformations of MicaSense RedEdge bands across firebreak patches covered by *Jaragua* grass at SR-EMSS, Costa Rica. Obtained using a *MicaSense RedEdge* ™ 3 camera onboard a *Draganflyer X4-P at* (a) 25 m, (b) 50 m, (c) 75 m, and (d) 100 m from the ground level. Therefore, (e) represent the aggregated values from all bands disregarding the acquisition altitude.

3. Chapter three – Detecting dead woody components using an Unmanned Aerial System and Machine Learning techniques at the tropical dry forest of Santa Rosa National Park, Costa Rica

3.1. Keywords

Costa Rica, forest mortality, machine learning, tropical dry forests, unmanned aerial systems.

3.2. Introduction

Increasing emissions of greenhouse gases are widely acknowledged by the scientific community as a significant cause of increases in the global mean temperature and changes in hydrological cycles. Even under conservative scenarios, future climate changes are likely to include further increases in mean temperature with significant drying in some regions (Seager et al. 2007); increases in frequency and severity of extreme droughts, and heat waves (Sterl et al. 2008). Field long-term studies have reported that in forests, mortality occurs in response to prolonged drought or after exposure to previous droughts that initiate a growth decline (Poorter et al. 2016; Breshears et al. 2009; McDowell et al. 2008; Clark 2004). Likewise, it has been observed that trees predisposed to dying have lower mean growth rates or greater growth sensitivity to climate in the years preceeding mortality (Williams et al. 2013).

Anomalously long or intense mortality events can have long-term impacts on a range of ecosystems and populations (Zeppel et al. 2013). Mortality can impact biodiversity, and ecosystem functions such as nutrient and carbon cycling, and biophysical and biogeochemical climate feedbacks. For instance, a mortality event can cause the increased growth of understory vegetation, thus possibly altering successional pathways with feedbacks to productivity and surface hydrology (McDowell et al. 2008). Therefore, tree death can both relieve competition and reduce facilitation in other plant communities, leading to counteracting forces on understory plants (McDowell et al. 2008). Mortality also reduces photosynthetic uptake, causing ecosystems to become a source of CO_2 for some time periods (Clark 2014).

Numerous hypotheses to explain mechanisms of survival and mortality have been generated via theoretical, and experimental analyses. For instance, the hydraulic-failure hypothesis forecasts that reduced soil water supply coupled with high evaporative demand causes xylem conduits to become air-filled, thus stopping the flow of water and desiccating plant tissues to a complete cellular death (McDowell et al. 2008; Rowland et al. 2015). On the other hand, the carbon-starvation hypothesis predicts that plants starve as a result of continued metabolic demand for carbohydrates and stomatal closure to prevent hydraulic failure (McDowell et al. 2008). This process may be exacerbated during drought by photo inhibition and increased respiratory demands associated with elevated temperatures (McDowell et al. 2018). Therefore, hydraulic failure occurs if drought is sufficiently intense that plants run out of water before they run out of carbon (Bretfeld, Ewers, and Hall 2018). It has been suggested that in tropical forests, mortality is most likely triggered by hydraulic processes, which lead to a hydraulic deterioration and rapid limitations in carbon uptake (Rowland et al. 2015).

Over the years machine learning (ML) has become a significant focus of remote sensing studies (Maxwell et al. 2018; Sanchez-Azofeifa et al. 2017a; Ghamisi et al. 2017; Plaza et al. 2009) showcasing computer algorithms than acquire knowledge from existing data, using inference strategies such as induction or deduction. A wide range of such studies has found that these methods tend to produce higher accuracies compared to traditional parametric classifiers (Maxwell et al. 2018, Li et al. 2018; Vargas-Sanabria and Campos-Vargas 2018; Li et al. 2017; Kuhn and Johnson 2013). ML algorithms can model complex classes, accept a variety of input predictor data and do not make assumptions about the data distribution (Maxwell et al. 2018). Furthermore, ML can process vast quantities of data from a variety of different sources. The state-of-the-art machine learning algorithms in remote sensing are divided into Artificial Neural Networks (ANN), Boosting Machines (BM), Decision Trees (DT), Deep Learning (DL), and Support Vector Machines (SVM).

The use of ANN for remote sensing data analysis has been motivated by the assumption that the human brain and artificial intelligence can associate elements in one set of data with elements in a second set. However, when ANN are applied to classification tasks, they only focus on the association of data from feature space to class space (Atkinson and Tatnall 1997). DL is similar to ANN however, DL is about deeper neural networks that provide a hierarchical representation

of the data by means of various convolutions, thus providing larger learning capabilities and higher precision (Kamilaris and Prenafeta-Boldú 2018). DL algorithms are one promising avenue of research into the automated analysis of complex data (Li et al. 2017) because DL develop a layered, hierarchical architecture of learning and representing data, where more abstract (higher-level) features are defined regarding less abstract (lower-level) features (Najafabadi et al. 2015).

DT are amongst the most intuitively simple classifiers thanks to their flexibility, intuitive simplicity, and computational efficiency (Ghamisi et al. 2017). The DT models create a recursive split of the input data into smaller subdivisions, based on a set of decision tests defined at each branch (or node) in the tree and their leaves (set of terminal nodes). Each node in a decision tree has only one parent node and two or more descendant nodes (Friedl and Brodley 1997). On the other hand, Random Forest (RF), a specific DT, is a classification model that produces multiple decision trees, using a randomly selected subset of training samples and variables. Specifically, it uses a set of classification and regression trees to make a prediction, where the trees are created by drawing a subset of training samples through replacement (Belgiu and Drăgu 2016). In other words, in RF the same sample can be selected several times, while others may not be selected at all. Likewise, BM models are created by generating an ensemble of weak (shallow) decision trees, where each successive tree is fitted with the remaining residuals from the previous combination of trees, a process known as 'boosting'(Maxwell et al. 2018). BM incorporate both bias and variance reduction, in an attempt to minimise the errors of the previous trees (Vaughn et al. 2018).

SVM has often been used in remote sensing because they make no assumptions on the underlying data distribution and their ability to handle high dimensional data with a limited number of training samples (Mountrakis, Im, and Ogole 2011). SVM proceed by defining an optimal separating hyperplane (the class boundary) within a multidimensional feature space that differentiates the training samples of two classes; where the best hyperplane is the one that leaves the maximum margin from both categories (Ghamisi et al. 2017).

Unmanned Aerial Systems (UAS, also known as drones) are well-suited tools for addressing current issues in remote sensing of tropical ecology and conservation (Sanchez-Azofeifa et al. 2017a). Particularly, small remote sensors onboard low flying unmanned aerial vehicles (UAV)

can collect a wide variety of plant canopy measurements, including broad and narrowband vegetation indices, chlorophyll fluorescence, and thermal stress, and enable the estimation of biomass, and assessment of carbon stock (Zarco-Tejada et al. 2014). Li et al. (2018) demonstrated that with a multispectral UAS and machine learning techniques can be quantified the relative coverage of dead trees, liana-infested, and non-liana-infested trees in a temporary plot at the SR-EMSS. However, that study was exploratory and was conducted only in a single plot with just two ML models. This paper wants to detect and quantify dead woody components such as stand and fallen death trees using a multispectral UAS and 10 machine learning models in five temporary plots that cover a gradient of secondary tropical dry forests at the SR-EMSS.

3.3. Materials and methods

3.3.1. Study site

The study area is located at the Santa Rosa National Park Environmental Monitoring Super Site (SR-EMSS), Guanacaste, Costa Rica (Figure. 3.1a). In this area, the mean temperature is 25 °C, and it receives an average annual rainfall of 1500 mm that ranges from 900 to 2600 mm. The dry season lasts for a minimum of 5–6 months, and it normally extends from approximately late December to mid-May (Sánchez-Azofeifa et al. 2017b). The landscape comprises a mosaic of forests in various stages of regeneration that once suffered from intense deforestation (Sánchez-Azofeifa et al. 2017b). The extent of the secondary tropical dry forests at SR-EMSS is not related to a deterministic forest regeneration process but rather, to a continuous stochastic process driven by wind and vertebrates combined by fire control efforts (Li et al. 2017).

In this study, a gradient of secondary tropical dry forest was sampled (Table 3.1) following the findings of Li et al. (2017). In general terms, the more early forests are composed of patches of woody vegetation, which include several species of shrubs, small trees, and young trees with a maximum height of approximately 6–8 m, that loose nearly all their leaves during the dry season (Sánchez-Azofeifa et al. 2017b; Kalacska et al. 2004). The early forests are dominated by species well adapted to open habitats like Silk cotton tree (*Cochlospermum vitifolium*), Madero negro (*Gliricidia sepium*) and Yayo (*Rehdera trinervis*), as well as also sun-loving species (heliophytes) that have anemochory and autochory dispersal syndromes (Hilje et al. 2015). The intermediate and more advanced stages show significant differences in structure and

composition. These differences are in general driven by species turn-over which in turn cause a very dynamic structure and forest species composition (Cao et al. 2015). These successional stages have two vegetation layers. The first layer encompasses fast-growing deciduous tree species that reach a maximum height of 10–15 m. The second layer is below the canopy and is composed of lianas (woody vines) along with adults of more shade-tolerant evergreen species and juveniles of many species (Hilje et al. 2015; Kalacska et al. 2004).

3.3.2. Field acquisition

From May to July 2017 five temporary plots at the SR-EMSS (Table 3.1) were surveyed by field geolocation and a UAS multispectral capture. (Figure 3.1a, Figure 3.2). Although this study focusses on the detection of dead woody components, in the field and in the data processing was also accounted for two complementary classes, understory and live-healthy components, in order to facilitate and complement our analysis. Specifically, the dead woody components included i) dead stand trees, ii) dead fallen trees, iii) non-photosynthetic woody components within the tree crown of live-not healthy trees, and iv) dead woody components from lianas (woody vines). The understory class included i) understory vegetation such as shrubs, small trees, and young trees located under the canopy, ii) canopy gaps with grass-like vegetation, wines, shrubs and, small trees, iii) exposed rocks and soils, and, iv) shadows. The live-healthy class included i) healthy canopy trees, and ii) healthy lianas within the tree crowns.

On each plot of 200m x 100m, geolocation of True Class Points (TCP) was performed for 50 dead woody components, 50 understory components, and 50 live-healthy components (Figure 3.1c, 3.1d). The geolocation was conducted using a field census across the five plots, and systematically surveying each plot with transects every 25m along the short side of the plot (Figure 3.1c, Figure 3.1d). A compass and a Trimble GeoXT6000 differential GPS with a Hurricane antenna (Figure 3.1b) with an average precision of 0.5 m horizontal and 0.54 m vertical were used. This practice is similar to that conducted in inventories in tropical forest management.

The UAS multispectral data were obtained using a MicaSense RedEdge ^{TM} 3 camera onboard a Draganfly XP-4, operated at 120 m height from the ground. The MicaSense RedEdge ^{TM} 3 camera had five lenses with a focal length of 5.5 mm, the lens field of view was 47.2°, and the

image encompassed 1280 x 960 pixels. Each lens provided a separate 16-bit GeoTIFF image, each centered on a specific wavelength: blue at 475 nm (with a Full Width at Half Maximum (FWHM) 20 nm), green at 560 nm (FWHM 20 nm), red at 668 nm (FWHM 10nm), red edge at 717nm (FWHM 10 nm), and near-infrared at 840 nm (FWHM 40 nm). The Draganfly XP-4 is a quadcopter with a three axes electronic gimbal. The airframe was equipped with three axes gyrostabilizer, magnetometer, and accelerometer.

Spectral signatures and multispectral images of three calibrated (at laboratory conditions) reference panels (a white Spectralon^{R} panel, a grey MicaSense-halon panel, and a flat black presentation cardboard) were collected prior to each flight and after each flight, to perform a calibration to at surface reflectance. Specifically, at each site, 20 MicaSense images (at 1.5m from the panel) and 20 spectral signatures (at 0.75m from the panel) of every reference materials were collected following the protocol of Kalacska et al. (2016). The spectral signatures were acquired with a UniSpec-SC spectrometer (PP Systems, Spectral range 310 – 1100nm; Raleigh resolution of < 10 nm, and a Bin size of 3.3 nm). The dark signal noise removal was performed by taking a dark scan for every ten sample measurements, while the instruments shutters were closed. The integration time was adjusted with the fibre-optic exposed to white reference panel every 10 samples. A white reference measurement was taken prior to each panel measurement. In all cases, reflectance spectra were obtained by determining the ratios of data acquired for a sample (an average of 10 scans) to data acquired for the white reflectance panel.

3.3.3. Data Preprocessing

An image preprocessing workflow was implemented in three steps: radiometric calibration, mosaicking, and data reduction and transformation.

3.3.3.1. Radiometric correction and mosaics generation

To radiometrically correct at surface reflectance the MicaSense imagery, the empirical line method suggested by Smith and Milton (1999) and Kalacska et al. (2016) was mplemented. Specifically, an equation for each MicaSense band (TIFF 16 bits) was generated, based on the comparison of values from three reference panels acquired with a MicaSense RedEdge ^{TM} 3 and a UniSpec-SC spectrometer. The extraction of the values from the MicaSense imagery was made

using the tool Extract from Raster of ArcGIS (ArcGIS Desktop, Redlands, CA: Environmental Systems Research Institute, v10.3). An average of all pixels in the panel, with the exception of the pixels in the borders of the panel, was estimated. For the *UniSpec* reflectance spectrum of each panel, the spectrum was resampled to the MicaSense bandpasses using ENVI (Exelis Visual Information Solutions, Boulder, Colorado, v5.3).

The generation of ortho-mosaics was performed in Pix4Dmapper (Pix4D Pro, Lausanne, Switzerland, v3.3.29). However, in this program, the radiometric correction step was skipped, because it was previously performed with the empirical line method. Five single band mosaics were obtained, one mosaic per MicaSense band. To orthorectify the mosaics 7-10 ground control points (GCP) distributed across each plot were used (Figure. 3.1c). Each GCP was geolocated using the Trimble GPS described in the TCP collection (Figure 3.1b).

3.3.3.2. Data transformation

Though multispectral sensors present advantages in comparison with RGB technology, their use means a substantial increase in data volume and data manipulation. Numerous methods have been developed to improve the separability between classes by highlighting useful information and removing data redundancy. In this study, three transformation methods were applied to the multispectral mosaics (Figure 3.2): Principal Components Analysis (PCA), Tasseled Cap (TC), and Texture Analysis (TA). A PCA was performed using all five multispectral band mosaics, retaining the first three PC from all 5 band mosaics. Likewise, a TC transformation was performed using the five multispectral bands to highlight the vegetation classes. However, the only component retained from the TC was the third TC component (known as the Yellow Stuff structure) because the first two TC define a plane very similar to the first two PCA, providing features essentially equivalent (Crist and Kauth 1986).

The texture components of high-resolution remote sensing data have been proven to be useful for the quantification of forest structure and biomass (Bastin et al. 2014), and in the estimation of the extension and succession of tropical dry forests (Li et al. 2017). In this study a linear filter named "Gabor filter" was used to derive texture features from the multispectral mosaics, using as input the five bands calibrated at surface reflectance. The Gabor filter searches for elements in a

localised region of an image with specific frequency content in particular directions (Bovik et al, 1990). The Gabor filter used was restricted to a maximum of five scales and ten directions.

3.3.4. Classiffication Models

The "No Free Lunch" theorem of computing sciences states that, without having substantive information about the modelling problem, there is no single model that is better than other models (Wolpert 1992). Wolpert (1996) specified that, for any two algorithms 'A' and 'B', there are "as many" targets for which algorithm 'A' has lower expected errors than algorithm 'B' and vice versa. In other words, there are "as many" targets for which any learning algorithm can get confused by the data, and performs worse than random guessing. In this context, Kuhn and Johnson (2013) suggested to try a wide variety of classification models, to determine which model performs better. Consequently, this study used 10 ML classification algorithms in remote sensing: Averaged Neural Network (ANN), Conditional Inference Tree (CIT), C4.5-like Trees (C45), Deep Neural Network (DNET), Gradient Boosting Machines (GBM), Random Forest (RF), Neural Network (NNT), Support Vector Machines with Linear Kernel (SVML), Support Vector Machines with Polynomial Kernel (SVMP), and Support Vector Machines with Radial Kernel (SVMR). This approach covers most of the available classification models of Support Vector Machines, Decision Trees, Boosting Machines, and Artificial Neural Networks (Table 3.2).

3.3.4.1. Creation of training and validation datasets

The implementation of the 10 ML models was performed using 450 pixel-samples per mosaic (scene), representing a total of 2250 samples acquired from the MicaSense camera and validated in the field. This data set was divided in two datasets, training and validation. The training dataset was used in the model implementation, while the validation dataset was used to estimate the performance of the trained models.

To obtain those data sets the following steps were followed: i) created a geospatial dataset from the TCP collected in the field, ii) extracted the values from the MicaSense mosaics using as reference the TCP acquired in the field, iii) divided the geospatial dataset in to training and validation sets. Specifically, the pixel-samples were created in *QGIS* using the geolocated TCP

collected in the field with the *Trimble* GPS. On each of these points, a sampling window of 3 x 3 pixels was created on *QGIS*, extracting the values from the transformed MicaSense mosaics (Figure 3.2.b). Thus, providing a data set with three classes: Dead woody components (Fallen and stand dead trees), healthy-live vegetation and gaps and understory vegetation. In the case of leafless crowns, care was taken to select pixels from central regions of crowns, and that the tree branching was dense enough to ensure that the class of interest would dominate the collected spectra. Because the signal from understory vegetation can have a significant impact on observed spectra. Therefore, this dataset was exported to *R program*, on which it was randomly divided onto a training dataset (70%) and a validation dataset (30%), using the function 'createDataPartition' of the package "raster" in R program.

3.3.5. Classification Models implementation

The best number of training samples to avoid overfitting in the classification models was estimated using the resampling technique bootstrap "632 method" contained in the "Caret" package. The "632 method" creates a performance estimate that is a combination of the simple bootstrap estimate and the estimate from re-predicting the training set (Efron and Tibshirani 1983). Bootstrap error rates tend to have less uncertainty than other methods such as k-fold cross-validation, especially, if the training set size is small (Kuhn and Johnson 2013). Likewise, the estimation of the optimal tune-up parameters for all models was performed with the functions 'expand.grid:caret' and 'tuneGrid:caret' using several combinations of values and parameters (Table 3.3).

Two kind of classification models were generated to quantify the extent of mortality across the five temporary plots, due to the complexity of scenes: 5 plot-specific models and a general model. Following the findings of Miltiadou et al. (2018), that found that the generation of a model with all possible training samples and possible patterns from all sampled plots can provide better results than a model generated from a single sampled-plot with less number of samples. The specific models refer to five models that were trained only with the data from one particular temporary plot. For example, the specific model one, only used data (trainig and valition) from samples collected in the plot one, the specific model two used only data from the temporary plot two, etc. On the other hand, the general model refers to a model that was trained and validated with the data from all five temporary plots.

3.3.6. Model validation and selection

The model validation and selection were assessed by considering the values of accuracy, kappa, and the time required to run each clasiffication model. The accuracy and kappa values were estimated on a per-pixel basis, rather than per crown or trunk basis because the classification was performed by pixels rather than by objects. Specifically, those metrics were estimated with the function 'confusionMatrix:caret', using the validation dataset, which corresponds to the remaining 30% of the values, which were previously separated. However, to compare the classification models was accounted for the accuracy, kappa and time values of only the best candidate models from each model type (Table 3.3) because on each model was tested several tune-up parameters. Consequently, the same model can provide different accuracy values even with the same training data, because of changes in the tune-up parameters. (Figure. 3.3, Figure. 3.4, Figure. 3.5, Figure. 3.6). For instance, Table 3.4 shows the highest accuracy values for every classification model used in Table 3.2. Three indicators were considered to select the best classification model accuracy, kappa and time because all classification models provided similar accuracy values. In consequence, to corroborate if there was any statistical difference in the model performance, an ANOVA was performed (Table 3.5).

3.3.7. Differences in the extension of dead woody components between plots

The coverage of the dead woody area and other complementary classes (m^2) were estimated by extracting the values from the five classified mosaics, using the results from the five specific models and the General model. Specifically, on QGIS all classified mosaics were cropped to a window frame of precisely 200 m x 100 m, in order to promote fair comparisons between plots. Then, all cropped mosaics were transformed from raster to vector using QGIS, on which was estimated the class area (m^2) of all classes from all classified mosaics. The differences in the coverage of dead wood components between plots were analized with an ANOVA and a Tukey test. The ANOVA and Tukey test were performed on *R program*, comparing the extension of dead wood components between plots.

3.4. Results

3.4.1. Effect of tuning parameters on the accuracy values

Our data showed that neither of the algorithms and set of parameters overun the others in all the situations, especially, in the quantification of dead woody components across the different successional stages of TDF forest at SR-EMSS (Figure. 3.3, Figure. 3.4, Figure. 3.5, Figure. 3.6). However, the wide range of available parameters and models used helped to choose the ideal set of models and parameters to classify dead woody components and others complementary classes such as live vegetation and understory.

The effects of the tuning parameters in all candidate models tested suggest that some of the classification models used were more sensitive to the tuning parameters than others. In general terms models such as RF (Figure. 3.3a), CIT (Figure 3.3b), SVML (Figure 3.3d), NNET (Figure 3.3f), ANNET (Figure 3.4a), SVMP (Figure 3.4b), GMD (Figure 3.5), and DNET (Figure 3.6) reached their maximum accuracy values at some point and then remain stable as the values of the driver parameters increased. Contrary to models such as SVMR (Figure 3.3c) and C45T (Figure 3.3e) reached their maximum accuracy values at some point and then their accuracy decreased as the values of the driver parameters increased (Figure 3.3e).

In regards the used tuning parameters values, it was observed that the models displayed a heterogenous selection of available parameters. For instance, models such as CIT, C45T, RF, SVML, and SVMR required a maximum of two tuning parameters while models such as SVMP, GBM, ANNT, and DNET required three or more tuning parameters, and even more complex settings like learning rates for GBM and DNET. Although models such as ANNET (Figure 3.4a) and GBM (Figure 3.5) required a more complex implementation than the others models (Table 3.3), they did not beat the other models in all temporary plots

DNET reported the lowest accuracy values in comparison with the others nine models (Table 3.4). It provided accuracy values lower than 95% in all models including the plot specific and the general models (Figure 3.6) likely as a consequence of the low number of hidden unit in the three layers and the relatively low number of training samples. In the case of plot Two (Figure 3.6b), plot Four (Figure 3.6b), and the General model (Figure 3.6f) the accuracy values were even lower, with considerable differences within models. The number of hidden units in Layer 1

and Layer 3 had no effect on the accuracy values (Figure 3.6). However, in plot Two, a small change in the patterns of the Layer 1 with ten hidden units in the Layer 2 was noticed.

3.4.2. Model selection

GBM, RF and SVMR reported the highest accuracy values in the classification of dead woody components across the five temporary plots while the lowest accuracy values were reported by CIT, DNET, and SVML (Table 3.4). The SVMR had the highest accuracy value with 0.982, followed by RF with 0.980 and GBM with 0.977. On the other hand, the processing times showed significant differences betwwen models and plots. SVMR reported the highest time (4689.9 min), followed by GBM, (2839.3 min) and RF (1523.2 min). SVMR showed higher accuracy values than RF; however, it also showed that it was very time consuming and its processing times can drastically vary across implementations (Standard deviation of 8735.6 min). The Neural Networks (ANNET, NNET and, DNET) were the most time-consuming models (Table 3.4 and Figure 3.7). The ANNT was the most time-consuming model, followed by NNET and SVMP. The most efficient models in term time were CIT, C45T and SVML, respectively. Consequently, the model RF was chosen to run the final classification because it had the highest accuracy and the lowest processing time (Table 3.4 and Figure 3.7).

The Repeated measures ANOVA showed that the averages of the processing times were significantly different among them with a confidence of 95% (Table 3.5). However, the same test also indicated that the differences in the averages of accuracy and kappa values, and in the interaction of the variables were not statistically different.

3.4.3. Mortality extension

The coverage of dead woody components in the five-temporary plot at SR-EMSS was estimated to range from 4.8% to 16.1% dependent on the site (Figure 3.8). The General model displayed higher areas covered by dead woody components in comparison with those estimated by each specific model (Figure 3.8 and Figure 3.10).

The lowest coverage of dead woody components was reported for plot Two, a secondary early-intermediate forest patch, followed by plot Three a secondary intermediate-intermediate forest patch with a high liana infestation. In those plots, the values from the General and specific

models (Figure 3.8) coincided, contrary to plot One, a secondary intermediate-late forest patch, and Five, a secondary intermediate-intermediate forest patch that showed differences in the results from the general and specific models. Moreover, plots One and Five inversely mirror each other in terms of coverage of dead woody components (Figure 3.8).

The highest coverage of dead woody components was reported for plot Four, a secondary early-early forest patch (Figure 3.8 and Figure 3.10). However, this plot showed the lowest accuracy values for both the General and specific models. Because this plot is in a very early successional stage the canopy cover is rare, the gaps are large, and grass such as Jaragua grass is present which could mimics the response of dead vegetation.

The repeated measures ANOVA showed, with confidentiality of 95%, that the averages of the processing times values were significantly different among models (Table 3.5). Likewise, the same test also indicated that the differences in the averages of accuracy and kappa values, and in the interaction of the variables were not statistically different. On the other hand, a Tukey test showed that the plots were clustered into three groups based on the mortality coverage. The first group, composed of plots Four, One and Five has the highest mortality coverage. A second group was composed of plot Three, and a third group by plot Two (Figure 3.9).

3.5. Discussion

3.5.1. Effect of tuning parameters on the accuracy values and Performance of selected models

This paper examined the effect of tuning parameters on the accuracy values of the classification of dead woody components. Though the best three classification models reported accuracy values higher than 0.97, these models with the worst set up parameters showed accuracy values close to 0.8. Thus, suggesting that ML should not be used as a black-box that provide an omnipotent straightforward answer to everything, because a reductionist and synthetic answer might not even exist (Castelvecchi 2016).

All ML models provided very high classification accuracy values for detecting dead woody components, understory and live-healthy vegetation thanks to the three classes were highly distinguishable between them. However, the results provided by RF, SVMP, and GBM highlighted because these three models provided higher accuracy and kappa values, and relatively shorter processing times than the other models tested.

Our results concur with other similar studies, such as Li et al. (2018) who discriminated between liana infested trees, non-liana infested trees, and dead trees using Deep Learning and SVM algorithms in a single plot at the same study site. Vaughn et al. (2018) who ensembled SVM and GBM to map individual dead trees in a Hawaiian island using high-resolution digital imagery. Meddens, Hicke, and Vierling (2011) that evaluated the potential of high-resolution multispectral imagery to map tree mortality in Colorado, EEUU; and Garrity et al. (2013) who quantified tree mortality in an EEUU southwestern woodland affected by drought, bark beetle outbreak, fire, and ecological restoration treatments.

Similar than Miltiadou et al. (2018) who demonstrated that increasing the number of training samples increased the accuracy of the detection of dead standing *Eucalyptus camaldulensis* in a native Australian forest. It was found that the increase in the number of samples and possible training patterns with the generation of a general model generally increased the accuracy values. However, in one of the plots (Plot Four) even with an increase in samples, the accuracy values remained lower than the others four plots, suggesting the necessity to include in the early successional forest stages, an extra class that accounts for bare soils and no woody dead materials such dry *Jaragua* grass.

3.5.2. Dead woody components and its ecological implications

This study demonstrated that it is possible to detect and quantify dead woody components in a gradient of the secondary tropical dry forest at SR-EMSS, Costa Rica. The coverage of dead woody components in the five temporary forest plots at SR-EMSS range from of 4.8% to 16.1%, with an overall accuracy of 98%, and a kappa value of 0.958.

Even though the coverages of the dead woody components are lower than 16.1%, this percentage could be relevant because according to Greenwood et al. (2017) about 70% of tree species could be operating in narrow hydraulic safety margins and are at high risk of embolism and related mortality if drought severity increases. Likewise, Poorter et al. (2016) found that in deciduous and arid habitats the recovery and loss of biomass were driven by water availability and stand age.

The impact of drought on forest functions and structure depends on which trees are most adversely affected. Worldwide, drought has consistently shown more detrimental impacts on

larger trees, causing significant decreases in woody growth and associated carbon sequestration in forests (Bennett et al. 2015). In forests, large trees play keystone ecological roles, by creating unique microenvironments which many plants and animals depend on for nesting cavities and substrate for epiphytes (Hilje et al. 2015). Furthermore, large canopy trees account for a more significant proportion of ecosystem-level transpiration than smaller trees, and their drought-related decline could create detrimental canopy transpiration contributions to cloud formation (Wullschleger, Hanson, and Todd 2001).

In TDF, other growth forms such as lianas (woody vines) can be abundant and play an important role in forest dynamics and mortality. In temperate and tropical forests Lai et al. (2017) found that lianas reduce growth and survival of host trees. Likewise, Tobin et al. (2012) pointed out that lianas have a greater competitive effect on canopy trees during the dry season than do trees of similar biomass because of the unique morphology of lianas. This is because lianas reach the canopy and deploy a crown with less investment in support tissues than trees leading to a more significant competitive impact on canopy trees than competing trees with similar biomass (Tobin et al. 2012). It has been suggested that in neotropical forests, liana coverage is increasing as a result of higher CO_2 concentration, increased disturbance and decreased precipitation (Kalacska, Bohlman, et al. 2007; Phillips et al. 2002; Schnitzer 2005; Wright et al. 2004).

3.5.3. Uncertainties and Sources of error

In an image of a tropical forest, there is a high complexity of shapes, textures, illumination conditions that increase the potential occurrence of false detections. Consequently, to reduce false-positives in the classification of this type of images, all potential error sources should be considered. Vaughn et al. (2018) noticed that as viewing angle and solar angles approach nadir, green undergrowth beneath a thin, leafless crown had a more dominant effect on reflectance, leading to a decreased detection of targets. This assumption contradicts the findings of Meddens et al. (2011) who argued that vegetation self-shadowing, standing position, and tree crown orientation might play different and critical roles in relatively high and medium resolution remote sensing. However, at a very high spatial resolution, as provided by an UAS, this might not be the case due to the increased probability to sense pixels corresponding to illuminated and shadowed parts of tree crowns (Meddens et al. 2011).

3.6. Conclusions

This study demonstrated that it is feasible to detect and quantify dead woody components such as dead stand and fallen trees at SR-EMSS using a multispectral UAS and ML techniques. The UAS allowed access to the canopy forest at such high resolution that dead woody components within a tree crown could be detected. The coverage of dead woody components in the five temporary forest plots at SR-EMSS range from of 4.8% to 16.1%, with an overall accuracy of 98%, and a kappa value of 0.958.

Even though the best candidate model of the ten classification models tested provided similar accuracy values. The effects of the tuning parameters in the candidate models tested suggest that some of the classification models used were more sensitive to the tuning parameters than others. Likewise, it was found that the tested models displayed a heterogeneous selection of available parameters. Consequently, a wide range of available parameters should be tested in the classification models used to obtain the best classification results possible. The generation of a general model increased the accuracy values at the plot level, thanks to the increase of the number of samples and possible training patterns; however, it can not be argued that that model provided better results than the plot specific model.

3.7. References

Arroyo-Mora, Pablo, G Arturo Sánchez-Azofeifa, Margaret E R Kalacska, Benoit Rivard, Julio C Calvo-Alvarado, Daniel H Janzen. 2005. "Secondary Forest Detection in a Neotropical Dry Forest Landscape Using Landsat 7 ETM + and IKONOS Imagery Published by: Association for Tropical Biology and Conservation." *Biotropica* 37 (4): 497–507. https://doi.org/10.1111/j. 1744-7429.2005.00068.x.

Atkinson, P. M., and A. R. L. Tatnall. 1997. "Introduction Neural Networks in Remote Sensing." *International Journal of Remote Sensing* 18 (4): 699–709. https://doi.org/10.1080/014311697218700.

Bastin, Jean François, Nicolas Barbier, Pierre Couteron, Benoît Adams, Aurélie Shapiro, Jan Bogaert, and Charles De Cannière. 2014. "Aboveground Biomass Mapping of African Forest Mosaics Using Canopy Texture Analysis: Toward a Regional Approach." *Ecological Applications* 24 (8): 1984–2001. https://doi.org/10.1890/13-1574.1.

Belgiu, Mariana, and Lucian Drăgu. 2016. "Random Forest in Remote Sensing: A Review of Applications and Future Directions." *ISPRS Journal of Photogrammetry and Remote Sensing* 114: 24–31. https://doi.org/10.1016/j.isprsjprs.2016.01.011.

Bennett, Amy C., Nathan G. Mcdowell, Craig D. Allen, and Kristina J. Anderson-Teixeira. 2015. "Larger Trees Suffer Most during Drought in Forests Worldwide." *Nature Plants* 1 (September). Nature Publishing Group: 1–5. https://doi.org/10.1038/nplants.2015.139.

Bovik, Alan Conrad, Marianna Clark, and Wilson S. Geisler. 1990. "Multichannel Texture Analysis Using Localized Spatial Filters." *IEEE Transactions on Pattern Analysis and Machine Intelligence* 12 (1): 55–73. https://doi.org/10.1109/34.41384.

Breiman, Leo, Adele Cutler, Andy Liaw, and Mathew Wiener. 2018. "Breiman and Cutler's Random Forests for Classification and Regression." CRAN R Core Team. R: A Language and Environment for Statistical Computing. *R Foundation for Statistical Computing*, Vienna, Austria. CRAN. https://doi.org/10.1023/A.

Bretfeld, Mario, Brent E. Ewers, and Jefferson S. Hall. 2018. "Plant Water Use Responses along Secondary Forest Succession during the 2015-2016 El Niño Drought in Panama." *New Phytologist* 2. https://doi.org/10.1111/nph.15071.

Clark, Deborah A. 2014. "Are Tropical Forests an Important Carbon Sink?" *Ecological Society of America* 12 (1): 3–7. https://doi.org/10.1890/1051-0761(2002)012[0003:ATFAIC]2.0.CO;2.

Crist, E. P., and R. J. Kauth. 1986. "The Tasseled Cap De-Mystified." *Photogrammetric Engineering & Remote Sensing* 52 (1): 81–86.

Crist, E P, and R C Cicone. 1984. "Application of the Tasseled Cap Concept to Simulated Thematic Mapper Data." *Photogrammetric Engineering Remote Sensing* 50 (3): 343–52.

Crist, Eric P., and Richard C. Cicone. 1984. "A Physically-Based Transformation of Thematic Mapper Data—The TM Tasseled Cap." *IEEE Transactions on Geoscience and Remote Sensing* GE-22 (3): 256–63. https://doi.org/10.1109/TGRS.1984.350619.

Efron, B, and R Tibshirani. 1983. “Estimating the Error Rate of a Prediction Rule.” *Journal of the American Statistical Association* 78 (382): 316–31. https://doi.org/10.1080/01621459.1983.10477973.

Friedl, Mark a. M.A., and Carla E. C.E. Brodley. 1997. “Decision Tree Classification of Land Cover from Remotely Sensed Data.” *Remote Sensing of Environment* 61 (3): 399–409. https://doi.org/10.1016/S0034-4257(97)00049-7.

Garrity, Steven R., Craig D. Allen, Steven P. Brumby, Chandana Gangodagamage, Nate G. McDowell, and D. Michael Cai. 2013. “Quantifying Tree Mortality in a Mixed-Species Woodland Using Multitemporal High Spatial Resolution Satellite Imagery.” *Remote Sensing of Environment* 129. Elsevier Inc.: 54–65. https://doi.org/10.1016/j.rse.2012.10.029.

Ghamisi, Pedram, Javier Plaza, Yushi Chen, Jun Li, and Antonio J. Plaza. 2017. “Advanced Spectral Classifiers for Hyperspectral Images: A Review.” *IEEE Geoscience and Remote Sensing Magazine* 5 (1): 8–32. https://doi.org/10.1109/MGRS.2016.2616418.

Greenwood, Sarah, Paloma Ruiz-Benito, Jordi Martínez-Vilalta, Francisco Lloret, Thomas Kitzberger, Craig D. Allen, Rod Fensham, et al. 2017. “Tree Mortality across Biomes Is Promoted by Drought Intensity, Lower Wood Density and Higher Specific Leaf Area.” *Ecology Letters* 20 (4): 539–53. https://doi.org/10.1111/ele.12748.

Hilje B, Calvo-Alvarado J, Jiménez-Rodríguez C, Sánchez-Azofeifa A. 2015. Tree Species Composition, Breeding Systems, and Pollination and Dispersal Syndromes in Three Forest Successional Stages in a Tropical Dry Forest in Mesoamerica. *Tropical Conservation Sciences*; 8(1):76-94. https://doi:10.1177/194008291500800109

Hornik, Kurt, Christian Buchta, Torsten Hothorn, Alexandros Karatzoglou, David Mayer, and Achim Zeileis. 2018. “Package ‘ RWeka ’.” CRAN R Core Team. R: A Language and Environment for Statistical Computing. R Foundation for Statistical Computing, Vienna, Austria. CRAN R Core Team. R: A language and environment for statistical computing. *R Foundation for Statistical Computing,* Vienna, Austria. https://cran.r-project.org/web/packages/RWeka/index.html.

Hothorn, Torsten, Kurt Hornik, Carolin Strobl, and Achim Zeileis. 2017. “A Laboratory for Recursive Partitioning.” CRAN R Core Team. R: A Language and Environment for Statistical Computing. R Foundation for Statistical Computing, Vienna, Austria language and Environment for Statistical Computing. *R Foundation for Statistical Computing*, Vienna, Austria. https://doi.org/10.1198/106186006X133933>.

Kalacska, M., G. A. Sanchez-Azofeifa, J. C. Calvo-Alvarado, M. Quesada, B. Rivard, and D. H. Janzen. 2004. “Species Composition, Similarity and Diversity in Three Successional Stages of a Seasonally Dry Tropical Forest.” *Forest Ecology and Management* 200 (1–3): 227–47. https://doi.org/10.1016/j.foreco.2004.07.001.

Kalacska, Margaret, J. Pablo Arroyo-Mora, Raymond Soffer, and George Leblanc. 2016. “Quality Control Assessment of the Mission Airborne Carbon 13 (MAC-13)

Hyperspectral Imagery from Costa Rica." *Canadian Journal of Remote Sensing* 42 (2): 85–105. https://doi.org/10.1080/07038992.2016.1160771.

Karatzoglou, Alexandros, Alex Smola, and Kurt Hornik. 2016. "Kernel-Based Machine Learning Lab." CRAN R Core Team. R: A Language and Environment for Statistical Computing. *R Foundation for Statistical Computing*, Vienna, Austria. CRAN. https://cran.r-project.org/web/packages/kernlab.

Kuhn, Max, and Kjell Johnson. 2013. Applied Predictive Modeling. *Applied Predictive Modeling*. https://doi.org/10.1007/978-1-4614-6849-3.

Kuhn, Max, Steve Weston, Chris Keefer, Allan Engelhardt, Tony Cooper, Zachary Mayer, Brenton Kenkel, et al. 2018. "Classification and Regression Training." Classification and Regression Training. CRAN R Core Team. R: A language and environment for statistical computing. *R Foundation for Statistical Computing*, Vienna, Austria. http://topepo.github.io/caret/index.html.

Lai, Hao Ran, Jefferson S. Hall, Benjamin L. Turner, and Michiel van Breugel. 2017. "Liana Effects on Biomass Dynamics Strengthen during Secondary Forest Succession." *Ecology* 98 (4): 1062–70. https://doi.org/10.1002/ecy.1734.

Li, Wei, Carlos Campos-Vargas, Philip Marzhahn, and Arturo Sanchez-Azofeifa. 2018. "Relative Coverage of Dead Trees, Liana-Infested and Non-Liana-Infested Trees Mapped in Tropical Dry Forest with UAs-Based Deep-Learning Framework." *International Journal of Applied Earth Observation and Geoinformation* 1 (2): 5.

Li Wei, Campos-Vargas Carlos, Marzahn Phillip, Sanchez-Azofeifa Arturo 2018. On the estimation of tree mortality and liana infestation using a deep self- encoding network. *International Journal of Applied Earth Observation and Geoinformation* 73:1–13.https://doi.org/10.1016/j.jag.2018.05.025.

Li, Wei, Sen Cao, Carlos Campos-Vargas, and Arturo Sanchez-Azofeifa. 2017. "Identifying Tropical Dry Forests Extent and Succession via the Use of Machine Learning Techniques." *International Journal of Applied Earth Observation and Geoinformation* 63 (July). Elsevier: 196–205. https://doi.org/10.1016/j.jag.2017.08.003.

Maxwell, Aaron E., Timothy A. Warner, and Fang Fang. 2018. "Implementation of Machine-Learning Classification in Remote Sensing: An Applied Review." *International Journal of Remote Sensing* 39 (9). Taylor & Francis: 2784–2817. https://doi.org/10.1080/01431161.2018.1433343.

McDowell, Nate, Craig D. Allen, Kristina Anderson-Teixeira, Paulo Brando, Roel Brienen, Jeff Chambers, Brad Christoffersen, et al. 2018. "Drivers and Mechanisms of Tree Mortality in Moist Tropical Forests." *New Phytologist*. https://doi.org/10.1111/nph.15027.

McDowell, Nate, William T Pockman, Craig D Allen, David D Breshears, Neil Cobb, Thomas Kolb, Jennifer Plaut, et al. 2008. "Mechanisms of Plant Survival and Mortality during Drought: Why Do Some Plants Survive While Others Succumb to Drought?" *New Phytologist* 178 (4): 719–39. https://doi.org/10.1111/j.1469-8137.2008.02436.x.

Meddens, Arjan J H, Jeffrey A. Hicke, and Lee A. Vierling. 2011. “Evaluating the Potential of Multispectral Imagery to Map Multiple Stages of Tree Mortality.” *Remote Sensing of Environment* 115 (7). Elsevier Inc.: 1632–42. https://doi.org/10.1016/j.rse.2011.02.018.

Miltiadou, Milto, Neil D F Campbell, Susana Gonzalez, Tony Brown, and Michael G Grant. 2018. “Detection of Dead Standing Eucalyptus Camaldulensis without Tree Delineation for Managing Biodiversity in Native Australian Forest.” *Int J Appl Earth Obs Geoinformation* 67 (October 2017). Elsevier: 135–47. https://doi.org/10.1016/j.jag.2018.01.008.

Mountrakis, Giorgos, Jungho Im, and Caesar Ogole. 2011. “Support Vector Machines in Remote Sensing: A Review.” *ISPRS Journal of Photogrammetry and Remote Sensing* 66 (3). Elsevier B.V.: 247–59. https://doi.org/10.1016/j.isprsjprs.2010.11.001.

Najafabadi, Maryam M., Flavio Villanustre, Taghi M. Khoshgoftaar, Naeem Seliya, Randall Wald, and Edin Muharemagic. 2015. “Deep Learning Applications and Challenges in Big Data Analytics.” *Journal of Big Data* 2 (1): 1–21. https://doi.org/10.1186/s40537-014-0007-7.

Plaza, Antonio, Jon Atli Benediktsson, Joseph W. Boardman, Jason Brazile, Lorenzo Bruzzone, Gustavo Camps-Valls, Jocelyn Chanussot, et al. 2009. “Recent Advances in Techniques for Hyperspectral Image Processing.” *Remote Sensing of Environment* 113 (SUPPL. 1). Elsevier Inc.: S110–22. https://doi.org/10.1016/j.rse.2007.07.028.

Phillips, O. L., Martinez, R. V., Arroyo, L., Baker, T. R., Killeen, T., Lewis, S. L., et al. (2002). Increased dominance of large lianas in Amazonian forests. Nature, 418, 770−774.

Poorter, Lourens, Frans Bongers, T. Mitchell Aide, Angélica M. Almeyda Zambrano, Patricia Balvanera, Justin M. Becknell, Vanessa Boukili, et al. 2016. “Biomass Resilience of Neotropical Secondary Forests.” *Nature* 530 (7589). Nature Publishing Group: 211–14. https://doi.org/10.1038/nature16512.

Ridgeway, Greg. 2017. “Generalized Boosted Regression Models Author.” CRAN R Core Team. R: A Language and Environment for Statistical Computing. R Foundation for Statistical Computing, Vienna, Austria. CRAN R Core Team. R: A language and environment for statistical computing. *R Foundation for Statistical Computing*, Vienna, Austria. https://cran.r-project.org/web/packages/gbm/index.html.

Ripley, Brian, and William Venables. 2016. “R Package ‘Nnet’: Feed-Forward Neural Networks and Multinomial Log-Linear Models.” CRAN R Core Team. R: A Language and Environment for Statistical Computing. *R Foundation for Statistical Computing*, Vienna, Austria. http://www.stats.ox.ac.uk/pub/MASS4/.

Rong, Xiao. 2014. “Deepnet: Deep Learning Toolkit in R.” CRAN R Core Team. R: A Language and Environment for Statistical Computing. R Foundation for Statistical Computing, Vienna, Austria.

Rowland, L., A. C.L. Da Costa, D. R. Galbraith, R. S. Oliveira, O. J. Binks, A. A.R. Oliveira, A. M. Pullen, et al. 2015. “Death from Drought in Tropical Forests Is Triggered by

Hydraulics Not Carbon Starvation." *Nature* 528 (7580). Nature Publishing Group: 119–22. https://doi.org/10.1038/nature15539.

Sanchez-Azofeifa, Arturo, Jose Antonio Guzmán, Carlos A. Campos, Saulo Castro, Virginia Garcia-Millan, Joanne Nightingale, and Cassidy Rankine. 2017. "Twenty-First Century Remote Sensing Technologies Are Revolutionizing the Study of Tropical Forests." *Biotropica* 49 (5): 604–19. https://doi.org/10.1111/btp.12454.

Sánchez-Azofeifa, Gerardo Arturo, J. Antonio Guzmán-Quesada, Mauricio Vega-Araya, Carlos Campos-Vargas, Sandra Milena Durán, Nikhil D'Souza, Thomas Gianoli, Carlos Portillo-Quintero, and Iain Sharp. 2017. "Can Terrestrial Laser Scanners (TLSs) and Hemispherical Photographs Predict Tropical Dry Forest Succession with Liana Abundance?" *Biogeosciences* 14 (4): 977–88. https://doi.org/10.5194/bg-14-977-2017.

Seager, Richard, Mingfang Ting, Isaac Held, Yochanan Kushnir, Jian Lu, Gabriel Vecchi, Huei-Ping Huang, et al. 2007. "Model Projections of an Imminent Transition to a More Arid Climate in Southwestern North America." *Science* 316 (5828): 1181–84.

Smith, Geoffrey M., and Edward J. Milton. 1999. "The Use of the Empirical Line Method to Calibrate Remotely Sensed Data to Reflectance." *International Journal of Remote Sensing* 20 (13): 2653–62. https://doi.org/10.1080/014311699211994.

Sterl, Andreas, Camiel Severijns, Henk Dijkstra, Wilco Hazeleger, Geert Jan van Oldenborgh, Michiel van den Broeke, Gerrit Burgers, Bart van den Hurk, Peter Jan van Leeuwen, and Peter van Velthoven. 2008. "When Can We Expect Extremely High Surface Temperatures?" *Geophysical Research Letters* 35 (14): 1–5. https://doi.org/10.1029/2008GL034071.

Tobin, Michael F., Alexandra J. Wright, Scott A. Mangan, and Stefan A. Schnitzer. 2012. "Lianas Have a Greater Competitive Effect than Trees of Similar Biomass on Tropical Canopy Trees." *Ecosphere* 3 (2): art20. https://doi.org/10.1890/ES11-00322.1.

Vargas-Sanabria, Daniela, and Carlos Campos-Vargas. 2018. "Sistema Multi-Algoritmo Para La Clasificación de Coberturas de La Tierra En El Bosque Seco Tropical Del Área de Conservación Guanacaste, Costa Rica." *Revista Tecnología En Marcha* 31 (1): 58. https://doi.org/10.18845/tm.v31i1.3497.

Vaughn, N.R., G.P. Asner, P.G. Brodrick, R.E. Martin, J.W. Heckler, D.E. Knapp, and R.F. Hughes. 2018. "An Approach for High-Resolution Mapping of Hawaiian Metrosideros Forest Mortality Using Laser-Guided Imaging Spectroscopy." *Remote Sensing*, This Issue, 1–17. https://doi.org/10.3390/rs10040502.

Williams, A. Park, Craig D. Allen, Alison K. Macalady, Daniel Griffin, Connie A. Woodhouse, David M. Meko, Thomas W. Swetnam, et al. 2013. "Temperature as a Potent Driver of Regional Forest Drought Stress and Tree Mortality." *Nature Climate Change* 3 (3). Nature Publishing Group: 292–97. https://doi.org/10.1038/nclimate1693.

Wolpert, David H. 1996. "The Existence of A Priori Distinctions Between Learning Algorithms." *Neural Computation* 8 (7): 1391–1420. https://doi.org/10.1162/neco.1996.8.7.1391.

Wolpert, David H. 1992. “On the Connection between In-Sample Testing and Generalization Error.” *Com p Lex Systems* 6: 47–94.

Wullschleger, Stan D., P. J. Hanson, and D. E. Todd. 2001. “Transpiration from a Multi-Species Deciduous Forest as Estimated by Xylem Sap Flow Techniques.” *Forest Ecology and Management* 143 (1–3): 205–13. https://doi.org/10.1016/S0378-1127(00)00518-1.

Zarco-Tejada, P. J., R. Diaz-Varela, V. Angileri, and P. Loudjani. 2014. “Tree Height Quantification Using Very High-Resolution Imagery Acquired from an Unmanned Aerial Vehicle (UAV) and Automatic 3D Photo-Reconstruction Methods.” *European Journal of Agronomy* 55. Elsevier B.V.: 89–99. https://doi.org/10.1016/j.eja.2014.01.004.

Zeppel, Melanie J., William R. Anderegg, and Henry D. Adams. 2013. “Meetings Forest Mortality Due to Drought : Latest Insights, Evidence and Unresolved Questions on Physiological Pathways and Consequences of Tree Death.” *New Phytologist* 197 (2): 372–74. https://doi.org/10.1111/nph.12090.

3.8. Figures and Tables

Table 3.1. Description of the five temporary forest plots surveyed on the estimation of dead woody components at SR-EMSS, Costa Rica.

Plot	Secondary succession	Description	Figure
One	Intermediate-late	Forest patch contiguous to an old-grow forest patch; however, this patch is also surrounded by early forests. The soils in this patch are shallow with large exposures of volcanic rocks.	3.1 a Principe
Two	Early-intermediate	Forest patch composed for grasses, shrubs, small decidudus trees, and some large evergreen trees of a Mesoamerican oak that grows from Mexico to northern Costa Rica. This patch is located in a particular soil which enhance the abundance of *Quercus oleoides* (White oak tree).	3.2 a Guacimo
Three	Intermediate-intermediate	Forest with a high liana infestation (Woody vines) which is located next to a firebreak. In consequence, this patch was affected in the past by several wildfires.	3.4 a Phenology
Four	Early-early	Forest patch with a low recovery, large gaps, high abundance of grasses, shrubs and small trees. The maximun height of the trees is approximately 6–8 m.	3.3 a Fire
Five	Intermediate-intermediate	Forest patch surrounded only by similar successional stages, with deep soils. Historically intensively used as cattle pasture during the Hacienda epochs from 1600 s to 1960.	3.5 a Perros

Table 3.2. Models implemented and their available and selected input parameters in five temporary forest plots at SR-EMSS, Costa Rica.

Model	Package	Method	Parameter	Descriptor	Reference
Support Vector Machines with Linear Kernel	kernlab	'svmLinear'	Cost	Cost	(Karatzoglou, Smola, and Hornik 2016)
Support Vector Machines with Polynomial Kernel		'svmPoly'	Degree Scale C	Polynomial degree Scale factor Cost	
Support Vector Machines with Radial Kernel		'svmRadial'	C Sigma	Cost Distance value	
Random Forest	'randomForest'	'rf'	Mty	Number of trees	(Breiman et al. 2018)
Conditional Inference Tree	'party'	'ctree'	maxdepth mincriterion	Max. depth of the tree Value of statistic (1-p_{value})	(Hothorn et al. 2017)
C4.5-like Trees	'rWeka'	'J48'	C M	Pruning confidence Min. instances/leaf	(Hornik et al. 2018)
Gradient Boosting Machines	'gbm'	'gbm'	n.trees interaction.depth shrinkage n.minobsinnode	Number of iterations Complexity of the tree Learning rate Min. number of training samples in a node	(Ridgeway 2017)
Neural Network	'nnet'	'avNNet'	Size Decay	Hidden units Weight decay	(Ripley and Venables 2016)
Averaged Neural Network		'nnet'	Size Decay Bag	Hidden units Weight decay Bagging	
Deep Neural Network	'deepnet'	'dnn'	layer1 layer2 layer3 hidden_dropout visible_dropout	Hidden units Hidden units Hidden units Dropout rate Bagging	(Rong 2014)

Table 3.3. Machine Learning models implemented and their selected and available input parameters in five temporary forest plots at SR-EMSS, Costa Rica.

Model	Acron	Tune up parameters	Avail. Values	Plot					Gen
				1	2	3	4	5	
Support Vector Machines with Linear Kernel	SVML	cost	c(1:100)	55	56	19	1	3	62
Support Vector Machines with Polynomial Kernel	SVMP	degree	c(1:10)	3	4	1	6	5	5
		scale	seq(1,10,100)	1	1	1	1	1	1
		C	c(1:100)	2	10	14	6	1	24
Support Vector Machines with Radial Kernel	SVMR	C	seq(1,10,100)	1	6	1	8	3	2
		sigma	c(0.5:100)	1	1	1	1	1	1
Random Forest	RF	mty	c(1:100)	1	1	60	2	4	2
Conditional Inference Tree	CIT	maxdepth	c(1:100)	3	9	4	16	2	13
		mincriterion	c(0.01:0.99)	0.01	0.01	0.01	0.01	0.01	0.01
C4.5-like Trees	C45T	C	c(0.05:1)	0.05	0.05	0.05	0.05	0.05	0.05
		M	c(1:100)	1	1	3	1	1	1
Gradient Boosting Machines	GMB	n.trees	c(1:100)	56	97	31	97	97	96
		interaction.depth	c(1:10)	10	10	6	10	1	10
		shrinkage	seq(0.1,0.5)	0.1	0.1	0.1	0.1	0.1	0.1
		n.minobsinnode	c(5,7,10)	10	10	5	5	5	10
Neural Network	NNET	size	c(1:100)	3	8	5	13	2	4
		decay	c(0.5: 0.1)	0.5	0.5	0.5	0.5	0.5	0.5
Averaged Neural Network	ANNT	size	c(1:100)	16	41	62	12	33	28
		decay	seq(0.01, 0.1, 0.5)	0.01	0.01	0.01	0.01	0.01	0.01
		bag	seq(T, F)	T	T	T	T	T	T
Deep Neural Network	DNET	layer1	c(1:10)	3	10	7	4	2	10
		layer2	c(1:10)	1	8	9	5	10	6
		layer3	c(0:10)	8	2	0	1	0	6
		hidden_dropout	seq(0, .1)	1	1	1	1	1	0
		visible_dropout	seq(0, 0.01)	0	0	0	1	0	0

Table 3.4. Average values of Accuracy, Kappa, and Processing times from the best candidate models across five temporary forest plots at SR-EMSS, Costa Rica.

	Accuracy		Kappa		Time	
Model	**Average**	**StaDev**	**Average**	**StaDev**	**Average**	**StaDev**
ANNT	0.968	0.035	0.955	0.050	69307.830	20306.710
C45T	0.967	0.032	0.950	0.045	373.777	56.677
CIT	0.958	0.036	0.948	0.047	173.878	119.465
DNET	0.945	0.005	0.955	0.021	4970.447	3550.205
GMB	0.977	0.023	0.970	0.031	2839.378	2195.188
NNET	0.955	0.054	0.940	0.075	9271.333	5272.399
RF	0.980	0.020	0.958	0.034	1523.245	989.001
SVML	0.950	0.056	0.938	0.069	595.568	1066.373
SVMP	0.977	0.024	0.972	0.031	8188.283	11149.980
SVMR	0.982	0.021	0.977	0.024	4689.915	8735.645

Table 3.5. Analysis of variance with repeated measures ANOVA of three performance variables (Accuracy, Kappa, and Time) across five temporary forest plots at SR-EMSS, Costa Rica.

Variable	**F- value**	**Significance**	
Time	82.963	0.000	***
Accuracy	2.236	0.209	
Kappa	12.719	0.174	
Interaction	1.045	0.365	

Table 3.6. Analysis of variance with a repeated measures ANOVA of the extension of dead woody components across five temporary forest plots at SR-EMSS, Costa Rica.

Variable	**F- value**	**significance**
Plot	3.296	0.246

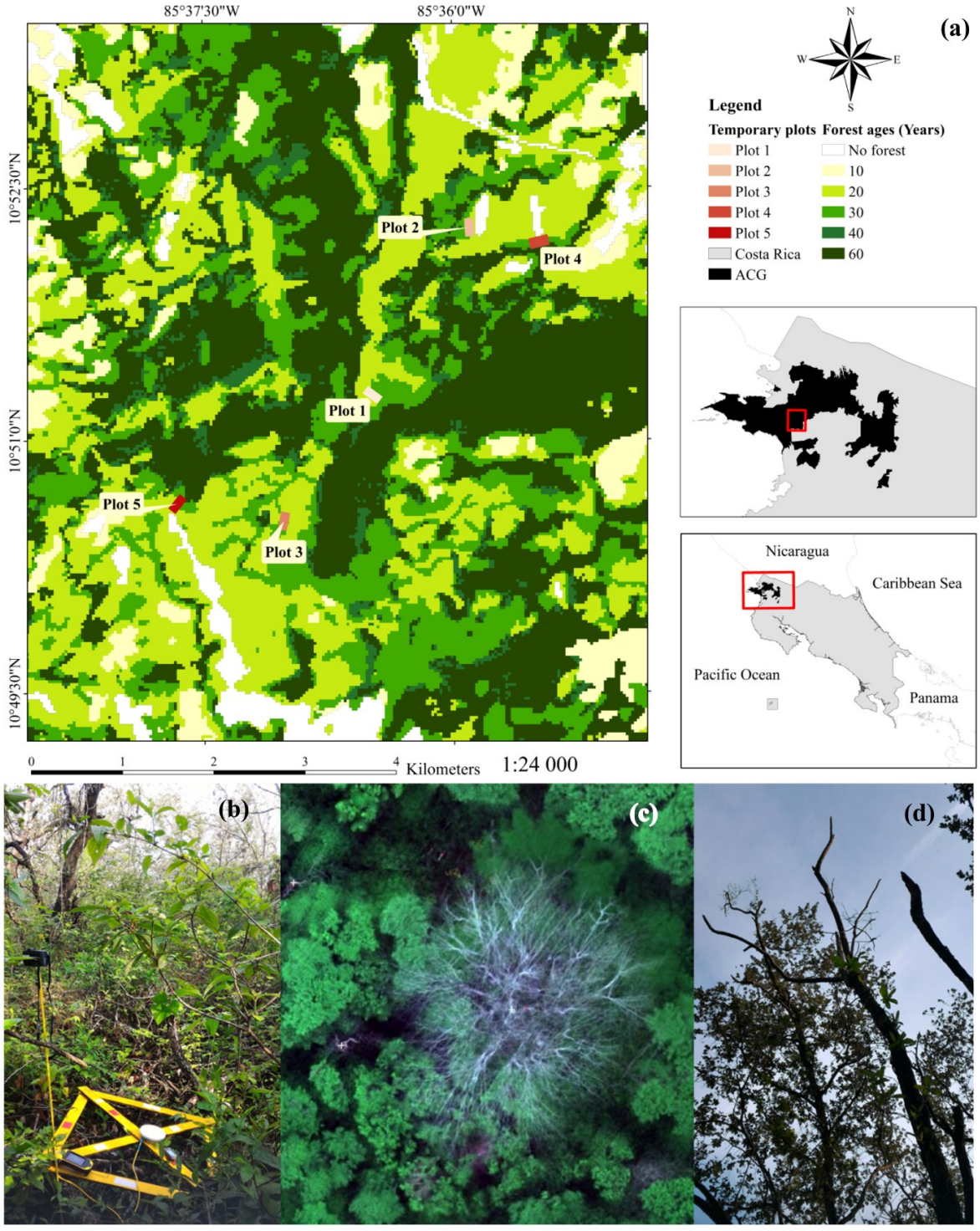

Figure 3.1. (a) location map of the SR-EMSS; (b) ground reference point and GPS; (c) dead stand tree from UAV R: band red, G: band green B: band blue; (d); dead stand tree viewed from ground

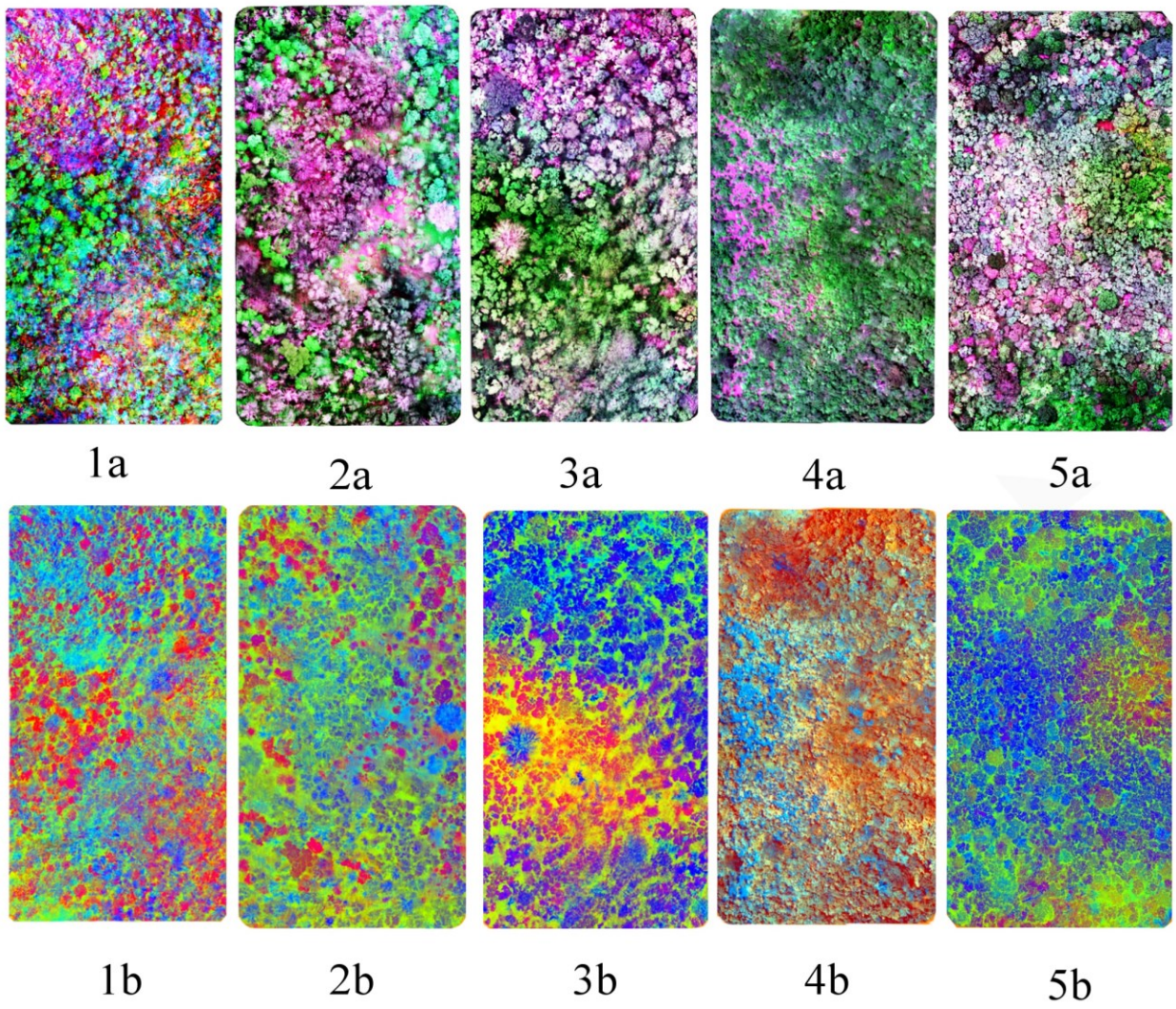

Figure 3.2. Color composites for each site. Top row R: band red, G: band green B: band blue. Bottow row: Transformation composite R: Tasseled Cap – Yellow Stuff structure, G: First Principal Component, B:Texture Mean Band blue. Column labels: (1) Intermediate-late, (2) Early -intermediate, (3)intermediate-intermediate (4) Early- early, (5) Intermediate-intermediate,

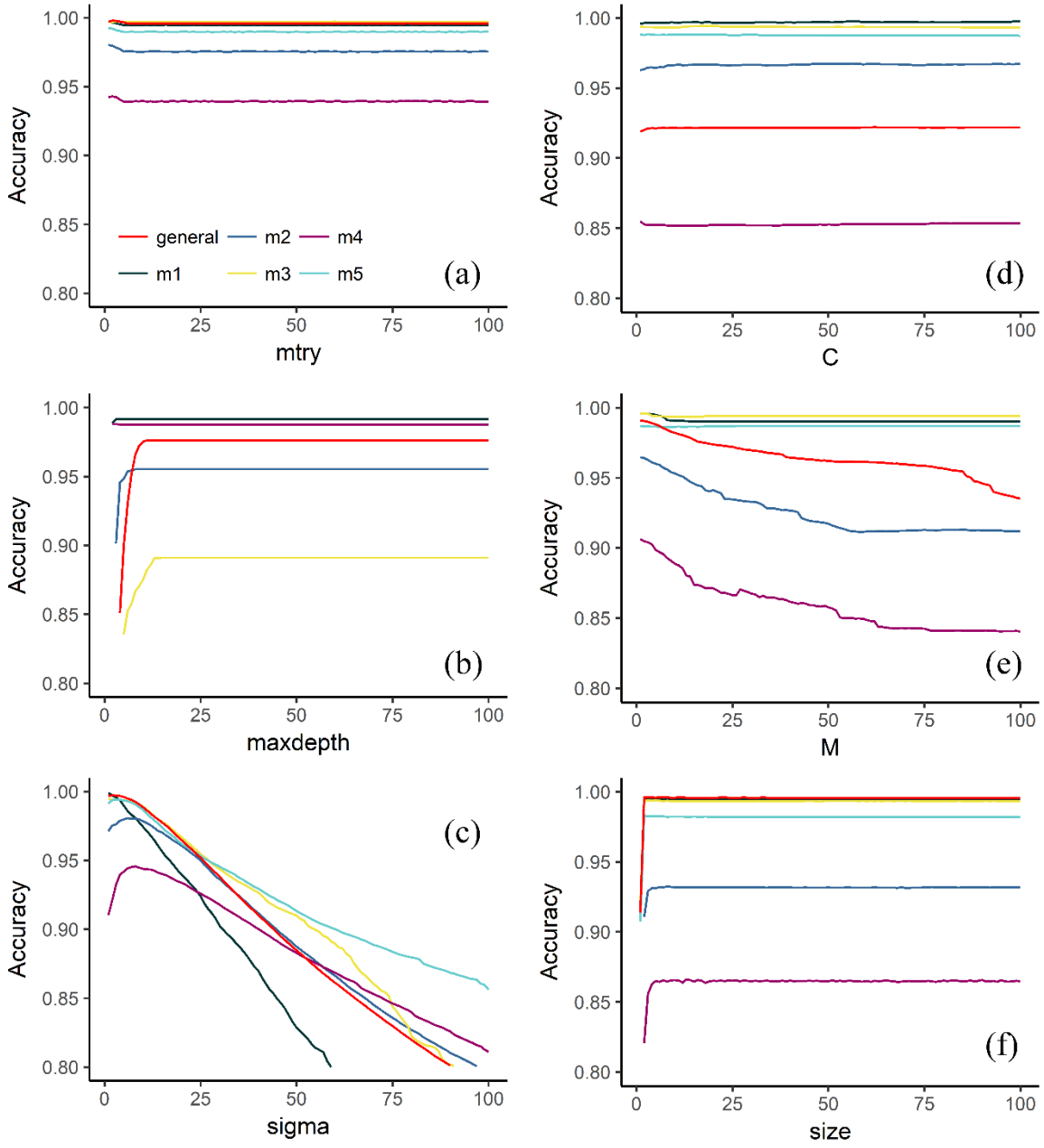

Figure 3.3. The accuracy of validation samples for six machine learning algorithms using the Bootstrap 632 method in five temporary forest plots at SR-EMSS, Costa Rica. (a) Random Forest, (b) Conditional Inference Tree, (c) Support Vector Machines with Radial Kernel, (d) Support Vector Machines with Linear Kernel, (e) C4.5-like Trees, (f) Neural Network.

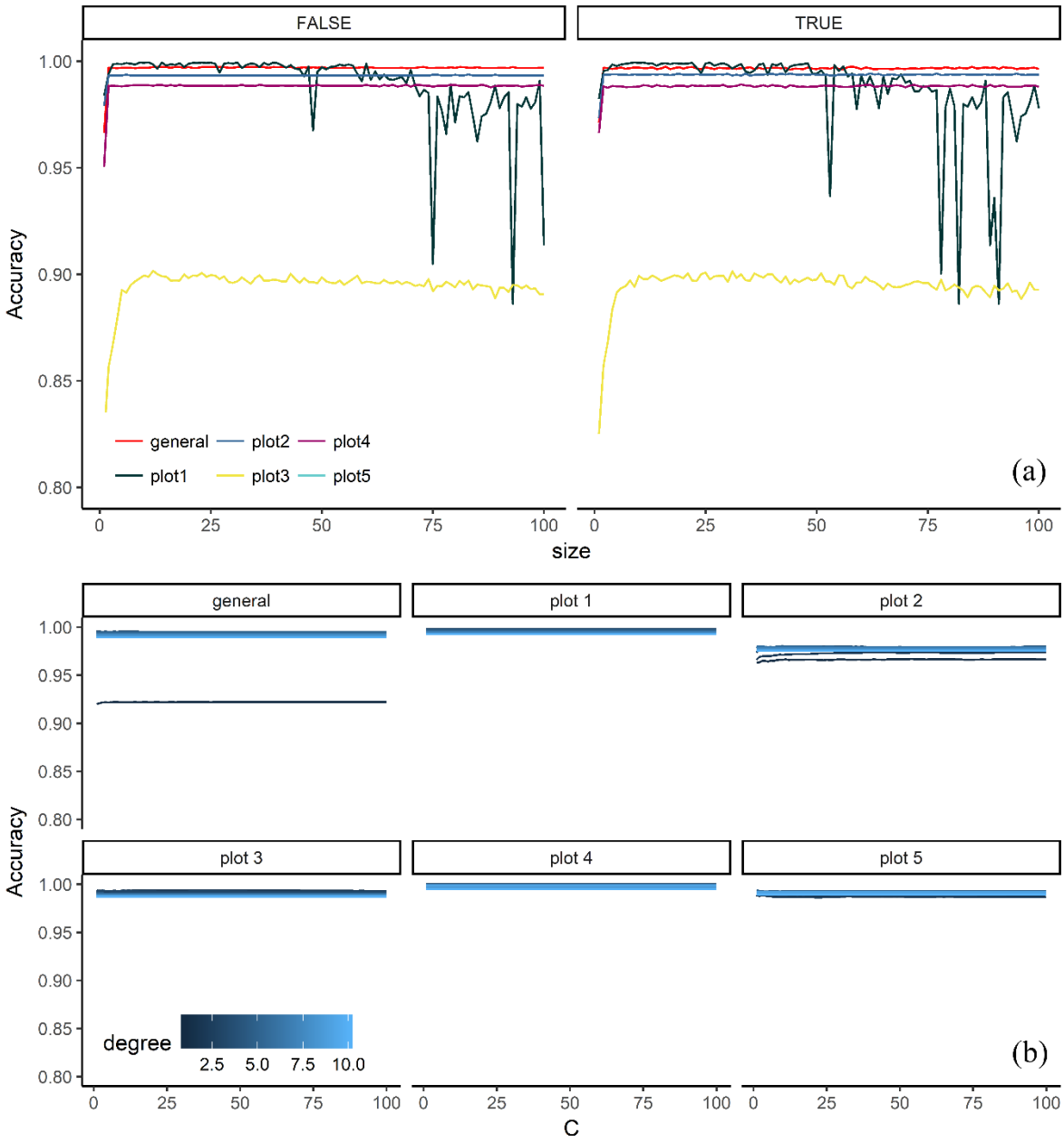

Figure 3.4. Accuracy of validation samples by two classification algorithms using the Bootstrap 632 method in five temporary forest plots at SR-EMSS, Costa Rica. (a) Averaged Neural Network with Bagging (TRUE, FALSE)', (b) Support Vector machine with polynomial kernel.

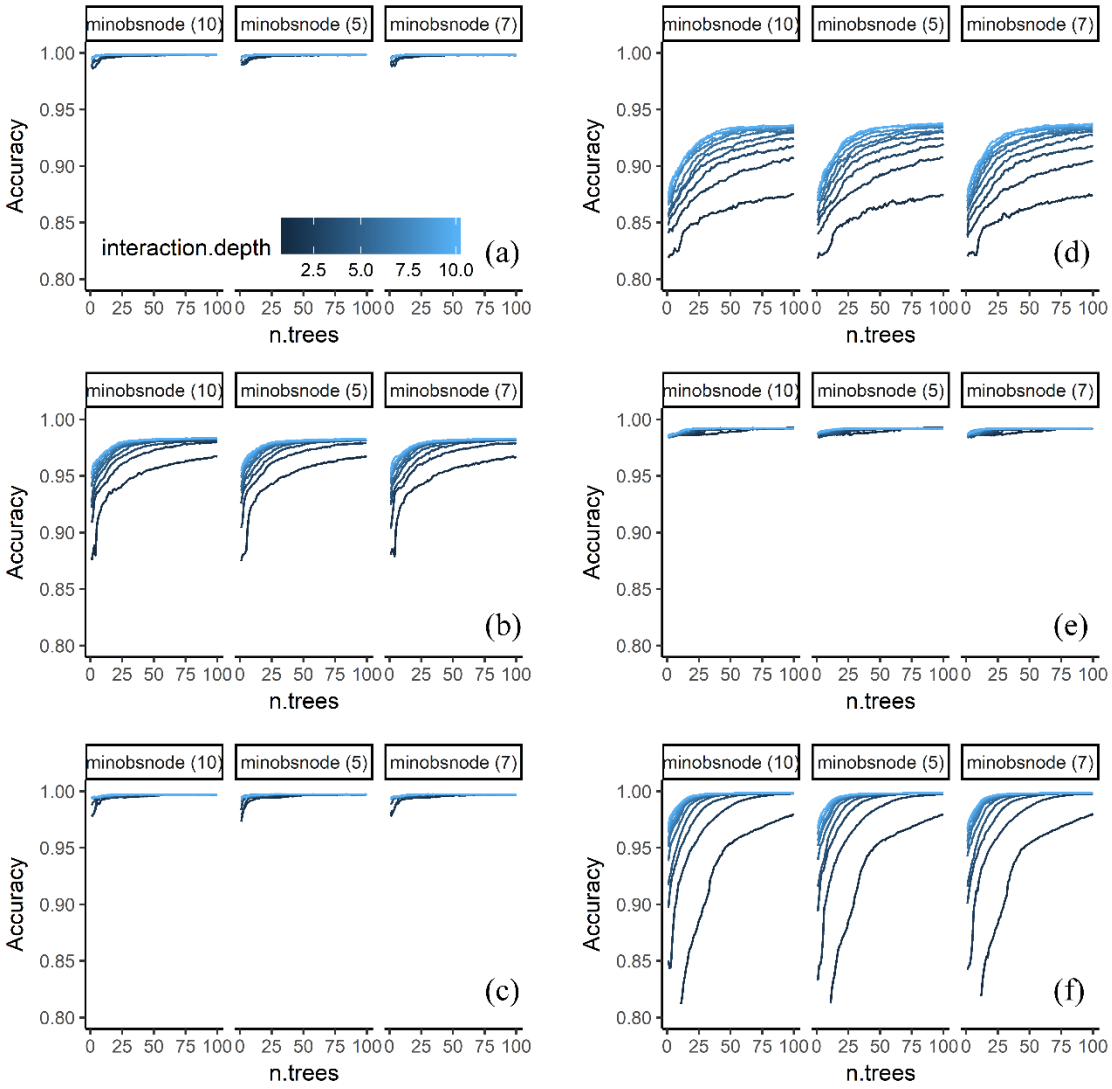

Figure 3.5. Accuracy of training samples by Gradient Boosting Machine using the Bootstrap 632 method in five temporary forest plots at SR-EMSS, Costa Rica. (a) plot One, (b) plot Two, (c) plot Three, (d) plot Four, (e) plot Five, (f) General model.

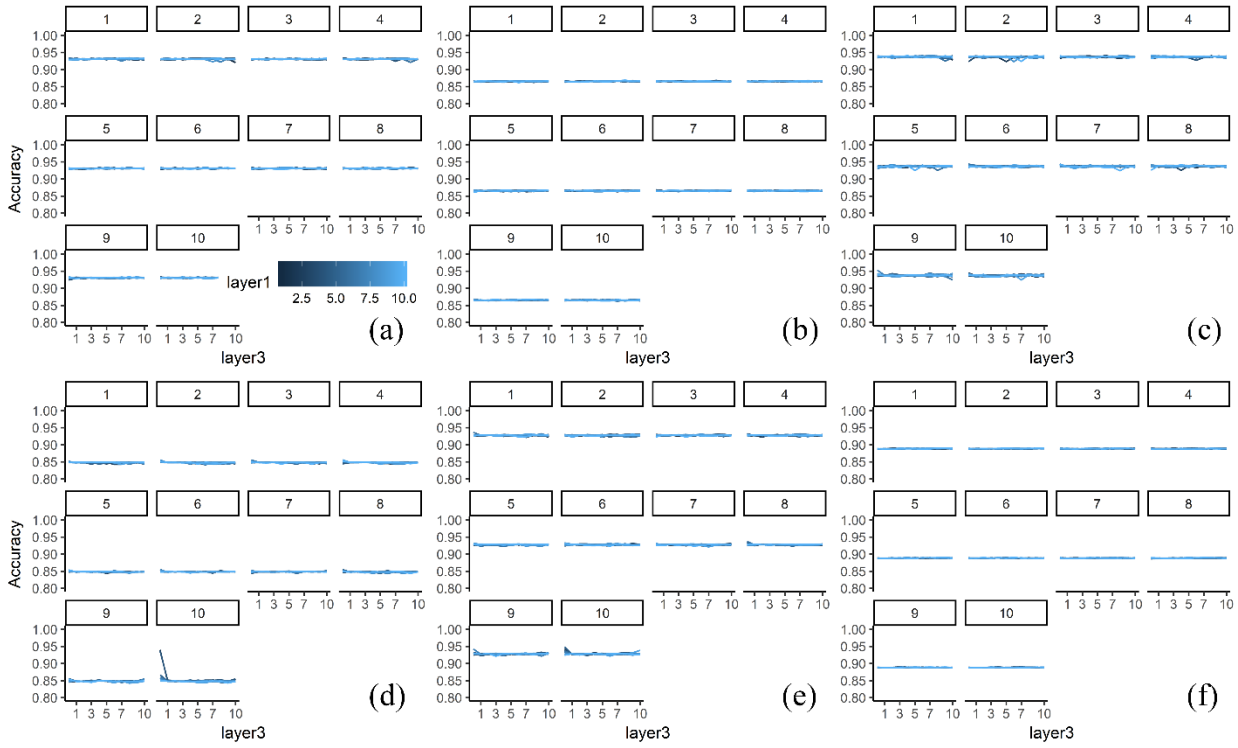

Figure 3.6. The accuracy of training samples by Deep Neural Network using the Bootstrap 632 method in five temporary forest plots at SR-EMSS, Costa Rica. (a) plot One, (b) plot Two, (c) plot Three, (d) plot Four, (e) plot Five, (f) General model.

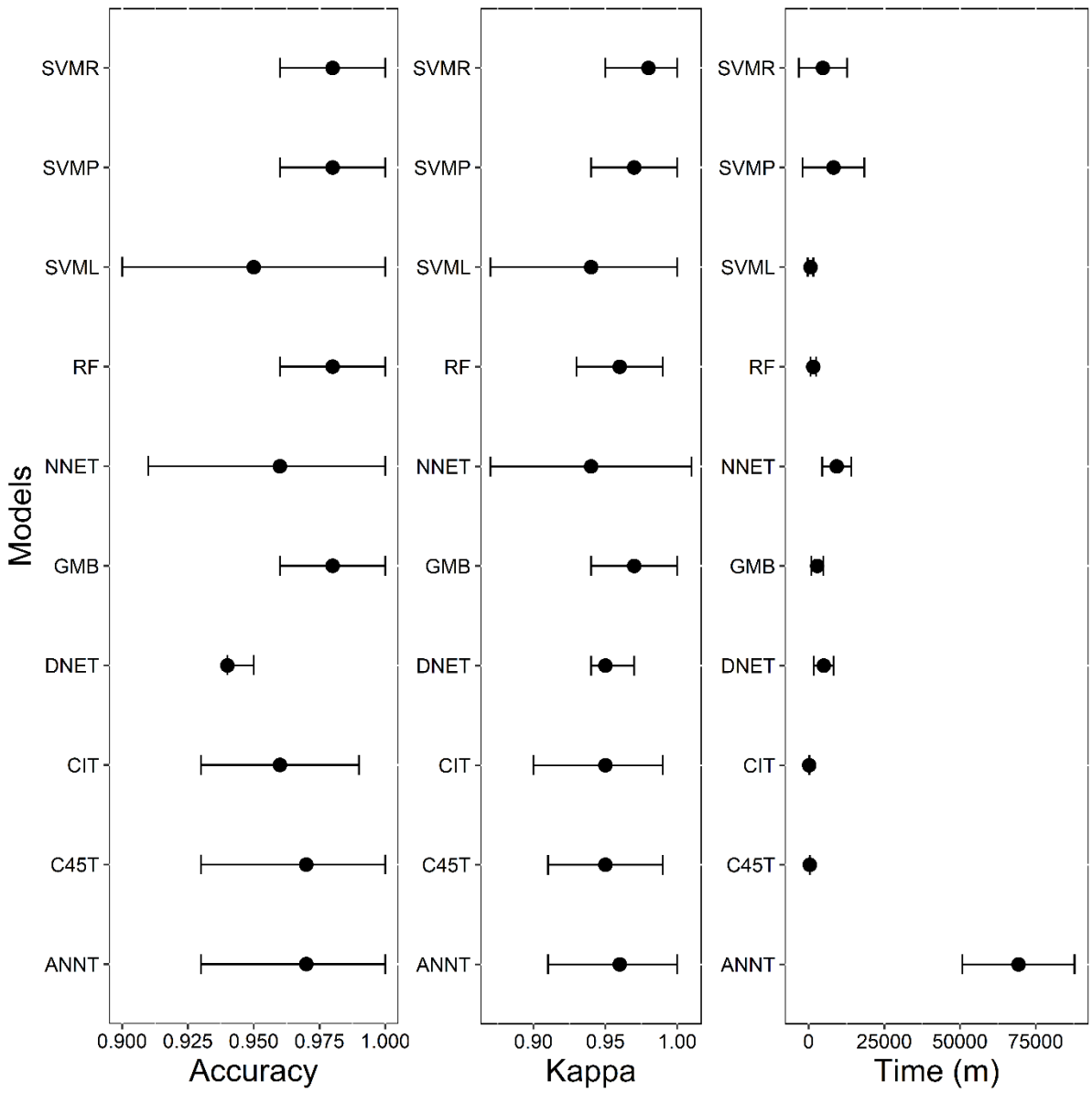

Figure 3.7. Accuracy, Kappa and processing times values of ten machine learning models for classification across five temporary forest plots at SR-EMSS, Costa Rica.

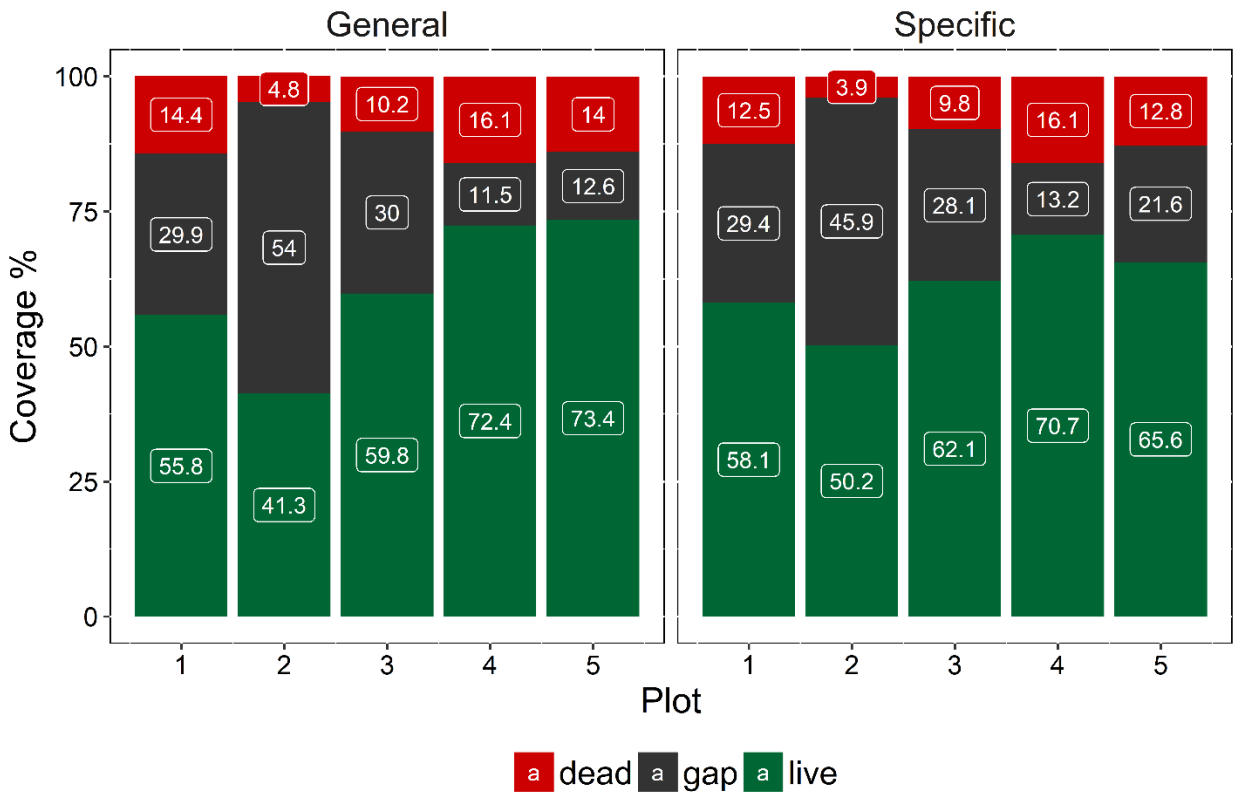

Figure 3.8. Class coverage of five secondary dry forest temporary plots at SR-EMSS, Costa Rica using five plots and a specific and a general classification model.

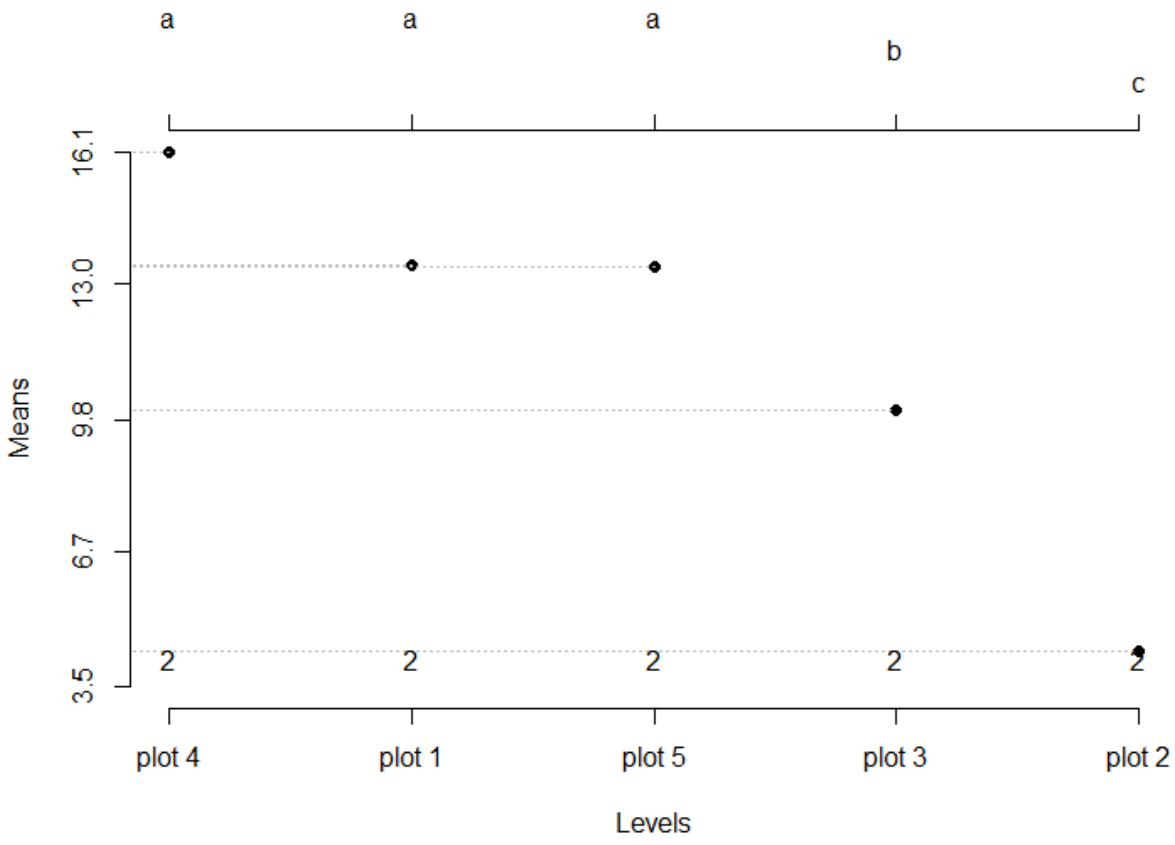

Figure 3.9. Tukey test results of mortality coverage in five secondary dry forest temporary plots at SR-EMSS, Costa Rica. Where (a), (b), and (c) represent possible the groups.

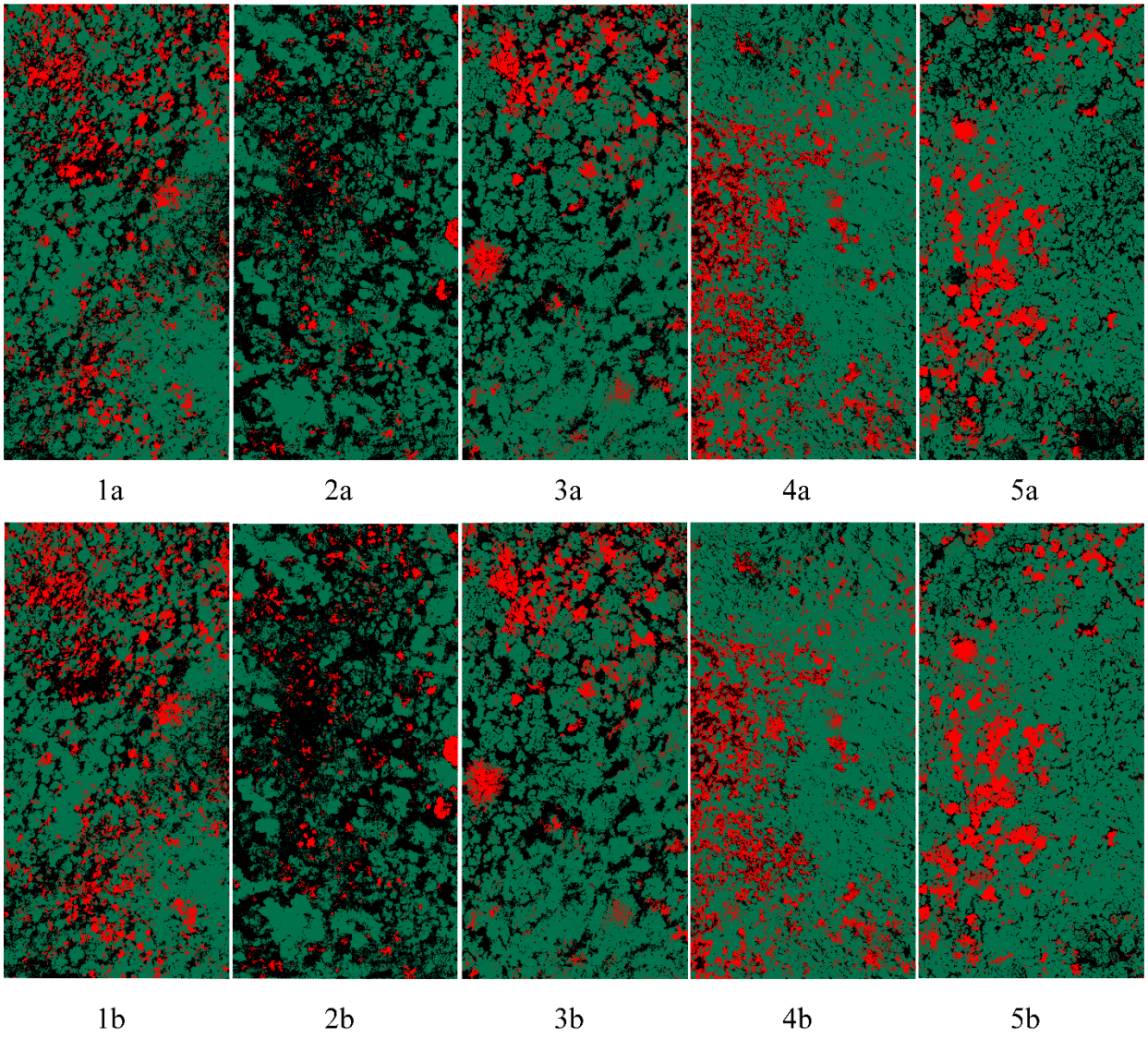

Figure 3.10. Classification results of mortality extension in five secondary dry forest temporary plots at SR-EMSS, Costa Rica, using Random Forest algorithm. Using a plot specific model (a), and a general model (b).

4. Chapter four – Conclusions

The main objective of this thesis was to assess the capabilities of a multi-spectral Unmanned Aerial System (UAS) at the Santa Rosa Environmental Monitoring Super Site, Costa Rica. Two studies were conducted, the first one, contained in *Chapter Two*, compared the relative error of reflectance values at the band-level as well as spectral vegetation indexes (VI) from a MicaSense Red Edge ™ 3 multispectral camera onboard of a Draganfly XP-4 helicopter at the SR-EMSS' grass-covered firebreaks using two radiometric transformations and four acquisition altitudes. This chapter contributed to the understanding of how to handle multispectral information acquired with an UAS beyond the use of end-user solutions that follow commercial processing chains. The second study, contained in *Chapter Three*, quantified the extension of dead woody components and live and understory vegetation using an UAS and Machine Learning techniques at the Tropical Dry forest of the Santa Rosa National Park Costa Rica. This study contributed to the understanding of techniques to quantify the extension of mortality at TDF and other tropical enviroments and combined two leading edge technologies namely UAS and Machine Learning.

4.1. Synthesis of significant contributions

Von Bueren et al. (2015) argued that multispectral cameras have the potential to be deployed within UAV only if the shortcomings of the radiometric calibration are addressed. The results from chapter Two demonstrated that using at least three reference materials (White panel, grey panel, and black panel) for the calibration to at surface reflectance provide better results than using a single white panel. A repeated measures ANOVA indicated that the differences between transformation methods were statistically significant only in Blue, Red, Red Edge and NIR bands, and not in the Green band. Consequently, it can be argued that the calibration to at surface reflectance by the empirical line method solved the shortcomings of the radiometric calibration at SR-MESS. The error at the band level stretched values up to 10%, attributed to random errors because the instrument optimization and the protocols used mitigated the appearance of synthetic errors. Likewise, the vegetation indexes reported error values close to 20%. Seven of the ten vegetation indexes (DVI, EVI, GDVI, GNDVI, GRVI, IPVI, MSR, NDVI, NLI, and SR) showed an underestimation in comparison with values derived from field spectrometer measurements.

The results from chapter Three demonstrated that multispectral UAS and Machine Learning are viable technologies to quantify the extent dead woody components such as dead stand and fallen trees at the SR-EMSS, Costa Rica. This study found that the coverage of dead woody components in the five temporary plots at SR-EMSS ranges from 4.8% to 16.1%. Chapter Three illustrated the "No Free Lunch" theorem of Wolpert (1992), who stated that without having substantive information about the modelling problem, there is no single model that is better than another model. Chapter Three showed that neither of the ML models with a single set of parameters could outperform in accuracy values the others ML models in all plots. Even though the best candidate model of the ten classification models tested provided similar accuracy values. Some classification models tested were more sensitive to the tuning parameters than others. Likewise, it was found that the best candidate models displayed a heterogeneous selection of available parameters. Consequently, a wide range of available parameters should be tested in the classification models used to obtain the best classification results possible. Similarly, to select a final classification model, it is required to consider factors such as the assumptions of the model chosen, the number and complexity of setting up parameters, the accuracy values, the kappa coefficient and processing times.

In synthesis, both chapters of this thesis showed the potential of a multispectral UAS as a research tool at the SR-EMSS. To calibrate the multispectral data used to at surface reflectance the empirical line method with three reference panels provided better results than using a single white reference panel, even though the camera manufacturer recommends the use of a single white reference panel. The UAS allowed access to the forest canopy at high resolution enabling the detection of dead woody component within a tree crown .

4.2. Challenges and considerations

The toughest challenge faced during this thesis was the learning process related to the operation of the UAS used during the field campaign. The operation of a UAS requires several skills and certifications. Similarly, there was a learning curve in regards to the computer code required to implement the Machine Learning models in *chapter Three*. The learning curve of the R program was overcome with the help of online courses, support groups, and code libraries. Another challenge of this thesis was the deletion of individual images during the mosaic generation on

PIX4D. Specifically, for no clear reason, PIX4D discarded many images in the mosaicking generation, only displaying a message that indicated that the images were not calibrated resulting in mosaics with large gaps or no information. Consequently, to fill those gaps missing images were added and replaced with images acquired at the same time period.

Sandbrook (2015) in "The social implications of using drones for biodiversity conservation" calls for self-regulation and mitigation of possible social impacts of using drones, including effects on safety, privacy, psychological well-being, and data security. Consequently, good ethical practices must be accounted to avoid negative social impacts and an undermining of the relatively good perception of drones in society in the long term.

4.3. Future Research

Further climate scenarios are likely to include significant increases in mean temperatures, carrying increases in frequency and severity of extreme droughts, and heat waves (Sterl et al. 2008). Tree mortality related to extreme drought has been reported worldwide; however, the triggering factors and susceptability vary across ecosystems, life forms and even within species. Large trees suffer most during a drought in forests worldwide (Bennett et al. 2015) while Lianas reduce growth and survival of host trees in temperate and tropical forests (Lai et al. 2017).

In this context, a further research path could be to fully scale-up the work of Li et al. (2018) by detecting dead trees, liana-infested, and non-liana-infested trees in a gradient of secondary dry forests at SR-EMSS. Another future path could be to locate emergent dead trees individually adapting the work of Alexander et al. (2018) who located emergent trees in a tropical rainforest using data from an UAS. However, to pursue an analysis with 3D information a high-resolution RGB camera or lidar should be considered because of the MicaSense RedEdge TM 3 not provides good 3D products. Sanchez-Azofeifa et al. (2017) proposed the fusion of thermal, VNIR, and hyperspectral sensors providing new opportunities for the discrimination of life form or species, and the analysis of biochemical and functional traits at canopy levels at very high spatial resolution.

The use of UAS, in general, carries some uncertainties that must be compensated to successfully obtain valuable data including platform movement that was minimal here due to stable flight conditions (minimal wind) and the compensation of any small platform instabilities by camera

gimbals. There are remaining uncertainties about whether the UAV cameras is truly pointing to the target at nadir, although the UAS is equipped with gyro-stabilization mechanisms such as GPS, IMU units, and camera gimbals (Von Bueren et al. 2015). The fusion of VNIR and SWIR sensors with thermal sensors intrinsically creates an operational constraint. because according to Mulero-Pázmány et al. (2014) the best time for the use of optical cameras is from late morning to midday. Thermal cameras, on the other hand, may have requirements for optimal results that span a larger time period. Likewise, there are other uncertainties related to the sensor viewing directions and possible differences in FOV between cameras.

Finally, another piece of research could be the estimation of canopy attributes using RGB images, adapting the work of Chianucci et al. (2016), or quantifying the spatial gap patterns in the TDF at the SR-EMSS, adapting the work of Getzin et al. (2014). However, the work with RGB images should be based on object-base and segmentation analysis because the images acquired with RGB technology have a low radiometric resolution. Consequently, RGB technology provides very high-resolution information but can store energy levels lower than 8 bits.

4.4. References

Alexander, Cici, Amanda H Korstjens, Emma Hankinson, Graham Usher, Nathan Harrison, Matthew G Nowak, Abdullah Abdullah, Serge A Wich, and Ross A Hill. 2018. "Locating Emergent Trees in a Tropical Rainforest Using Data from an Unmanned Aerial Vehicle (UAV*)." International Journal of Applied Earth Observation and Geoinformation* 72 (May). Elsevier: 86–90. https://doi.org/https://doi.org/10.1016/j.jag.2018.05.024.

Bennett, Amy C., Nathan G. Mcdowell, Craig D. Allen, and Kristina J. Anderson-Teixeira. 2015. "Larger Trees Suffer Most during Drought in Forests Worldwide." *Nature Plants* 1 (September). Nature Publishing Group: 1–5. https://doi.org/10.1038/nplants.2015.139.

Chianucci, Francesco, Leonardo Disperati, Donatella Guzzi, Daniele Bianchini, Vanni Nardino, Cinzia Lastri, Andrea Rindinella, and Piermaria Corona. 2016. "Estimation of Canopy Attributes in Beech Forests Using True Colour Digital Images from a Small Fixed-Wing UAV." *International Journal of Applied Earth Observation and Geoinformation* 47. Elsevier B.V.: 60–68. https://doi.org/10.1016/j.jag.2015.12.005.

Getzin, S., Nuske, R. S., & Wiegand, K. (2014). Using unmanned aerial vehicles (UAV) to quantify spatial gap patterns in forests. *Remote Sensing*, *6*(8), 6988–7004. http://doi.org/10.3390/rs6086988

Lai, Hao Ran, Jefferson S. Hall, Benjamin L. Turner, and Michiel van Breugel. 2017. "Liana Effects on Biomass Dynamics Strengthen during Secondary Forest Succession." *Ecology* 98 (4): 1062–70. https://doi.org/10.1002/ecy.1734.

Li Wei, Campos-Vargas Carlos, Marzahn Phillip, Sanchez-Azofeifa Arturo 2018. On the estimation of tree mortality and liana infestation using a deep self- encoding network. *International Journal of Applied Earth Observation and Geoinformation* 73:1–13.https://doi.org/10.1016/j.jag.2018.05.025.

Mulero-Pázmány, M., Stolper, R., Van Essen, L. D., Negro, J. J., & Sassen, T. (2014). Remotely piloted aircraft systems as a rhinoceros anti-poaching tool in Africa. *PLoS ONE*, *9*(1), 1–10. http://doi.org/10.1371/journal.pone.0083873

Sanchez-Azofeifa, Arturo, Jose Antonio Guzmán, Carlos A. Campos, Saulo Castro, Virginia Garcia-Millan, Joanne Nightingale, and Cassidy Rankine. 2017. "Twenty-First Century Remote Sensing Technologies Are Revolutionizing the Study of Tropical Forests." *Biotropica* 49 (5): 604–19. https://doi.org/10.1111/btp.12454.

Sandbrook, Chris. 2015. "The Social Implications of Using Drones for Biodiversity Conservation." *Ambio* 44 (4). Springer Netherlands: 636–47. https://doi.org/10.1007/s13280-015-0714-0.

Sterl, Andreas, Camiel Severijns, Henk Dijkstra, Wilco Hazeleger, Geert Jan van Oldenborgh, Michiel van den Broeke, Gerrit Burgers, Bart van den Hurk, Peter Jan van Leeuwen, and Peter van Velthoven. 2008. "When Can We Expect Extremely High Surface Temperatures?" *Geophysical Research Letters* 35 (14): 1–5. https://doi.org/10.1029/2008GL034071.

Von Bueren, S. K., A. Burkart, A. Hueni, U. Rascher, M. P. Tuohy, and I. J. Yule. 2015. "Deploying Four Optical UAV-Based Sensors over Grassland: Challenges and Limitations." *Biogeosciences* 12 (1): 163–75. https://doi.org/10.5194/bg-12-163-2015.

Wolpert, David H. 1992. "On the Connection between In-Sample Testing and Generalization Error." *CompLex Systems* 6: 47–94.

Bibliography

Aasen, Helge, Eija Honkavaara, Arko Lucieer, and Pablo Zarco-Tejada. 2018a. "Quantitative Remote Sensing at Ultra-High Resolution with UAV Spectroscopy: A Review of Sensor Technology, Measurement Procedures, and Data Correction Workflows." *Remote Sensing* 10(7):1091.

Aasen, Helge, Eija Honkavaara, Arko Lucieer, and Pablo Zarco-Tejada. 2018b. "Quantitative Remote Sensing at Ultra-High Resolution with UAV Spectroscopy: A Review of Sensor Technology, Measurement Procedures, and Data Correction Workflows." *Remote Sensing* 10(7):1091. Retrieved (http://www.mdpi.com/2072-4292/10/7/1091).

Ahmed, Oumer S. et al. 2017. "Hierarchical Land Cover and Vegetation Classification Using Multispectral Data Acquired from an Unmanned Aerial Vehicle." *International Journal of Remote Sensing* 38(8–10):2037–52. Retrieved (http://dx.doi.org/10.1080/01431161.2017.1294781).

Alexander, Cici et al. 2018. "Locating Emergent Trees in a Tropical Rainforest Using Data from an Unmanned Aerial Vehicle (UAV)." *International Journal of Applied Earth Observation and Geoinformation* 72(May):86–90. Retrieved (https://www.sciencedirect.com/science/article/pii/S0303243418303660).

Ambrosia, V. G. et al. 2011. "The Ikhana Unmanned Airborne System (UAS) Western States Fire Imaging Missions: From Concept to Reality (2006–2010)." *Geocarto International* 26(2):85–101. Retrieved (http://dx.doi.org/10.1080/10106049.2010.539302).

Anderegg, William R. L., Jeffrey M. Kane, and Leander D. L. Anderegg. 2012. "Triggered by Drought and Temperature Stress." *Nature Climate Change* (September). Retrieved (http://dx.doi.org/10.1038/nclimate1635).

Anderson, Karen and Kevin J. Gaston. 2013. "Lightweight Unmanned Aerial Vehicles Will Revolutionize Spatial Ecology." *Frontiers in Ecology and the Environment* 11(3):138–46.

Arroyo-Mora, Pablo et al. 2005. "Secondary Forest Detection in a Neotropical Dry Forest Landscape Using Landsat 7 ETM + and IKONOS Imagery Published by : Association for Tropical Biology and Conservation." *Biotropica* 37(4):497–507. Retrieved (http://www.jstor.org/stable/30043218).

Asner, Gregory P. 1998. "Biophysical and Biochemical Sources of Variability in Canopy Reflectance." *Remote Sensing of Environment* 64(3):234–53.

Atkinson, P. M. and A. R. L. Tatnall. 1997. "Introduction Neural Networks in Remote Sensing." *International Journal of Remote Sensing* 18(4):699–709. Retrieved (http://www.tandfonline.com/doi/abs/10.1080/014311697218700).

Babey, S. K. and Raymond J. Soffer. 1992. "Radiometric Calibration of the Compact Airborne Spectrographic Imager (Casi)." *Canadian Journal of Remote Sensing* 18(4):233–42.

Ballesteros, R., J. F. Ortega, D. Hernández, and M. A. Moreno. 2014. "Applications of Georeferenced High-Resolution Images Obtained with Unmanned Aerial Vehicles. Part I: Description of Image Acquisition and Processing." *Precision Agriculture* 15(6):579–92.

Banninger, C. 1988. “Changes In Canopy Leaf Area Index And Biochemical Constituents Of A Spruce Forest As Measured By The AIS-2 Airborne Imaging Spectrometer.” Pp. 2085–89 in *12th Canadian Symposium on Remote Sensing Geoscience and Remote Sensing Symposium,* vol. 4. IEEE. Retrieved (http://ieeexplore.ieee.org/document/577783/).

Bastin, Jean François et al. 2014. “Aboveground Biomass Mapping of African Forest Mosaics Using Canopy Texture Analysis: Toward a Regional Approach.” *Ecological Applications* 24(8):1984–2001.

Belgiu, Mariana and Lucian Drăgu. 2016. “Random Forest in Remote Sensing: A Review of Applications and Future Directions.” *ISPRS Journal of Photogrammetry and Remote Sensing* 114:24–31.

Bendig, Juliane et al. 2015. “Combining UAV-Based Plant Height from Crop Surface Models, Visible, and near Infrared Vegetation Indices for Biomass Monitoring in Barley.” *International Journal of Applied Earth Observation and Geoinformation* 39:79–87. Retrieved (http://dx.doi.org/10.1016/j.jag.2015.02.012).

Bennett, Amy C., Nathan G. Mcdowell, Craig D. Allen, and Kristina J. Anderson-Teixeira. 2015. “Larger Trees Suffer Most during Drought in Forests Worldwide.” *Nature Plants* 1(September):1–5.

Birth, Gerald S. and George R. McVey. 1968. “Measuring the Color of Growing Turf with a Reflectance Spectrophotometer1.” *Agronomy Journal* 60(6):640. Retrieved (https://www.agronomy.org/publications/aj/abstracts/60/6/AJ0600060640).

Van Bloem, S., P. Murphy, and A. Lugo. 2004. “Tropical Dry Forests.” *Encyclopedia of Forest Sciences* 24(1):1767–75.

Bovik, Alan Conrad, Marianna Clark, and Wilson S. Geisler. 1990. “Multichannel Texture Analysis Using Localized Spatial Filters.” *IEEE Transactions on Pattern Analysis and Machine Intelligence* 12(1):55–73. Retrieved (http://ieeexplore.ieee.org/ielx1/34/1584/00041384.pdf?tp=&arnumber=41384&isnumber=1584%5Cnhttp://ieeexplore.ieee.org/xpls/abs_all.jsp?arnumber=41384).

Breiman, Leo, Adele Cutler, Andy Liaw, and Mathew Wiener. 2018. “Breiman and Cutler’s Random Forests for Classification and Regression.” *CRAN R Core Team. R: A Language and Environment for Statistical Computing. R Foundation for Statistical Computing, Vienna, Austria*. Retrieved (https://www.stat.berkeley.edu/~breiman/RandomForests/).

Breshears, David D. et al. 2009. “Research Communications Research Communications Tree Die-off in Response to Global Change-Type Drought: Mortality Insights from a Decade of Plant Water Potential Measurements.” *Frontiers in Ecology and the Environment* 7(4):185–89.

Bretfeld, Mario, Brent E. Ewers, and Jefferson S. Hall. 2018. “Plant Water Use Responses along Secondary Forest Succession during the 2015-2016 El Niño Drought in Panama.” *New Phytologist* 2. Retrieved (http://doi.wiley.com/10.1111/nph.15071).

Von Bueren, S. K. et al. 2015. “Deploying Four Optical UAV-Based Sensors over Grassland: Challenges and Limitations.” *Biogeosciences* 12(1):163–75.

Campos-Vargas, Carlos, Rodolfo Mora-Zamora, and Andres Segura-Castillo. 2015. "Geovisión : Una Infraestructura Abierta de Datos Espaciales Geovisión : Una Infraestructura Abierta de Datos Espaciales." *Tecnología En Marcha* 28(3):15–24.

Candiago, Sebastian, Fabio Remondino, Michaela De Giglio, Marco Dubbini, and Mario Gattelli. 2015. "Evaluating Multispectral Images and Vegetation Indices for Precision Farming Applications from UAV Images." *Remote Sensing* 7(4):4026–47.

Cao, Sen et al. 2015. "Mapping Tropical Dry Forest Succession Using Multiple Criteria Spectral Mixture Analysis." *ISPRS Journal of Photogrammetry and Remote Sensing* 109(November 2017):17–29. Retrieved (http://dx.doi.org/10.1016/j.isprsjprs.2015.08.009).

Carvalhais, Nuno et al. 2014. "Global Covariation of Carbon Turnover Times with Climate in Terrestrial Ecosystems." *Nature* 514(7521):213–17.

Castelvecchi, Davide. 2016. "Can We Open the Black Box of AI?" *Nature* 538(7623):20–23.

Castro-Esau, K. L., G. A. Sánchez-Azofeifa, and T. Caelli. 2004. "Discrimination of Lianas and Trees with Leaf-Level Hyperspectral Data." *Remote Sensing of Environment* 90(3):353–72.

Castro-Esau, K. L., G. A. Sánchez-Azofeifa, and B. Rivard. 2006. "Comparison of Spectral Indices Obtained Using Multiple Spectroradiometers." *Remote Sensing of Environment* 103(3):276–88.

Chianucci, Francesco et al. 2016. "Estimation of Canopy Attributes in Beech Forests Using True Colour Digital Images from a Small Fixed-Wing UAV." *International Journal of Applied Earth Observation and Geoinformation* 47:60–68. Retrieved (http://www.sciencedirect.com/science/article/pii/S0303243415300702).

Clark, D. A. 2004. "Sources or Sinks? The Responses of Tropical Forests to Current and Future Climate and Atmospheric Composition." *Philosophical Transactions of the Royal Society B: Biological Sciences* 359(1443):477–91. Retrieved September 22, 2013 (http://rstb.royalsocietypublishing.org/cgi/doi/10.1098/rstb.2003.1426).

Clark, Deborah A. 2014. "Are Tropical Forests an Important Carbon Sink?" *Ecological Society of America* 12(1):3–7.

Colomina, I. and P. Molina. 2014. "Unmanned Aerial Systems for Photogrammetry and Remote Sensing: A Review." *ISPRS Journal of Photogrammetry and Remote Sensing* 92:79–97. Retrieved (http://dx.doi.org/10.1016/j.isprsjprs.2014.02.013).

Crippen, Robert E. 1990. "Calculating the Vegetation Index Faster." *Remote Sensing of Environment* 34(1):71–73.

Crist, E. P. and R. J. Kauth. 1986. "The Tasseled Cap De-Mystified." *Photogrammetric Engineering & Remote Sensing* 52(1):81–86.

Cunliffe, Andrew M., Richard E. Brazier, and Karen Anderson. 2016. "Ultra-Fine Grain Landscape-Scale Quantification of Dryland Vegetation Structure with Drone-Acquired Structure-from-Motion Photogrammetry." *Remote Sensing of Environment* 183:129–43. Retrieved (http://dx.doi.org/10.1016/j.rse.2016.05.019).

Curran, Paul J. 1989. “Remote Sensing of Foliar Chemistry.” *Remote Sensing of Environment* 30(3):271–78.

Dandois, Jonathan P., Marc Olano, and Erle C. Ellis. 2015. “Optimal Altitude, Overlap, and Weather Conditions for Computer Vision Uav Estimates of Forest Structure.” *Remote Sensing* 7(10):13895–920.

Dash, Jonathan P., Michael S. Watt, Grant D. Pearse, Marie Heaphy, and Heidi S. Dungey. 2017. “Assessing Very High Resolution UAV Imagery for Monitoring Forest Health during a Simulated Disease Outbreak.” *ISPRS Journal of Photogrammetry and Remote Sensing* 131:1–14. Retrieved (http://dx.doi.org/10.1016/j.isprsjprs.2017.07.007).

Dunford, R., K. Michel, M. Gagnage, H. Piégay, and M. L. Trémelo. 2009. “Potential and Constraints of Unmanned Aerial Vehicle Technology for the Characterization of Mediterranean Riparian Forest.” *International Journal of Remote Sensing* 30(19):4915–35.

Efron, B. and R. Tibshirani. 1983. “Estimating the Error Rate of a Prediction Rule.” *Journal of the American Statistical Association* 78(382):316–31. Retrieved (http://citeseer.ist.psu.edu/47726.html).

Friedl, Mark a. M. A. and Carla E. C. E. Brodley. 1997. “Decision Tree Classification of Land Cover from Remotely Sensed Data.” *Remote Sensing of Environment* 61(3):399–409. Retrieved (http://www.sciencedirect.com/science/article/pii/S0034425797000497%5Cnhttp://www.sciencedirect.com/science/article/pii/S0034425797000497/pdf?md5=1cbeb1ccbff2690c404d2bbceb14066e&pid=1-s2.0-S0034425797000497-main.pdf%5Cnhttp://www.sciencedirect.com/science).

Gao, Bo Cai, Alexander Goetz, and J. Zamudio. 1991. “RETRIEVALS OF SURFACE REFLECTANCES FROM AVIRIS DATA.” Pp. 2069–77 in *IGARSS’91 Remote Sensing: Global Monitoring for Earth Management Geoscience and Remote Sensing Symposium*, vol. 2077.

Garrity, Steven R. et al. 2013. “Quantifying Tree Mortality in a Mixed Species Woodland Using Multitemporal High Spatial Resolution Satellite Imagery.” *Remote Sensing of Environment* 129:54–65. Retrieved (http://dx.doi.org/10.1016/j.rse.2012.10.029).

Getzin, Stephan, Robert S. Nuske, and Kerstin Wiegand. 2014. “Using Unmanned Aerial Vehicles (UAV) to Quantify Spatial Gap Patterns in Forests.” *Remote Sensing* 6(8):6988–7004.

Ghamisi, Pedram, Javier Plaza, Yushi Chen, Jun Li, and Antonio J. Plaza. 2017. “Advanced Spectral Classifiers for Hyperspectral Images: A Review.” *IEEE Geoscience and Remote Sensing Magazine* 5(1):8–32.

Gitelson, Anatoly A. and Mark N. Merzlyak. 1998. “Remote Sensing of Chlorophyll Concentration in Higher Plant Leaves.” *Advances in Space Research* 22(5):689–92.

Goel, N. S. and W. Qin. 1994. “Influences of Canopy Architecture on Relationships between Various Vegetation Indices and LAI and FPAR: A Computer Simulation.” *Remote Sensing Reviews* 10(4):309–47.

Goldman, Daniel B. and Chen Jiun-Hung. 2010. "Vignette and Exposure Calibration and Compensation." *IEEE Transactions on Pattern Analysis and Machine Intelligence* 32(12):2276–88.

Greenwood, Sarah et al. 2017. "Tree Mortality across Biomes Is Promoted by Drought Intensity, Lower Wood Density and Higher Specific Leaf Area." *Ecology Letters* 20(4):539–53.

Harris, A., J. A. Gamon, G. Z. Pastorello, and C. Y. S. Wong. 2014. "Retrieval of the Photochemical Reflectance Index for Assessing Xanthophyll Cycle Activity: A Comparison of near-Surface Optical Sensors." *Biogeosciences* 11(22):6277–92.

Hilje, Branko, Julio Calvo-Alvarado, César Jiménez-Rodríguez, and Arturo Sánchez-Azofeifa. 2015. "Tree Species Composition, Breeding Systems, and Pollination and Dispersal Syndromes in Three Forest Successional Stages in a Tropical Dry Forest in Mesoamerica." *Tropical Conservation Science* 8(1):76–94. Retrieved (http://journals.sagepub.com/doi/10.1177/194008291500800109).

Hornik, Kurt et al. 2018. "Package ' RWeka '." *CRAN R Core Team. R: A Language and Environment for Statistical Computing. R Foundation for Statistical Computing, Vienna, Austria*. Retrieved (https://cran.r-project.org/web/packages/RWeka/index.html).

Hothorn, Torsten, Kurt Hornik, Carolin Strobl, and Achim Zeileis. 2017. "A Laboratory for Recursive Partytioning." *CRAN R Core Team. R: A Language and Environment for Statistical Computing. R Foundation for Statistical Computing, Vienna, Austrialanguage and Environment for Statistical Computing. R Foundation for Statistical Computing, Vienna, Austria* 25. Retrieved (https://cran.r-project.org/web/packages/kohonen/kohonen.pdf).

Huete, A. et al. 2002. "Overview of the Radiometric and Biophysical Performance of the MODIS Vegetation Indices." *Remote Sensing of Environment* 83(1–2):195–213.

Janzen, Daniel H. 2000. "Costa Rica's Area de Conservación Guanacaste: A Long March to Survival through Non-Damaging Biodevelopment." *Biodiversity* 1(February):7–20. Retrieved (http://dx.doi.org/10.1080/14888386.2000.9712501%5Cnhttp://www.tandfonline.com/doi/abs/10.1080/14888386.2000.9712501#.U2kDRvldX8U).

Kalacska, M., G. A. Sanchez-Azofeifa, et al. 2007. "Ecological Fingerprinting of Ecosystem Succession: Estimating Secondary Tropical Dry Forest Structure and Diversity Using Imaging Spectroscopy." *Remote Sensing of Environment* 108(1):82–96.

Kalacska, M. et al. 2004. "Species Composition, Similarity and Diversity in Three Successional Stages of a Seasonally Dry Tropical Forest." *Forest Ecology and Management* 200(1–3):227–47.

Kalacska, M., S. Bohlman, G. A. Sanchez-Azofeifa, K. Castro-Esau, and T. Caelli. 2007. "Hyperspectral Discrimination of Tropical Dry Forest Lianas and Trees: Comparative Data Reduction Approaches at the Leaf and Canopy Levels." *Remote Sensing of Environment* 109(4):406–15.

Kalacska, Margaret, J. Pablo Arroyo-Mora, Raymond Soffer, and George Leblanc. 2016.

"Quality Control Assessment of the Mission Airborne Carbon 13 (MAC-13) Hyperspectral Imagery from Costa Rica." *Canadian Journal of Remote Sensing* 42(2):85–105. Retrieved (http://www.tandfonline.com/doi/full/10.1080/07038992.2016.1160771).

Kamilaris, Andreas and Francesc X. Prenafeta-Boldú. 2018. "Deep Learning in Agriculture: A Survey." *Computers and Electronics in Agriculture* 147(July 2017):70–90.

Karatzoglou, Alexandros, Alex Smola, and Kurt Hornik. 2016. "Kernel-Based Machine Learning Lab." *CRAN R Core Team. R: A Language and Environment for Statistical Computing. R Foundation for Statistical Computing, Vienna, Austria*. Retrieved (https://cran.r-project.org/web/packages/kernlab).

Knoth, Christian, Birte Klein, Torsten Prinz, and Till Kleinebecker. 2013. "Unmanned Aerial Vehicles as Innovative Remote Sensing Platforms for High-Resolution Infrared Imagery to Support Restoration Monitoring in Cut-over Bogs." *Applied Vegetation Science* 16(3):509–17.

Kuhn, Max and Kjell Johnson. 2013. *Applied Predictive Modeling*. Retrieved (http://www.amazon.com/Applied-Predictive-Modeling-Max-Kuhn/dp/1461468485/ref=pd_bxgy_b_img_z).

Lai, Hao Ran, Jefferson S. Hall, Benjamin L. Turner, and Michiel van Breugel. 2017. "Liana Effects on Biomass Dynamics Strengthen during Secondary Forest Succession." *Ecology* 98(4):1062–70.

Laliberte, Andrea. 2009. "Unmanned Aerial Vehicle-Based Remote Sensing for Rangeland Assessment, Monitoring, and Management." *Journal of Applied Remote Sensing* 3(1):033542. Retrieved (http://remotesensing.spiedigitallibrary.org/article.aspx?doi=10.1117/1.3216822).

Leblanc, George, Charles Francis, Raymond Soffer, Margaret Kalacska, and Julie de Gea. 2016. "Spectral Reflectance of Polar Bear and Other Large Arctic Mammal Pelts; Potential Applications to Remote Sensing Surveys." *Remote Sensing* 8(4):273. Retrieved (http://www.mdpi.com/2072-4292/8/4/273).

Li, Wang et al. 2016. "Remote Estimation of Canopy Height and Aboveground Biomass of Maize Using High-Resolution Stereo Images from a Low-Cost Unmanned Aerial Vehicle System." *Ecological Indicators* 67:637–48. Retrieved (http://dx.doi.org/10.1016/j.ecolind.2016.03.036).

Li, Wei, Carlos Campos-Vargas, Philip Marzahn, and Arturo Sanchez-Azofeifa. 2018. "On the Estimation of Tree Mortality and Liana Infestation Using a Deep Self-Encoding Network." *International Journal of Applied Earth Observation and Geoinformation* 73(May):1–13. Retrieved (https://doi.org/10.1016/j.jag.2018.05.025).

Li, Wei, Sen Cao, Carlos Campos-Vargas, and Arturo Sanchez-Azofeifa. 2017. "Identifying Tropical Dry Forests Extent and Succession via the Use of Machine Learning Techniques." *International Journal of Applied Earth Observation and Geoinformation* 63(July):196–205. Retrieved (https://doi.org/10.1016/j.jag.2017.08.003).

Maxwell, Aaron E., Timothy A. Warner, and Fang Fang. 2018. "Implementation of Machine-

Learning Classification in Remote Sensing: An Applied Review." *International Journal of Remote Sensing* 39(9):2784–2817. Retrieved (https://www.tandfonline.com/doi/full/10.1080/01431161.2018.1433343).

McDowell, Nate et al. 2018. "Drivers and Mechanisms of Tree Mortality in Moist Tropical Forests." *New Phytologist*. Retrieved (http://doi.wiley.com/10.1111/nph.15027).

McDowell, Nate et al. 2008. "Mechanisms of Plant Survival and Mortality during Drought: Why Do Some Plants Survive While Others Succumb to Drought?" *New Phytologist* 178(4):719–39. Retrieved (http://doi.wiley.com/10.1111/j.1469-8137.2008.02436.x).

Meddens, Arjan J. H., Jeffrey A. Hicke, and Lee A. Vierling. 2011. "Evaluating the Potential of Multispectral Imagery to Map Multiple Stages of Tree Mortality." *Remote Sensing of Environment* 115(7):1632–42. Retrieved (http://dx.doi.org/10.1016/j.rse.2011.02.018).

Miltiadou, Milto, Neil D. F. Campbell, Susana Gonzalez, Tony Brown, and Michael G. Grant. 2018. "Detection of Dead Standing Eucalyptus Camaldulensis without Tree Delineation for Managing Biodiversity in Native Australian Forest." *Int J Appl Earth Obs Geoinformation* 67(October 2017):135–47. Retrieved (https://doi.org/10.1016/j.jag.2018.01.008).

Miura, Tomoaki and Alfredo R. Huete. 2009. "Performance of Three Reflectance Calibration Methods for Airborne Hyperspectral Spectrometer Data." *Sensors* 9(2):794–813.

Mountrakis, Giorgos, Jungho Im, and Caesar Ogole. 2011. "Support Vector Machines in Remote Sensing: A Review." *ISPRS Journal of Photogrammetry and Remote Sensing* 66(3):247–59. Retrieved (http://dx.doi.org/10.1016/j.isprsjprs.2010.11.001).

Mulero-Pázmány, Margarita, Roel Stolper, L. D. Van Essen, Juan J. Negro, and Tyrell Sassen. 2014. "Remotely Piloted Aircraft Systems as a Rhinoceros Anti-Poaching Tool in Africa." *PLoS ONE* 9(1):1–10.

Najafabadi, Maryam M. et al. 2015. "Deep Learning Applications and Challenges in Big Data Analytics." *Journal of Big Data* 2(1):1–21.

Panagiotidis, Dimitrios, Azadeh Abdollahnejad, Peter Surový, and Vasco Chiteculo. 2017. "Determining Tree Height and Crown Diameter from High-Resolution UAV Imagery." *International Journal of Remote Sensing* 38(8–10):2392–2410. Retrieved (https://www.tandfonline.com/doi/full/10.1080/01431161.2016.1264028).

Phillips, Oliver L. et al. 2002. "Increasing Dominance of Large Lianas in Amazonian Forests." *Nature* 418(6899):770–74.

Plaza, Antonio et al. 2009. "Recent Advances in Techniques for Hyperspectral Image Processing." *Remote Sensing of Environment* 113(SUPPL. 1):S110–22. Retrieved (http://dx.doi.org/10.1016/j.rse.2007.07.028).

Poorter, Lourens et al. 2016. "Biomass Resilience of Neotropical Secondary Forests." *Nature* 530(7589):211–14. Retrieved (http://dx.doi.org/10.1038/nature16512).

Portillo-Quintero, C. A. and G. A. Sanchez-Azofeifa. 2010. "Extent and Conservation of Tropical Dry Forests in the Americas." *Biological Conservation* 143(1):144–55. Retrieved (http://dx.doi.org/10.1016/j.biocon.2009.09.020).

Pozo, Susana Del, Pablo Rodríguez-Gonzálvez, David Hernández-López, and Beatriz Felipe-García. 2014. "Vicarious Radiometric Calibration of a Multispectral Camera on Board an Unmanned Aerial System." *Remote Sensing* 6(3):1918–37.

Ridgeway, Greg. 2017. "Generalized Boosted Regression Models Author." *CRAN R Core Team. R: A Language and Environment for Statistical Computing. R Foundation for Statistical Computing, Vienna, Austria*. Retrieved (https://cran.r-project.org/web/packages/gbm/index.html).

Ripley, Brian and William Venables. 2016. "R Package 'Nnet': Feed-Forward Neural Networks and Multinomial Log-Linear Models." *CRAN R Core Team. R: A Language and Environment for Statistical Computing. R Foundation for Statistical Computing, Vienna, Austria*. Retrieved (http://www.stats.ox.ac.uk/pub/MASS4/).

Rong, Xiao. 2014. "Deepnet: Deep Learning Toolkit in R." *CRAN R Core Team. R: A Language and Environment for Statistical Computing. R Foundation for Statistical Computing, Vienna, Austria*.

Rowland, L. et al. 2015. "Death from Drought in Tropical Forests Is Triggered by Hydraulics Not Carbon Starvation." *Nature* 528(7580):119–22. Retrieved (http://dx.doi.org/10.1038/nature15539).

Rullan-Silva, C. D., A. E. Olthoff, J. A. Delgado de la Mata, and J. A. Pajares-Alonso. 2013. "Remote Monitoring of Forest Insect Defoliation. A Review." *Forest Systems* 22(3):377–91. Retrieved (http://apps.webofknowledge.com.ezproxy.library.wur.nl/full_record.do?product=WOS&search_mode=GeneralSearch&qid=4&SID=S271NJZlBMwJtwNh9OP&page=2&doc=15%5Cnhttp://revistas.inia.es/index.php/fs/article/view/4417).

Sanchez-Azofeifa, Arturo et al. 2017. "Twenty-First Century Remote Sensing Technologies Are Revolutionizing the Study of Tropical Forests." *Biotropica* 49(5):604–19.

Sánchez-Azofeifa, Arturo et al. 2009. "Differences in Leaf Traits, Leaf Internal Structure, and Spectral Reflectance between Two Communities of Lianas and Trees: Implications for Remote Sensing in Tropical Environments." *Remote Sensing of Environment* 113(10):2076–88. Retrieved October 7, 2013 (http://linkinghub.elsevier.com/retrieve/pii/S003442570900159X).

Sánchez-Azofeifa, Arturo, Julio Calvo-Alvarado, Mário Marcos do Espírito-Santo, Geraldo Fernandes, and Jennifer Powers. 2013. "Tropical Dry Forests in the Americas." Pp. 1–15 in *Tropical Dry Forests in the Americas*. CRC Press. Retrieved (http://www.crcnetbase.com/doi/abs/10.1201/b15417-2).

Sanchez-Azofeifa, G. A., K. L. Castro, B. Rivard, M. R. Kalascka, and R. C. Harriss. 2003. "Remote Sensing Research Priorities in Tropical Dry Forest Environments." *Biotropica* 35(2):134–42. Retrieved (http://doi.wiley.com/10.1111/j.1744-7429.2003.tb00273.x).

Sánchez-Azofeifa, Gerardo Arturo et al. 2017. "Can Terrestrial Laser Scanners (TLSs) and Hemispherical Photographs Predict Tropical Dry Forest Succession with Liana Abundance?" *Biogeosciences* 14(4):977–88. Retrieved (https://www.biogeosciences.net/14/977/2017/).

Sandbrook, Chris. 2015. “The Social Implications of Using Drones for Biodiversity Conservation.” *Ambio* 44(4):636–47.

Schnitzer, Stefan A. 2005. “A Mechanistic Explanation for Global Patterns of Liana Abundance and Distribution.” *The American Naturalist* 166(2):262–76. Retrieved (http://www.journals.uchicago.edu/doi/10.1086/431250).

Seager, Richard et al. 2007. “Model Projections of an Imminent Transition to a More Arid Climate in Southwestern North America.” *Science* 316(5828):1181–84.

Smith, Geoffrey M. and Edward J. Milton. 1999. “The Use of the Empirical Line Method to Calibrate Remotely Sensed Data to Reflectance.” *International Journal of Remote Sensing* 20(13):2653–62.

Sripada, Ravi P., Ronnie W. Heiniger, Jeffrey G. White, and Alan D. Meijer. 2006. “Aerial Color Infrared Photography for Determining Early In-Season Nitrogen Requirements in Corn.” *Agronomy Journal* 98(4):968–77.

Sterl, Andreas et al. 2008. “When Can We Expect Extremely High Surface Temperatures?” *Geophysical Research Letters* 35(14):1–5.

Tobin, Michael F., Alexandra J. Wright, Scott A. Mangan, and Stefan A. Schnitzer. 2012. “Lianas Have a Greater Competitive Effect than Trees of Similar Biomass on Tropical Canopy Trees.” *Ecosphere* 3(2):art20. Retrieved (http://doi.wiley.com/10.1890/ES11-00322.1).

Tucker, Compton J. 1979. “Red and Photographic Infrared Linear Combinations for Monitoring Vegetation.” *Remote Sensing of Environment* 8(2):127–50.

Vargas-Sanabria, Daniela and Carlos Campos-Vargas. 2018. “Sistema Multi-Algoritmo Para La Clasificación de Coberturas de La Tierra En El Bosque Seco Tropical Del Área de Conservación Guanacaste, Costa Rica.” *Revista Tecnología En Marcha* 31(1):58. Retrieved (http://revistas.tec.ac.cr/index.php/tec_marcha/article/view/3497).

Vaughn, N. R. et al. 2018. “An Approach for High-Resolution Mapping of Hawaiian Metrosideros Forest Mortality Using Laser-Guided Imaging Spectroscopy.” *Remote Sensing, This Issue* 1–17.

Vescovo, Loris et al. 2012. “New Spectral Vegetation Indices Based on the Near-Infrared Shoulder Wavelengths for Remote Detection of Grassland Phytomass.” *International Journal of Remote Sensing* 33(7):2178–95.

Viña, Andrés, Anatoly A. Gitelson, Anthony L. Nguy-Robertson, and Yi Peng. 2011. “Comparison of Different Vegetation Indices for the Remote Assessment of Green Leaf Area Index of Crops.” *Remote Sensing of Environment* 115(12):3468–78. Retrieved (http://dx.doi.org/10.1016/j.rse.2011.08.010).

Williams, A. Park et al. 2013. “Temperature as a Potent Driver of Regional Forest Drought Stress and Tree Mortality.” *Nature Climate Change* 3(3):292–97. Retrieved (http://dx.doi.org/10.1038/nclimate1693).

Wolpert, David H. 1992. “On the Connection between In-Sample Testing and Generalization

Error.” *Com p Lex Systems* 6:47–94.

Wolpert, David H. 1996. “The Existence of A Priori Distinctions Between Learning Algorithms.” *Neural Computation* 8(7):1391–1420. Retrieved (http://www.mitpressjournals.org/doi/10.1162/neco.1996.8.7.1391).

Wright, S. Joseph, Osvaldo Calderón, Andrés Hernandéz, and Steven Paton. 2004. “Are Lianas Increasing in Importance in Tropical Forests ? A 17-Year Record from Panama ARE LIANAS INCREASING IN IMPORTANCE IN TROPICAL FORESTS ? A 17-YEAR RECORD FROM PANAMA.” 85(2):484–89.

Wullschleger, Stan D., P. J. Hanson, and D. E. Todd. 2001. “Transpiration from a Multi-Species Deciduous Forest as Estimated by Xylem Sap Flow Techniques.” *Forest Ecology and Management* 143(1–3):205–13.

Yuan, Chi, Youmin Zhang, and Zhixiang Liu. 2015. “A Survey on Technologies for Automatic Forest Fire Monitoring, Detection, and Fighting Using Unmanned Aerial Vehicles and Remote Sensing Techniques.” *Canadian Journal of Forest Research* 45(7):783–92.

Zahawi, Rakan A. et al. 2015. “Using Lightweight Unmanned Aerial Vehicles to Monitor Tropical Forest Recovery.” *Biological Conservation* 186:287–95.

Zarco-Tejada, P. J., R. Diaz-Varela, V. Angileri, and P. Loudjani. 2014. “Tree Height Quantification Using Very High Resolution Imagery Acquired from an Unmanned Aerial Vehicle (UAV) and Automatic 3D Photo-Reconstruction Methods.” *European Journal of Agronomy* 55:89–99. Retrieved (http://dx.doi.org/10.1016/j.eja.2014.01.004).

Zeppel, Melanie J., William R. Anderegg, and Henry D. Adams. 2013. “Meetings Forest Mortality Due to Drought : Latest Insights , Evidence and Unresolved Questions on Physiological Pathways and Consequences of Tree Death.” *New Phytologist* 197(2):372–74.

Appendices

Appendices chapter Two

Appendices 2.1. Example of error values at band and index level acquired at 25 m of altitude.

field	treat	height	e_b1	e_b2	e_b3	e_b4	e_b5	e_dvi	e_evi	e_gdvi	e_ngdvi	e_ndvi	e_grvi	e_ipvi	e_mnli	e_msr	e_nli	e_sr
1	2	h25	-5.8	-6.3	-5.2	-8.3	-7.3	12.1	-15.3	-11	-11.6	-12.8	-2.7	-6.4	-15.8	-12.5	17.4	-4.4
2	2	h25	-5.5	-6.1	-5.6	-8.2	-6.8	11.2	-15.1	-10.7	-11	-11.6	-1.8	-5.8	-14.9	-11.5	16.2	-2.7
3	2	h25	-5.4	-6.3	-5.7	-8.3	-6.8	11.1	-16.1	-10.5	-10.7	-11.5	-1.4	-5.7	-14.8	-11.4	16.2	-2.6
4	2	h25	-5.3	-6	-4.8	-8.1	-6.5	11.7	-14.5	-10.5	-10.7	-12	-1.3	-6	-15.2	-11.8	16.2	-3.3
5	2	h25	-4.6	-5.9	-5.9	-8.2	-7	11.1	-0.5	-11.1	-11.5	-11.5	-2.7	-5.8	-14.8	-11.4	16.4	-2.7
6	2	h25	-7	-7.6	-7	-8.6	-7.7	10.7	-12.2	-10.1	-10.2	-11.3	-0.4	-5.7	-14.3	-11.2	-17	-2.3
7	2	h25	-6.9	-7.3	-7	-8.3	-7.4	10.4	-11.4	-10.1	-10.2	-10.7	-0.4	-5.4	-14	-10.7	16.3	-1.3
8	2	h25	-7.5	-8.4	-8.5	-8.9	-8.6	10.1	-11.5	-10.2	-10.7	-10.3	-1.3	-5.2	-12.9	-10.3	17.7	-0.7
9	2	h25	-7.7	-8.5	-8.3	-8.4	-8	-9.7	-8.5	-9.5	-8.6	-9.2	3.3	-4.6	-12.7	-9.2	16.2	-1.8
10	2	h25	-7.9	-8.4	-8.4	-9.3	-8.6	10.2	-11	-10.2	-10.7	-10.7	-1.3	-5.3	-13.1	-10.6	17.8	-1.3
11	2	h25	-7.4	-8.8	-8.5	-9.1	-7.9	-9.4	-0.6	-9.1	-7.3	-8.3	7.5	-4.2	-12.3	-8.2	15.5	-4

Note: The total data set it is not provided because it requires 1744 rows to be displayed.

Appendices chapter Three

Appendices 3.1 Tukey test results of 10 classification models according to (a) Time and (b) Accuracy average values.

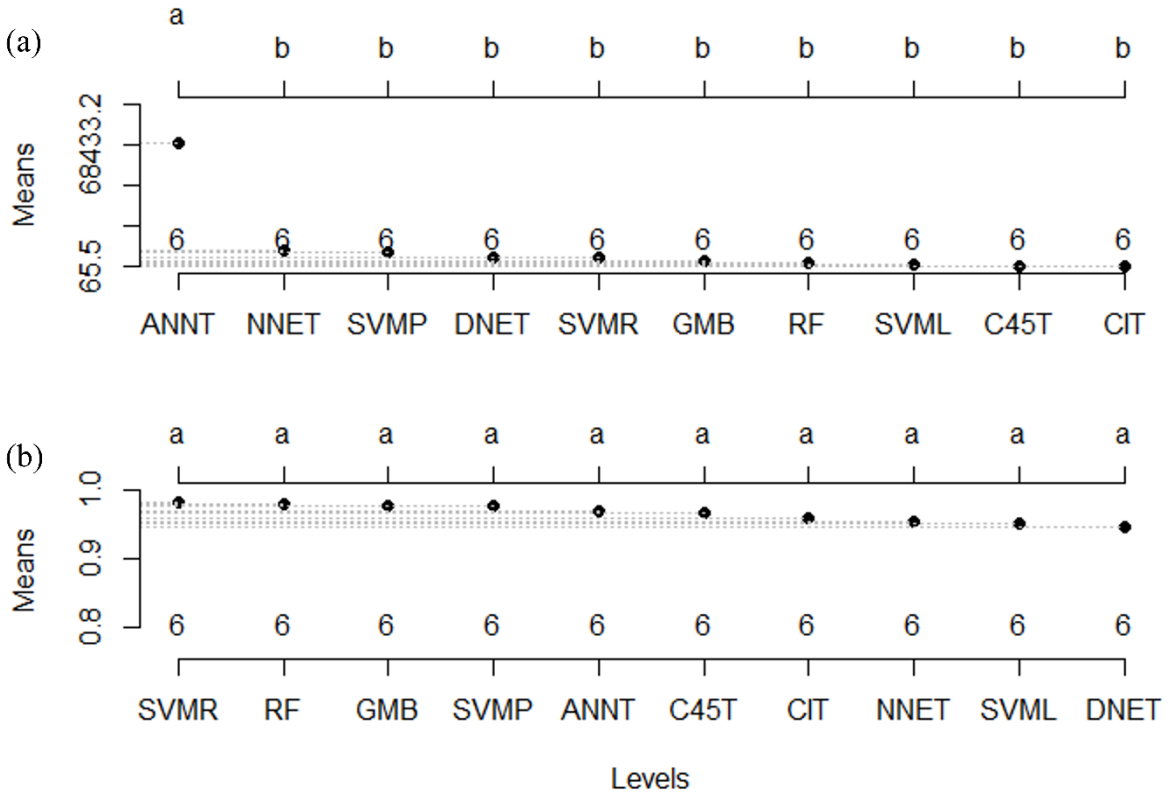

Appendices 3.2. Tukey test results of five specific models and a general model at SR-EMSS.

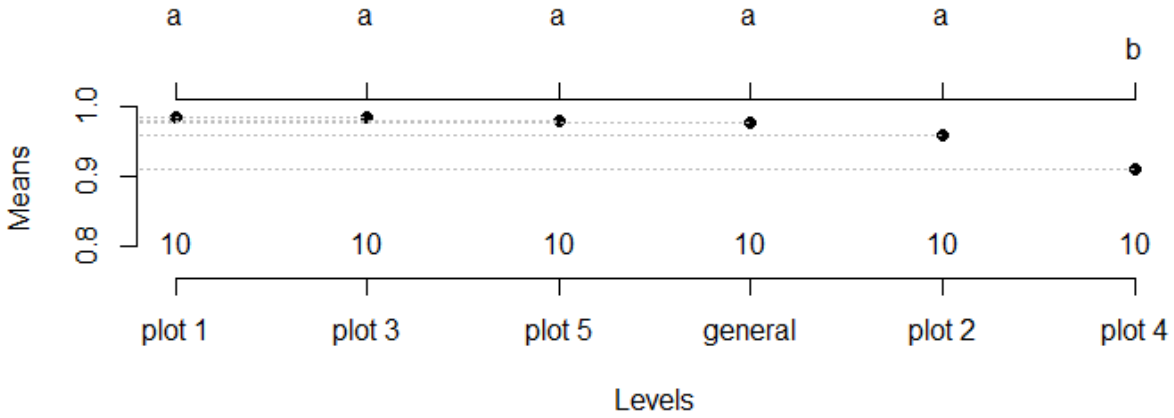

Appendices 3.3. Tukey Test of an ANOVA with a significance level of 0.95 across five temporary forest plots at Costa Rica.

Models	diff	lwr	upr	p adj
C45T-CIT	199.8983	-15330.8	15730.56	1.000
SVML-CIT	421.69	-15109	15952.35	1.000
RF-CIT	1349.367	-14181.3	16880.02	1.000
GMB-CIT	2665.5	-12865.2	18196.16	1.000
SVMR-CIT	4516.037	-11014.6	20046.69	0.993
DNET-CIT	4796.568	-10734.1	20327.23	0.989
SVMP-CIT	8014.405	-7516.25	23545.06	0.786
NNET-CIT	9097.455	-6433.2	24628.11	0.643
ANNT-CIT	69133.95	53603.29	84664.61	0.000
SVML-C45T	221.7917	-15308.9	15752.45	1.000
RF-C45T	1149.468	-14381.2	16680.13	1.000
GMB-C45T	2465.602	-13065.1	17996.26	1.000
SVMR-C45T	4316.138	-11214.5	19846.8	0.995
DNET-C45T	4596.67	-10934	20127.33	0.992
SVMP-C45T	7814.507	-7716.15	23345.16	0.809
NNET-C45T	8897.557	-6633.1	24428.21	0.671
ANNT-C45T	68934.05	53403.4	84464.71	0.000
RF-SVML	927.6767	-14603	16458.33	1.000
GMB-SVML	2243.81	-13286.8	17774.47	1.000
SVMR-SVML	4094.347	-11436.3	19625	0.997
DNET-SVML	4374.878	-11155.8	19905.54	0.995
SVMP-SVML	7592.715	-7937.94	23123.37	0.833
NNET-SVML	8675.765	-6854.89	24206.42	0.701
ANNT-SVML	68712.26	53181.6	84242.92	0.000
GMB-RF	1316.133	-14214.5	16846.79	1.000
SVMR-RF	3166.67	-12364	18697.33	1.000
DNET-RF	3447.202	-12083.5	18977.86	0.999
SVMP-RF	6665.038	-8865.62	22195.7	0.915
NNET-RF	7748.088	-7782.57	23278.75	0.816
ANNT-RF	67784.59	52253.93	83315.24	0.000
SVMR-GMB	1850.537	-13680.1	17381.19	1.000
DNET-GMB	2131.068	-13399.6	17661.73	1.000
SVMP-GMB	5348.905	-10181.8	20879.56	0.978
NNET-GMB	6431.955	-9098.7	21962.61	0.930
ANNT-GMB	66468.45	50937.79	81999.11	0.000
DNET-SVMR	280.5317	-15250.1	15811.19	1.000
SVMP-SVMR	3498.368	-12032.3	19029.03	0.999
NNET-SVMR	4581.418	-10949.2	20112.08	0.992
ANNT-SVMR	64617.92	49087.26	80148.57	0.000
SVMP-DNET	3217.837	-12312.8	18748.49	0.999
NNET-DNET	4300.887	-11229.8	19831.54	0.995

ANNT-DNET	64337.38	48806.73	79868.04	0.000
NNET-SVMP	1083.05	-14447.6	16613.71	1.000
ANNT-SVMP	61119.55	45588.89	76650.2	0.000
ANNT-NNET	60036.5	44505.84	75567.15	0.000

Appendices 3.4. Accuracy, kappa and processing time of ten Machine learning models across five temporary forest plots at SR-EMSS, Costa Rica.

mid	Model	Accuracy	kappa	Time (min)	Plot
1	RF	0.99	0.99	661.73	plot 1
1	RF	0.98	0.97	1751.45	plot 2
1	RF	0.99	0.98	734.74	plot 3
1	RF	0.94	0.92	2100.5	plot 4
1	RF	0.99	0.98	765.54	plot 5
1	RF	0.99	0.91	3125.51	plot 6
2	C45T	0.99	0.98	308.79	plot 1
2	C45T	0.95	0.93	430.07	plot 2
2	C45T	0.99	0.99	304.32	plot 3
2	C45T	0.91	0.87	366.45	plot 4
2	C45T	0.97	0.95	408.21	plot 5
2	C45T	0.99	0.98	424.82	plot 6
3	CIT	0.99	0.98	104.67	plot 1
3	CIT	0.95	0.94	183.62	plot 2
3	CIT	0.98	0.98	97.17	plot 3
3	CIT	0.89	0.86	164.19	plot 4
3	CIT	0.97	0.95	88.92	plot 5
3	CIT	0.97	0.98	404.7	plot 6
4	GMB	0.99	0.99	1488.44	plot 1
4	GMB	0.98	0.97	2770.14	plot 2
4	GMB	0.99	0.99	1408.78	plot 3
4	GMB	0.93	0.91	2248.28	plot 4
4	GMB	0.98	0.97	1919.75	plot 5
4	GMB	0.99	0.99	7200.88	plot 6
5	SVML	0.99	0.99	72.82	plot 1
5	SVML	0.96	0.94	128.61	plot 2
5	SVML	0.99	0.99	103.16	plot 3
5	SVML	0.85	0.81	396.28	plot 4
5	SVML	0.99	0.98	113.64	plot 5
5	SVML	0.92	0.92	2758.9	plot 6
6	SVMP	0.99	0.98	750.32	plot 1
6	SVMP	0.97	0.97	2747.55	plot 2
6	SVMP	0.99	0.99	917.91	plot 3
6	SVMP	0.93	0.91	27437.53	plot 4
6	SVMP	0.99	0.99	1125.25	plot 5

6	SVMP	0.99	0.99	16151.14	plot 6
7	SVMR	0.99	0.99	658.36	plot 1
7	SVMR	0.98	0.97	1933.04	plot 2
7	SVMR	0.99	0.99	732.28	plot 3
7	SVMR	0.94	0.93	1573.6	plot 4
7	SVMR	1	0.99	752.65	plot 5
7	SVMR	0.99	0.99	22489.56	plot 6
8	NNET	0.99	0.99	5291.85	plot 1
8	NNET	0.92	0.89	10203.23	plot 2
8	NNET	0.99	0.99	4862.61	plot 3
8	NNET	0.86	0.81	9885	plot 4
8	NNET	0.98	0.97	6405.29	plot 5
8	NNET	0.99	0.99	18980.02	plot 6
9	ANNT	0.99	0.99	51439.75	plot 1
9	ANNT	0.96	0.94	91222.38	plot 2
9	ANNT	0.99	0.99	49492.1	plot 3
9	ANNT	0.9	0.86	79925.06	plot 4
9	ANNT	0.98	0.97	52601.26	plot 5
9	ANNT	0.99	0.98	91166.43	plot 6
10	DNET	0.94	0.94	3468.43	plot 1
10	DNET	0.94	0.96	3755.14	plot 2
10	DNET	0.95	0.95	3392.74	plot 3
10	DNET	0.95	0.96	3855.23	plot 4
10	DNET	0.94	0.99	3152.38	plot 5
10	DNET	0.95	0.93	12198.76	plot 6